Experimental Investigation of the Ternary Mg-Al-Sr System

MD Anwar Parvez

A Thesis

In

The Department

of

Mechanical and Industrial Engineering

Presented in Partial Fulfillment of the Requirements
for the Degree of Master of Applied Science (Mechanical Engineering) at
Concordia University
Montreal, Quebec, Canada

January 2004

ABSTRACT

Experimental Investigation of the Ternary Mg-Al-Sr System

MD Anwar Parvez

In this work, the ternary Mg-Al-Sr system was investigated experimentally by differential scanning calorimeter (DSC), X-ray Diffraction (XRD) and metallography. The experimental work focused on the critical regions after reviewing the phase diagrams developed by thermodynamic modeling. DSC has permitted real time measurement of the temperature and enthalpy of the phase transformation. The experimental results were compared with the pertinent thermodynamic findings as well as with the literature data. The thermodynamic calculations are consistent with experimental results in few samples especially in the liquidus temperature, whereas discrepancy was observed in several cases especially in the solid phase transformation temperature that suggests this system should be remodeled. Two ternary eutectic transformations have been observed. XRD was used to identify the phases in the studied samples where Al_4Sr and (Mg) were found to be the dominating phases. Distinct unknown peaks were observed in the investigated samples. In this investigation, four new phase fields have been tentatively identified. The new phase may be ternary intermetallics or ternary or binary solid solutions. Thermodynamic calculations were also utilized to understand the microstructures and the phase relationships. The microstrutural evolution in two post-DSC samples has also been investigated and compared with the as-cast condition.

ACKNOWLEDGEMENTS

The author would like to express his sincere appreciation, gratitude and thanks to his supervisor, Dr. Mamoun Medraj, for his paternal guidance, invaluable and constructive suggestions throughout the period of this investigation. His intelligent supervision with overflowing enthusiasm helped the author to put the research ideas in the form that this report presents.

The assistance of Dr. Elhachmi Essadiqi of CANMET-MTL and Dr. Muntasar of Department of Chemistry, Concordia University is gratefully acknowledged.

The author would also like to thank the members of Dr. Medraj's research group, particularly Xiazhao Wang for his kind help and cooperation. In addition, the author would like to acknowledge the financial assistance provided by the Natural Science and Engineering Research Council (NSERC) to keep the research work going.

The author would like to thank his parents for their love, support and constant encouragement. Last by not least, the author would like to thank his wife, Jubaida for her invaluable support and help without which this thesis would not have been completed.

TABLE OF CONTENTS

LIST OF FIGURES

LIST OF TABLES

LIST OF ABBREVIATIONS

DSC	Differential Scanning Calorimetry
DTA	Diffrential Thermal Analysis
XRD	X-ray Diffraction
TG	Thermogravimetry
TMA	Thermomechanical Analysis
OM	Optical Microscopy
SEM	Scanning Electron Microscopy
EDS	Energy Dispersive Spectroscopy
EDX	Energy Dispersive X-ray Spectrometer

CHAPTER 1

Introduction

Magnesium is the eight most abundant metals on the earth surface at approximately 2.5% of its composition. It is an alkaline earth element (Group II) that crystallizes in a hexagonal structure (hcp-A3). Magnesium is the lightest metallic material used for structural applications with a density of 1.738 g/cm^3 in comparison with the densities of Al (2.70g/cm^3) and Fe (7.86g/cm^3). Magnesium also has a very good strength to weight ratio of common structural metals and has the exceptional die-casting characteristics [1,2]. In addition, on a per-pound basis in 2002, magnesium costs about 1.8 times as much as aluminum, whereas on a volume basis it costs only 1.2 times more. This makes magnesium alloys one of the most promising light-weight materials for automotive applications [3].

Emerging goals for reduced emission and fuel economy in passenger vehicles is exerting a driving force for expanding the use of magnesium [4]. The current use of magnesium in automotive application includes cross-car instrument panel beams, steering wheel armatures, cam covers and valve covers. The market for automotive magnesium parts has grown rapidly, nearly 15 % per year during the 1990s. The average magnesium content in the 2002 model cars was 4 kg. Figure 1-1 shows the North American automotive magnesium usage for different car manufacturers [5].

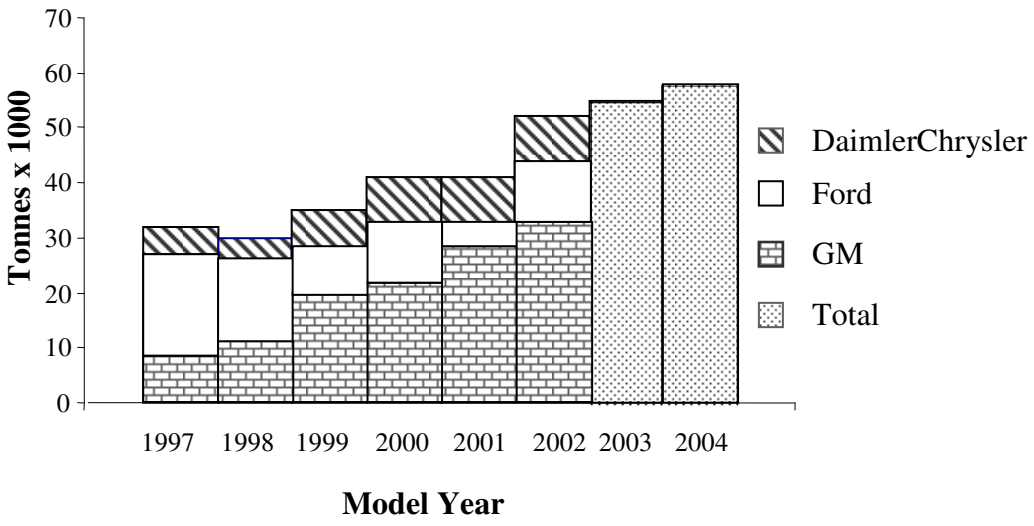

Figure 1-1: North American Automotive Magnesium Usage [5].

Die-casting is one of the most effective fabrication methods to produce magnesium components in automotive industry. However, the number of available Mg-based alloys for die-casting is very limited. AZ91 (Mg-9wt.% Al-1wt.%Zn) is the principal alloy, which represents 80% of the magnesium casting components [6]. These alloys are not suitable for applications over 95°C such as powertrain components in automobile applications (Figure 1-2) because of their restricted creep properties which limited the current application of magnesium to non-critical parts such as valve covers and instrument panels. In contrast to steels and many Al-alloys, the conventional Mg-alloys have a relatively low resistance to creep [7]. Magnesium faces a challenge in meeting the performance requirements of the components, which operate at elevated temperature. When the temperature is increased, strength becomes more time-dependent and loads which caused no permanent deformation at room temperature cause slow and continuous deformation with time. In recent years even higher demands have been made on thermally stressed components for example in engine construction.

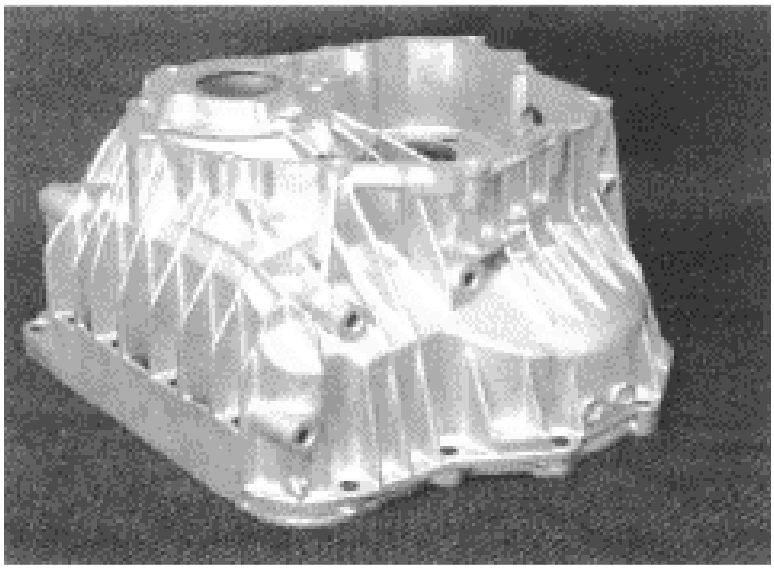

Figure 1-2: Gear Box made of Mg-alloy (Courtesy: Volkswagen)

1.1 Creep behavior of magnesium and its alloys

Grain boundary sliding has been observed to be the main creep mechanism in magnesium alloys in the stress-temperature ranges of interest for automotive application. Magnesium seems to creep even at low temperature by a stress-recovery mechanism. The creep mechanisms at low temperature are basal slip within the grains and sub-grains formation while at the higher temperatures diffusion-dependent mechanisms become predominant [7].

Mg-Al alloys are one major group among the magnesium-based alloys. The strength of these alloys is improved by forming a solid solution where 11.5 at.% Al is soluble in the Mg-matrix at 437°C. The microstructure of these alloys is characterized by the Mg-γ ($Mg_{17}Al_{12}$) eutectic at the grain boundaries. The non-stoichiometric phase γ is

incoherent with the α-Mg matrix. In addition to this poor coherency, if Mg-Al alloys are exposed to elevated temperatures (> 150°C) for longer time, the supersaturated Mg solid solution transforms to Mg-matrix with coarsely dispersed γ precipitates and contributes to grain boundary migration and creep deformation. γ is also prone to aging and has poor metallurgical stability, which limited the application at higher temperature [3,9].

1.2 Development of creep resistant magnesium alloys

Early developments in improving the creep properties of Magnesium were made in the 1960's by Volkswagen. It was based on the Mg-Al-Si system. These alloys exhibit marginally improved creep resistance but are quite difficult to die-cast. But it has paved the way for much of the current research [8].

The 90's have seen renewed activity in the development of elevated temperature magnesium diecasting alloys. Developments in recent years have led to the discovery of certain alloys containing rare earth elements and calcium. The AE42 (Mg-4 at.% Al-2 at.% rare earths) has improved creep resistance over the other alloys. For example, magnesium-thorium alloys displays excellent creep properties (350°C) and used in the aircraft engines. However, these alloys have cost disadvantages due to expensive rare-earth additions [9]. Also, thorium is a radioactive element.

Magnesium alloys, which are used commercially, contain Al and Zn. Some attempts were made in the last decades to replace the rare earths metals by Ca. But these

alloys suffer from inferior diecastability (e.g. Mg-Al-Ca) or have disadvantages in terms of marginal performance improvements (e.g. Mg-Al-Ca-RE and Mg-Al-Ca-Sr-RE). Die-sticking and hot-cracking behavior also caused problems. This alloy system has been considered subsequently for semi-solid forming applications. Later, Mg-Al-Zn-Ca show much improved castability but the alloy seems to work only in an extremely narrow composition range and the properties of the alloy vary due to macro segregation of the heavier Zn. Newly developed Mg-Al-Ca-based alloys with micro-alloying additions of Si and Sr showed better creep properties and diecastability [9,10].

It is very important to have magnesium alloys with acceptable creep resistance and affordable cost to automotive industry. The intermetallics in theses alloys should be thermally and metallurgically stable and would be expected to yield effective grain boundary strengthening and resistance to flow during creep loading. In addition, it should have adequate corrosion resistance, castability and strength. Strontium, an alkaline earth elements, is one of those metals which play a very positive role as an agent modifying or improving the casting and mechanical or structural properties of commercial Mg-based alloys. The microporosity of Mg-based alloys by low-pressure castings can also be overcome by an addition of Sr [11].

1.3 Mg-Al-Sr

The Mg-Al-Sr system has emerged in recent years as promising material system for the heat resistant light-weight Mg alloys. Recently Noranda developed alloys based on Mg-Al-Sr system, which will be used by BMW for the manufacturing of die-cast engine blocks. It exhibits excellent mechanical properties, good corrosion resistance and excellent castability. Timminco Ltd., which produces Al-Sr master alloys, has also patented master Al-Sr-Mg compositions with an increased Sr content. Figure 1-3 shows a comparison of creep deformation of different diecast Mg-alloys. It can be seen from this figure that Mg alloys with Sr addition outperformed the other alloy systems in terms of creep resistance. Tensile and yield strength of the alloys at 150°C was found to be superior to AE42. Figure 1-4 shows that the corrosion resistance of the Mg-Al-Sr alloys is similar to AZ91D and better than the AE42, which indicates that strontium does not have adverse effect on corrosion properties. The microstructure of this alloy is characterized by highly stable compound Al_4Sr and (Mg) lamellar phase, which improved the creep resistance [2].

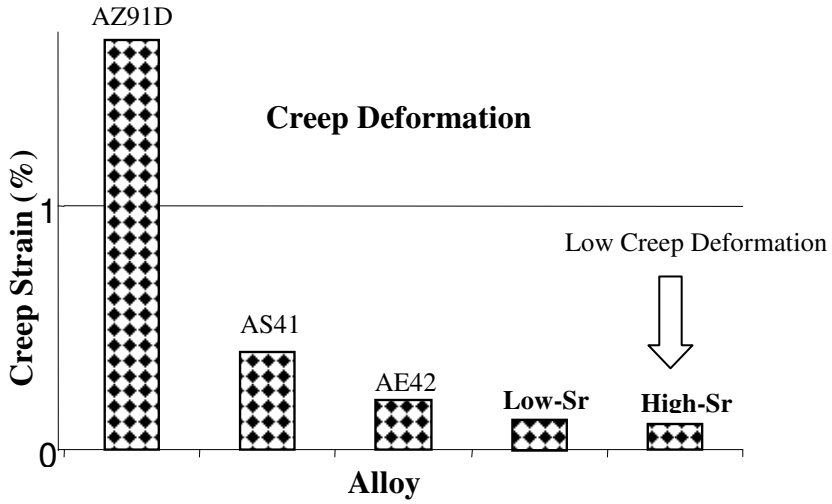

Figure 1-3: Comparison of creep deformation of die-cast Mg-alloys (35MPa, 150°C, 200h) [2].

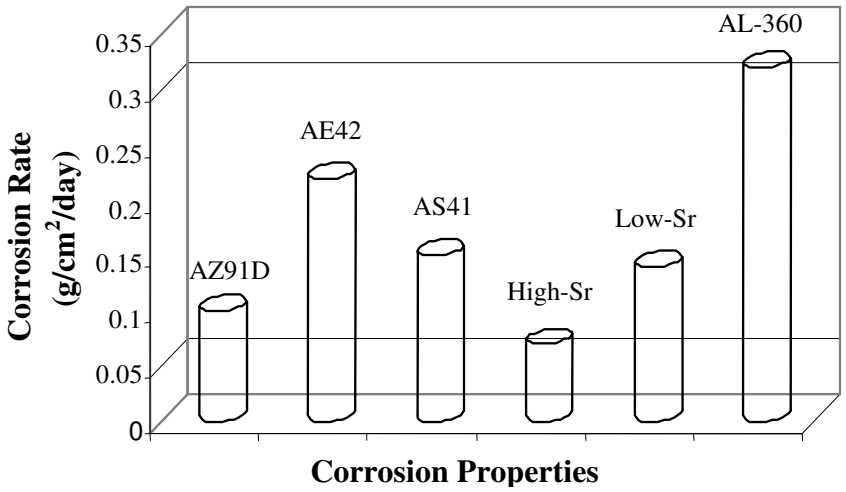

Figure 1-4: Comparison of corrosion properties [2].

Development of a reliable thermodynamic database for multicomponent alloys requires a combination of experiments and computational thermochemistry [12,13]. Within the ternary Mg-Al-Sr system, there is a huge amount of possibilities to select alloy compositions. The importance of phase diagram is enormous in all parts of material development because the diagram can illustrate the phase relations and phase stability under given conditions. It also assists in selecting promising alloys.

To date little effort has been made to construct the phase relationships of Mg-Al-Sr system. The published experimental works on the phase equilibria of Mg-Al-Sr system are self-contradictory. The calculated phase diagram exhibited substantial disagreement with the experimental data. The ternary system was modeled without using ternary phases or ternary interaction parameters. A considerable discrepancy among the published results and very few experimental data demands new experimental investigation for the verification and reassessment of this highly potential system.

1.4 Objectives

The objective of this study is to carry out a systematic investigation on the ternary Mg-Al-Sr system by Differential Scanning Calorimeter (DSC), X-ray Diffraction (XRD) and metallogaphy. Experimental results will be verified with the pertinent thermodynamic calculations. Specific objectives include:

- Real time measurement of the phase change involved in the system with temperature and enthalpy of transformation using DSC.
- Identification of the phases that form in the studied samples upon cooling to room temperature using XRD.
- Analysis of the morphology and the network nature of the grain boundary phases by metallography.
- Calculation of the isothermal section, vertical sections and phase assemblage diagrams for the studied samples using the Mg-Al-Sr thermodynamic database and with the aid of FactSage [14] computer program.
- Verification of the experimental results with the pertinent thermodynamic findings and available literature data.

CHAPTER 2

Literature Review

The Mg-Al-Sr phase diagram is very complicated due to the interaction between the components. This chapter outlines some past research works on this system. The fundamentals of the DSC and XRD are also being addressed.

2.1 Mg-Al-Sr ternary system

2.1.1 Experimental work

To date little effort has been made to construct the phase relationships of Mg-Al-Sr system. Prince *et al.* [15] summarized the work done on the Mg-Al-Sr system. The experimental work on the phase equilibria of Mg-Al-Sr system is primarily originated from one research group. However, inconsistency was noticed between their works, which were published from 1980 to 1982.

Makmudov *et al.* [16] studied solid solubility at 400°C for the Mg and Al-rich region and reported a ternary compound X of unknown stoichiometry which is in equilibrium with (Mg), $Mg_{17}Sr_2$ and γ. In 1981, Makmudov *et al.* [17] used the methods of DTA, microstructural and X-ray spectrum analysis and microhardness measurement for constructing the liquidus surfaces of Mg-Sr_2Mg_{17}-γ and Al-$SrAl_4$-β system. They reported two ternary eutectic points, one with a composition of 71 at.% Mg, 27 at.% Al and 2 at.% Sr and occurs at 430°C and another with a composition of 35 at.% Mg, 63.6

at.% Al and 1.4 at.% Sr and occurs at 445°C. Makhmudov *et al.* [18] determined the 400°C isothermal section by examining over 200 alloys. The 400°C isothermal section shows a triangulation involving (Mg), $Mg_{17}Sr_2$ and the γ phase. But it seems unlikely, as the thermodynamic stabilities of these compounds are low as compared to Al_4Sr and Al_2Sr. Makhmudov *et al.* [18] observed large solubilities in the solid phases. The Al_4Sr phase dissolves 20 at.% Mg and Mg_2Sr dissolves 10 at.% Al in the Mg-Al-Sr system. They also reported a ternary compound with stoichiometry of $Al_{34}Mg_6Sr_{60}$ (Al_6MgSr_{10}), which is different from the earlier reported X compound. The authors showed that this ternary system consists of 12 fields of single-phase alloys, 22 fields of two-phase alloys and 11 fields of three-phase alloys.

In 1982 Makmudov *et al.* [19] examined the quasibinary sections of the Mg-Al-Sr system by DTA, XRD, metallography and microhardness measurements. The examined sections are: γ-Sr_2Mg_{17}, β-Sr_2Mg_{17}, $SrMg_2$-$SrAl_4$, Sr_2Mg_{17}-$SrAl_4$, β-$SrAL_4$. All these sections are pseudobinary eutectic. The solubility limits at 300°C and 400°C were determined after annealing the alloys for 300 hours. These solubilities do not agree with the 400°C isothermal section given by Makhmudov *et al.* [1817] in 1981. No comment was made over the discrepancies. In 1982, Makhmudov *et al.* [20] used the simplex lattice design method to derive polynomial equations relating liquidus temperatures to alloy composition in the Sr-$SrMg_2$-$SrAl_4$ partial ternary system.

Prince *et al.* [15] developed a tentative liquidus surface by using the experimental results of Makhmudov *et al.* [17,18,19,20]. This diagram is shown in Figure 2-1. Al_4Sr and Mg_2Sr largely dominated the phase diagram. Figure 2-1 indicates that P_4 is a saddle

point on curve $U_2P_4U_4$ and the reaction at p_4 is more likely to be L+ $SrAl_4 \Leftrightarrow \tau$. However, Makhmudov *et al.* [20] reported the reaction at p_4 as $L+SrAl_4 \Leftrightarrow SrAl_2+\tau$, which shows a disagreement with the liquidus surface. The reaction at U_1 is given as $L+Al_4Sr \Leftrightarrow Al_2Sr+Al_7Sr_8$ by [19]. This is not possible since $Al_4Sr+Al_7Sr_8$ separated from U_1 to U_4 according to Figure 2-1. However, it is also not possible to reconcile the differences between two experimental works without conducting further experiments.

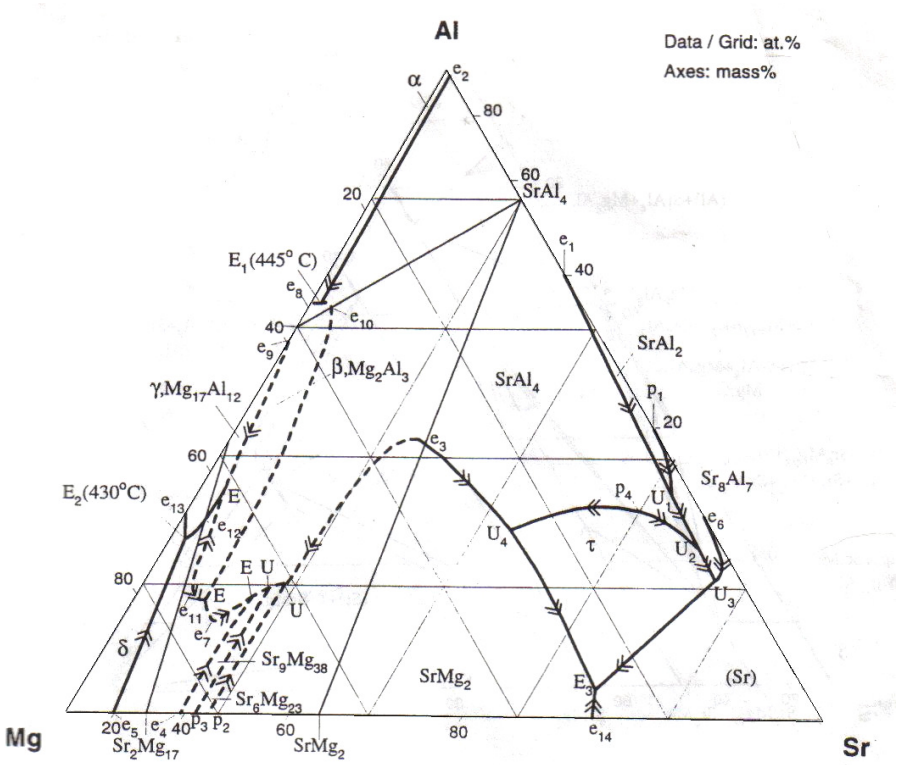

Figure 2-1: Tentative Liquidus Surface [15].

Baril *et al.* [21] reported XRD patterns and microstructures for five samples in the Mg-Al-Sr system. These samples are very close to Mg-rich corner and containing 93.85 to 95 wt.% Mg. The microstructure is characterized by the Al_4Sr-(Mg) lamellar phase that forms at the interdendritic/grain boundary region of the primary (Mg) matrix. Figure

2-2 shows the second phase compounds: A-type (divorced eutectic type) and B-type (non-lamellar type). These second phase compounds are located at the grain boundaries of (Mg) [2]. The second phase structure has been influenced by Sr content. The reduction in Sr content seems to increase the dissolved aluminum and thus increases the effect of solid solution strengthing mechanism. Lower Sr content Mg-Al-Sr alloy was recommended to be used for applications requiring moderate creep resistance such as oil pans and engine cradles. The improvement in ductility and tensile strength is associated with a reduction of the total second-phase volume fraction. The precipitation of low-melting phase (γ) is detrimental to creep resistance.

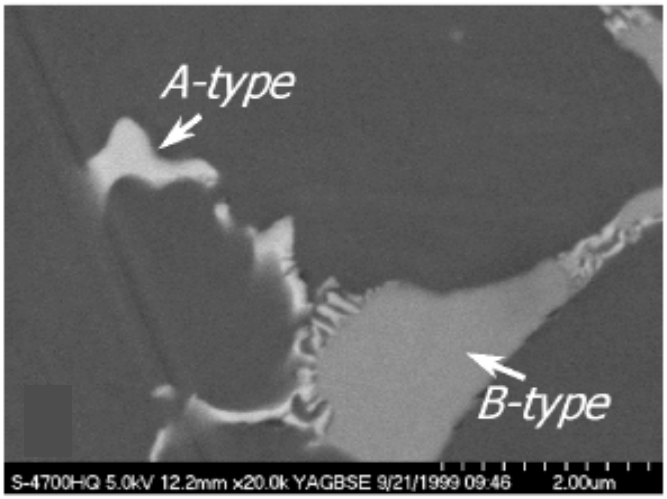

Figure 2-2: SEM micrograph.

The second-phase morphologies are lamellar, divorced eutectic and massive. Distinct peaks associated with this phase are observed in the XRD pattern of AJ52x alloy (Mg-5 wt.% Al-1.95 wt.% Sr). The phase was tentatively designated as $Al_3Mg_{13}Sr$. The stoichiometry is not yet clearly identified and the chemical composition is not compatible

with the ternary compound Al_6MgSr_{10} reported by Makhmudov *et al.* [18]. The presence of this phase in Mg-Al-Sr is detrimental to strength and ductility. Furthermore, the second-phase particle was observed to be relatively low indicating structural stability.

In 2004, Landriault Emmanuelle [22] characterized the Mg-Al-Sr-based alloys, developed by Noranda, and studied their behavior at elevated temperature. XRD measurement showed the presence of two phases in the Mg matrix. The first one was identified as Al_4Sr and the second phase could not be identified. XRD analysis showed no indication of any variation of lattice parameters with time for the Mg matrix and the Al_4Sr lamellae in the heat-treated specimens at 150°C. The duration of the treatment showed no significant influence on the proportions of the Al_4Sr and the matrix of the alloy. However, the proportion of the unknown phase diminished between 45 and 150 hours. After 150 hours of testing, no further variation in the proportion of the unknown phase was observed. In her work, microscopic observations combined with X-ray spectrometry and electron diffraction have revealed the presence of a lamellar constituent located at grain boundaries. X-ray spectrometry analysis, as for the Al_4Sr lamellae, revealed a depletion of the Sr content of the unknown phase as well as the enrichment in Mg. Furthermore, XRD analysis showed that the phase is undergoing a transformation after 4000 hours of creep testing at 150°C. Figure 2-3 shows the optical micrograph of the AJ52x sample in the as-cast condition and heat treated at 150°C for 500 hours and for 4000 hours. After the homogenization, the network becomes less complete.

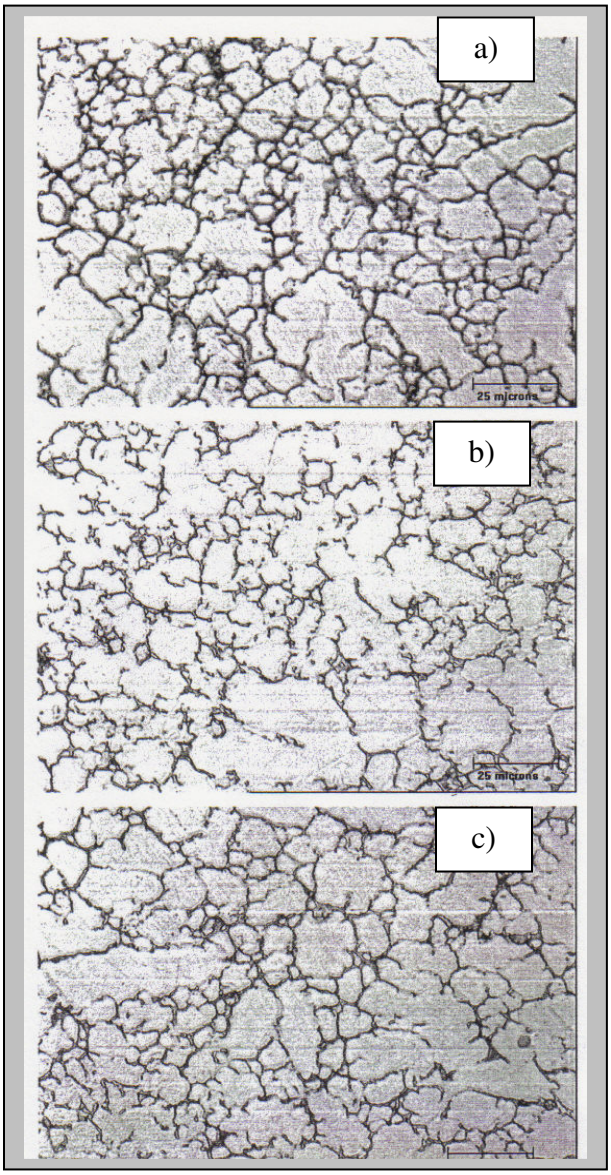

Figure 2-3: Optical micrograph of the AJ52x sample a) as-cast, b) heat treated at 150°C for 500 hours, c) heat treated at 150°C for 4000 hours [22].

2.1.2 Thermodynamic optimization and calculation

Chartrand and Pelton [23] critically reviewed and calculated the thermodynamic properties of the Mg-Al-Sr ternary and related binary sub-systems. The ternary diagram was calculated with first approximation without taking into account the formation of ternary solutions and compounds. No ternary terms were added to the thermodynamic model parameters of the liquid. This is due to the fact that there are uncertainties related to the existence, stability, homogeneity range and the melting and decomposition temperature of the ternary compounds. The thermodynamic properties of the ternary liquid were estimated from the optimized binary parameters using the modified quasi-chemical model for the ternary liquid phase. The projected liquidus of the calculated Mg-Al-Sr system in atomic percent is shown in Figure 2-4. Six ternary eutectic and four ternary peritectic invariants are observed on the calculated liquidus surface.

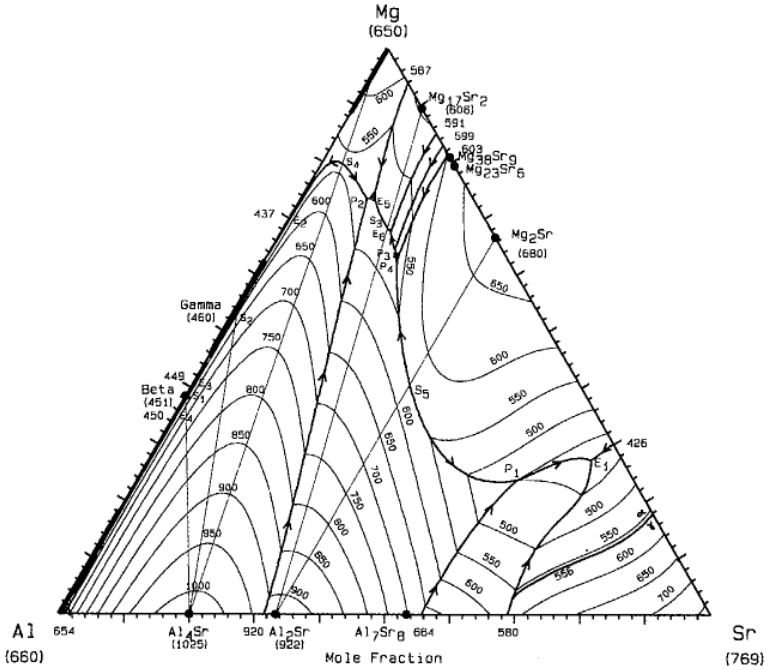

Figure 2-4: Mg-Al-Sr calculated phase diagram in atomic percent [23].

The calculated liquidus projection as shown in Figure 2-3 has thirteen primary crystallization fields: (Mg), (Al), α-(Sr), γ-(Sr), γ, β-Mg_2Al_3, Al_4Sr, Al_2Sr, Al_7Sr_8, $Mg_{17}Sr_2$, $Mg_{38}Sr_9$, $Mg_{23}Sr_6$ and Mg_2Sr. Liquidus surfaces of Al_4Sr, Al_2Sr and Mg_2Sr dominated the phase diagram.

In 2003, Koray *et al.* [24] calculated the liquidus projection of the ternary Mg-Al-Sr system (Figure 2-5). The ternary system was calculated without using any ternary phase or ternary interaction parameters. It is very similar to Chartrand and Pelton's [23] calculation except for the narrower phase field of Mg_2Sr.

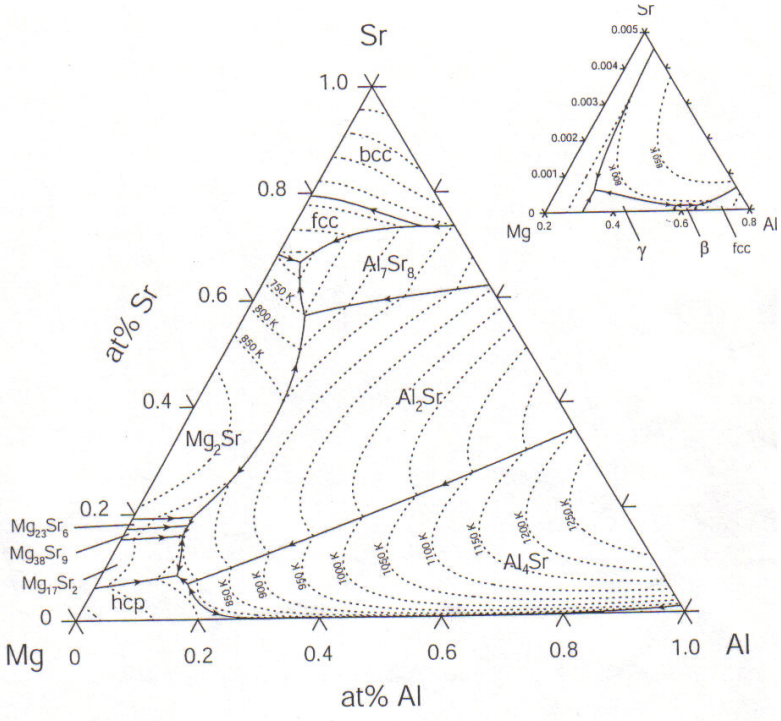

Figure 2-5: The calculated Mg-Al-Sr liquidus projection [24].

In Mg-Al-Sr ternary system, the binary sub-systems Mg-Al, Al-Sr and Mg-Sr contributed to the properties of the ternary system therefore they will be discussed in the following sections.

2.2 Mg-Al System

The Mg-Al system has been explored in several experimental studies due to its particular importance to the Al industry. A large amount of experimental information on the phase diagram (liquidus, solidus and solvus), the crystal structures of the phases and the thermodynamics have been reported. However, phase diagram compilations in the past showed numerous disagreements [23,25-27].

Murray [25] reviewed and optimized the Mg-Al phase diagram based on the work done prior to 1982**.** He indicated that R ($Al_{30}Mg_{23}$) phase, sometimes referred to as ε phase, has a composition of 42 at.% Mg. ζ ($Al_{49}Mg_{32}$) phase was considered in later optimization instead of R phase [26]. The existence of the ζ phase and the temperature range of the ε or R phase had been conflicting. Chartrand and Pelton [23] optimized the Mg-Al system and indicated some differences with other researchers. They did not include ζ phase in their optimization. Saunders [26] reported that the solubility limit for Mg in Al is lower than Murray's assessment while the solubility range of γ phase at low temperature was greater.

Ludecke *et al.* [27] reviewed the chronological development of the Mg-Al binary phase diagram from 1953 to 1982. There is a good agreement between different authors regarding the solid solubility of Mg and Al and liquidus, solidus and solvus lines. However, there are contradictory results, concerning the line compounds in the 40 to 55 at.% Mg concentration ranges.

Zho *et al.* [28] evaluated the Mg-Al binary system by thermodynamic calculation. The liquid, Al (fcc) and Mg (hcp) were described as disordered solution phases. Furthermore, the γ phase was treated as ordered solid solution phase. Goel *et al.* [29] experimentally determined the Mg-Al phase diagram using liquid diffusion couple technique. Their phase diagram shows good agreement with the diagram reported by Murray [25] except for the temperature range of the R phase. Moser *et al.* [30] determined thermodynamic data for liquid Mg-Al alloys using emf, vapor pressures and calorimetric techniques.

Su *et al.* [31] assumed a high-temperature phase, named λ, with a composition between 57 to 58 at.% Al. They reported that the rhombohedral ε phase was formed following a peritectoid reaction and not a peritectic reaction. Tomasz *et al.* [32] found ε phase to be stable at higher temperature than that was reported by Su *et al.* [31]. Liang *et al.* [33] identified some discrepancies between the experimental data in the composition range of the central part. These discrepancies can be summarized as: the existence of phase ζ, the temperature range of the phase designated ε and the occurrence of a possible γ′ phase of unknown structure within the γ region. However, they could not give any boundary between γ and γ′ and indicated that the λ phase is a corresponding modulation of the γ phase. They also reported that Donnadieu *et al.* used electron diffraction technique to show that there is no existence of hypothetical λ phase. Liang *et al.* [33] also suggested that ζ phase may be either the sequence of metastable quasiperiodic phase. In their recent investigations, Koray *et al.* [24,34] adopted the thermodynamic optimization by Liang *et al.* [33]. The invariant reactions matched very well with the finding's of

Chartrand and Pelton [23]. The calculated phase diagram of Mg-Al system, based on Koray's database is shown in Figure 2-6.

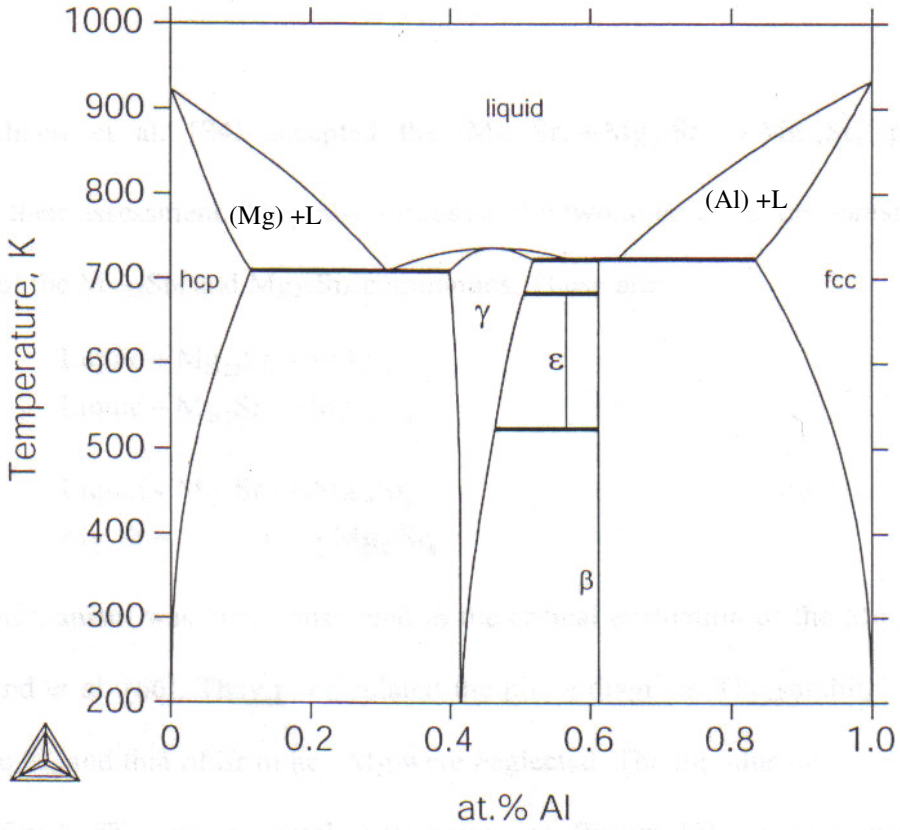

Figure 2-6: Calculated Mg-Al phase diagram [24].

2.3 Al-Sr System

The Al-Sr system is appealing because Sr is widely introduced into Al-Si casting alloys as a modifier [34]. The Al-Sr binary system has been explored in numerous experimental phase diagrams, thermodynamics and crystal structure investigations. It is a system with three compounds and two eutectic and two peritectic reactions.

A large amount of data for the Al-Sr binary system is documented by Alcock and Itkin [35]. It consists of the liquid L, fcc terminal solid solution, βSr, αSr. Chartrand and Pelton [23] reassessed this system by focusing on the experimental data from Closset *et al.* [36]. Their results are different from those of Alcock and Itkin [35], Bruylev *et al.* [37] and Vakhobov *et al.* [38] in Sr-rich region. Chartrand and Pelton reported γSr phase instead of βSr phase. In Sr-rich region, Alcock and Itkin [35] reported that Al_2Sr_3 and βSr formed a eutectic reaction at 81.75 at.% Sr at 590°C whereas this reaction was reported at 68 at.% Sr at 556°C by Chartrand and Pelton [23].

The recalculated phase diagram by Srikanth and Jacob [39] is in good agreement with Alcock and Itkin [35] up to 84 at.% Sr. There is a considerable discrepancy, however between the calculated and experimental liquidus near the Sr-rich end. The eutectic temperature is also higher than the previous findings. Wang *et al.* [40] reviewed and thermodynamically assessed the Al-Sr system. Their calculated phase diagram is similar to that of Alcock and Itkin [35]. Although large discrepancy exists in the Sr-rich region, the thermodynamic data agrees well with Chartrand and Pelton [23] in this region. The assessed and calculated liquidus lines provided by Alcock and Itkin [35], Chartrand and Pelton [23] and Srikanth and Jacob [39] are highly conflicting when the Sr concentrations are higher than ~33 at.%. In addition, the temperature for the eutectic reaction, $L \Leftrightarrow Al_7Sr_8$+Sr-bcc, has shown some discrepancy which was calculated as 830K by [36] and 853K by [23].

There are three intermetallic compounds in this binary system: Al_4Sr, Al_2Sr and AlSr as revealed by the crystallographic investigations. Among which Al_4Sr has

congruent melting point while the rest melt through a peritectic reaction. The primary Al_4Sr is dendritic in the samples prepared by electrolysis but stablike in the samples prepared by mixing method [41]. Several investigators specified Al_7Sr_8 or Al_2Sr_3 compound instead of AlSr. Both AlSr and Al_7Sr_8 are thermodynamically plausible and Closset *et al.* [36] reported that it is not possible to distinguish the two by diffraction analysis.

Zhang Jian [42] found that the model considering four compounds gives the best agreement with the measured results. He also reported that the results of Srikanth and Jacob [39] for ΔG° determination has the least agreement with his results. While there are several measurements of the enthalpies and activities of liquid Al–Sr alloys there are no experimental measurements of the enthalpies of formation of Al–Sr compounds till date.

Table 2-1: Comparison of the calculated enthalpies of formation of the intermetallic compounds

Compound	ΔH (KJ/mole)			
	Alcock and Itkin [35]	Srikanth and Jacob [39]	Chartrand and Pelton [23]	Wolverton *et al.* [43]
Al_4Sr	-25	-34.6	-31.2	-22.8
Al_2Sr	-45	-45.4	-28.4	-27.9
Al_7Sr_8	-65	-14.2	-19.3	-

Interestingly enough, despite the fact that these estimated thermodynamic properties of the solids are quite different from one another, in each case they all yield a good description of the observed Al–Sr phase diagram. This fact suggests that the

thermodynamic data are not uniquely determined by the phase diagram. Wolverton *et al.* [43] used first principal method to calculate the enthalpies of formation that are believed to be reliable. But they still suggest performing an experimental work to get the accurate data for the enthalpies of formation.

Chartrand and Pelton [23] and Closset *et al.* [36] reported a melting point of Al_4Sr around ~1025°C. Whereas recent studies using the new activity data and from the results of Wolverton *et al.* [43] showed that the melting point was found to be a little higher around 1040°C. Wang *et al.* [40] reported in their optimization that the compound Al_2Sr is formed via a peritectic reaction $L + Al_4Sr \Leftrightarrow Al_2Sr$. The previous calculations [23,36] cannot reflect this experimental feature. In 2003, Koray [24] calculated Al-Sr phase diagram using the database by Wang *et al.* [40].

In 2004, Liu *et al.* [44] reported a new compound Al_3Sr_8 that is isostructural with the recently discovered Al_3Ca_8 compound. This is predicted to lie above the ground state hull. Al_3Sr_8 was not observed experimentally in this system; however, it was observed that the liquidus around the Al_3Sr_8 composition is higher than the surrounding composition. Interestingly, near AlSr stoichiometry, Al_5Sr_4 structure (observed in Al-Ba) has been reported that breaks at the ground state hull. Other compounds near Al_2Sr stoichiometry such as $Al_{13}Sr_7$ and Al_9Sr_5 have been reported via local density approximation (LDA) and generalized gradient approximation (GGA).

Hitherto, Al-Sr phase diagram is not well established near the Sr-rich corner. There are also discrepancies among the findings in Al-rich region. So it needs additional

work to refine the thermodynamics and new experimental investigations are necessary to identify the potential existence of Al_3Sr_8 and Al_5Sr_4 compounds which will definitely alter the thermodynamic optimization of Mg-Al-Sr ternary diagram. The calculated phase diagrams by Liu *et al.* [44] and Koray [24] are shown in Figure 2-7.

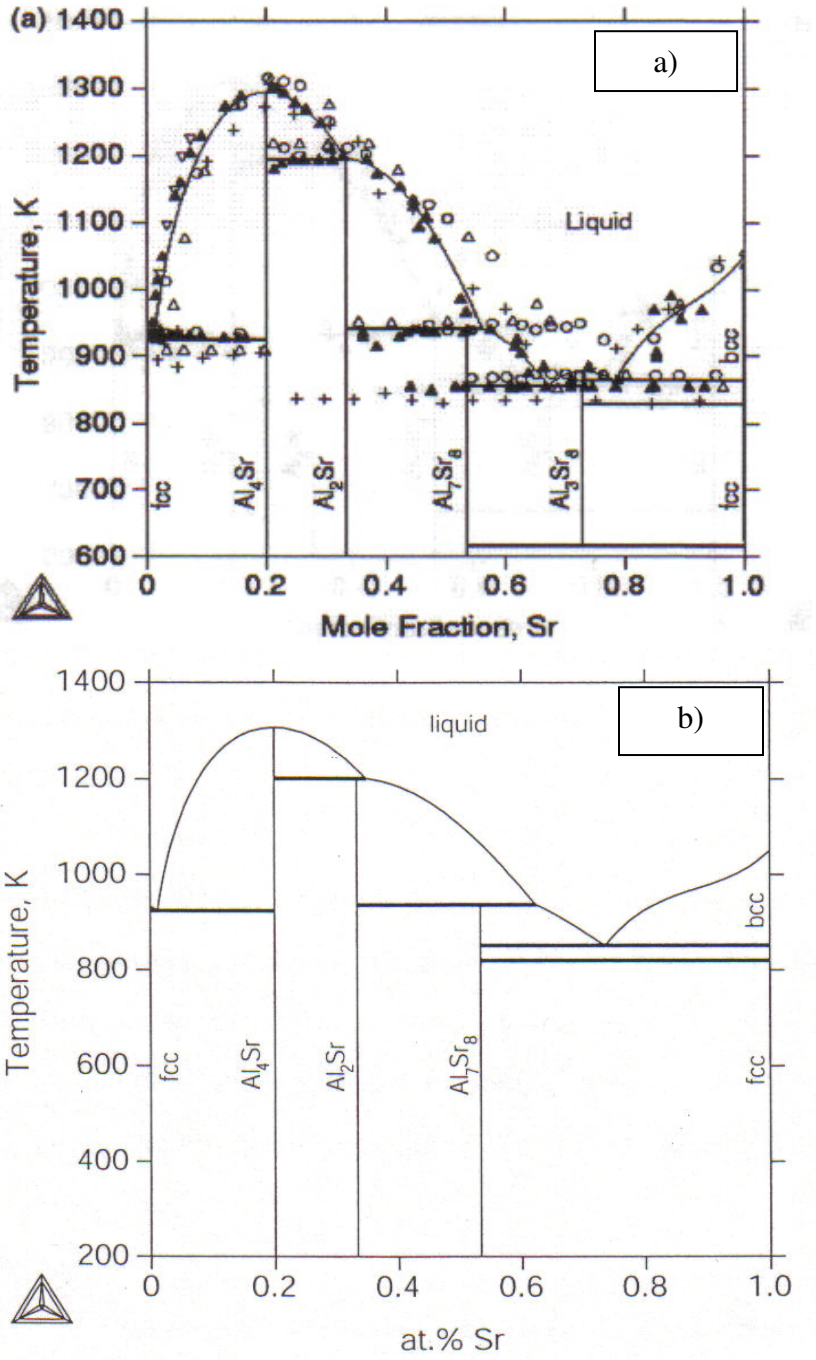

Figure 2-7: Calculated Al-Sr phase diagram a) Liu et al. [44] and b) Koray [24].

2.4 Mg-Sr System

Thermodynamic modelling and experimental measurements on Mg-Sr system are few. Nayeb-Hashemi *et al.* [45] collected the Mg-Sr binary system information in their review of this phase diagram. The first phase diagram for this system was reported by Vosskhuler [46] in 1939. He determined the liquidus temperatures of alloys containing 0 to 15.6 at.% Sr. Others determined the liquidus temperatures across the phase diagram [47,48]. There is good agreement among the results in the composition range 0 to 15 at.% Sr. However, Brown [47] reported that the liquidus temperatures lie at significantly higher temperature. This is because as Brown [47] pointed out the Sr-rich samples were contaminated with hydrogen and formed strontium hydride.

Ray according to Nayeb-Hashemi *et al.* [45] and Brown [47] determined the Sr solidus experimentally. The solidus temperature reported by Brown is significantly below that of Ray [45]. Whereas Nayeb-Hashemi [45] showed the Sr solidus by a dashed line due to the uncertainty in their calculated phase diagram.

Thermal analyses and metallographic examinations indicated a very small solid solubility of Sr in Mg. Brown [47] placed the maximum solid solubility of Mg in Sr near 6.3 at.% Mg and Ray placed it near 14.5 at. % Mg. However, a very small solubility of Mg in Sr is predicted by Chartrand and Pelton [23] by comparison with Mg solubility in similar systems e.g., Mg-Ca and Mg-Ba.

Vosskhuler [46] reported the existence of Mg_9Sr compound with congruent melting at 606°C. Klemm *et al.* [48] also reported a second intermetallic compound in the Mg-rich region without specifying the formula. Klemm *et al.* [48] and Ray according to Nayeb-Hashemi *et al.* [45] reported the existence of Mg_9Sr compound and its melting point as 603°C and 609°C, respectively. A possible existence of an Mg_3Sr compound was speculated but it was not shown on the phase diagram. A possible invariant arrest by a dashed line at 604°C in the composition range of ~20 to 30 at.% Sr was also indicated [45]. In contrast, Ray according to Nayeb-Hashemi *et al.* [45] observed thermal arrests at 608°C (~18-33 at.% Sr) and 599°C(~17 to 25 at.% Sr) and assigned these to the peritectic formation of Mg_3Sr and Mg_9Sr_2, respectively. He reported the existence of Mg_2Sr compound, which melt congruently at 680°C. The formula for the compound designated, as Mg_9Sr was later corrected to $Mg_{17}Sr_2$. Using XRD analysis, the compound designated Mg_4Sr by Klemm *et al.* [48] and Mg_9Sr_2 by Ray was found to have FCC structure and the formula was later changed to $Mg_{23}Sr_6$.

Brown [47] investigated the system by DTA using very slow heating and cooling rates. He observed only one thermal arrest and assigned it to the formation of $Mg_{23}Sr_6$. A second thermal arrest below the eutectic isotherm was also reported in the composition range 10.53 to 20.69 at.% Sr. This is assigned to the peritectoid formation of Mg_4Sr. He also reported the existence of Mg_2Sr compound, which melts congruently at 689°C [47]

In their review, Nayeb-Hashemi *et al.* [45] rejected the HCP structure of pure Sr. They concluded that the HCP form of Sr appeared to be a phase stabilized by hydrogen

contamination. They reported that there are four intermetallics in addition to the liquid, Mg-HCP, γSr-BCC and αSr-FCC phases.

Chartrand and Pelton [23] reviewed the contradictory information obtained previously and recalculated the phase diagram. The liquid was modeled by using the experimental values of enthalpy of mixing and activity of Mg in the liquid at 757°C, which were measured by Sommer [49]. Chartrand and Pelton [23] used the experimental results of Brown [47] whereas Ray's data were considered by Nayeb-Hashemi *et al.* [45]. Four intermetallic compounds were reported: $Mg_{17}Sr_2$, $Mg_{38}Sr_9$, $Mg_{23}Sr_6$ and Mg_2Sr. The calculated parameters for the solid intermetallic phases showed no decomposition at room temperature. The calculated phase diagram by Koray [24] based on the self-consistent thermodynamic database of Chartrand and Pelton [23] is shown in Figure 2-8.

Though few investigations have been conducted on Mg-Sr system, reasonable phase diagram has been obtained with some contradiction regarding the solubility of Mg in Sr. Research efforts can be made to find out the solubility of Mg in Sr as the attention on Mg-Al-Sr system has renewed the interest on Mg-Sr system.

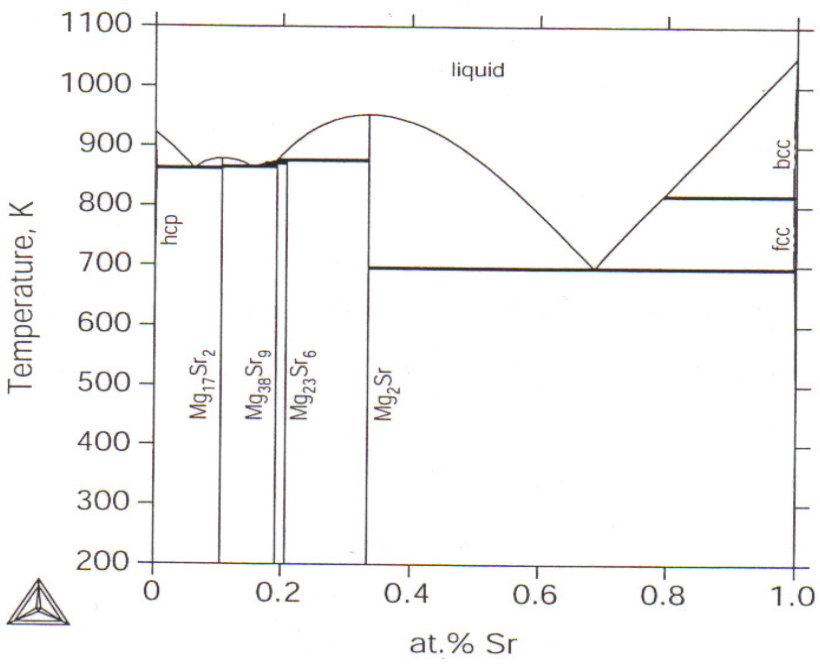

Figure 2-8: Calculated Mg-Sr phase diagram [24].

2.5 Discrepancies between experimental and thermodynamic calculation

A review of the literature concerning the phase equlibria in Mg-Al-Sr ternary system revealed a strong disagreement between the experimental data and thermodynamic calculation. The substantial discrepancies within the existing data and the paucity of the available data demand new experimental investigations.

The extended solubilities between solid phases reported by Makhmudov *et al.* [18,19] were not considered in the thermodynamics assessment of Chartrand and Pelton [23] because of the uncertainties related to them. Comparison between Figures 2-9 and 2-10 reveals that the critical points, such as eutectic, peritectic and saddle points, reported by Chartrand and Pelton [23] do not accord with the experimental results compiled by

Prince *et al.* [15]. Moreover, the phase equilibria and triangulation of the ternary system shown in Figure 2-10, strongly contradict those determined by Makhmudov *et al.* [18]. The 400°C isothermal section as shown in Figure 2-9 shows the triangulations involving Al_4Sr in equilibrium with $Mg_{17}Sr_2$, $Mg_{23}Sr_6$ and Mg_2Sr. However Chartrand and Pelton [23] showed that these compounds are calculated to be in triangulations with Al_2Sr. From these discrepancies, it is believed that this thermodynamic evaluation of the ternary system should be considered as tentative. Furthermore, in the experimental work of Makhmudov *et al.* [19], the binary compound $Mg_{38}Sr_9$ was not included in their Mg-Al-Sr phase diagram.

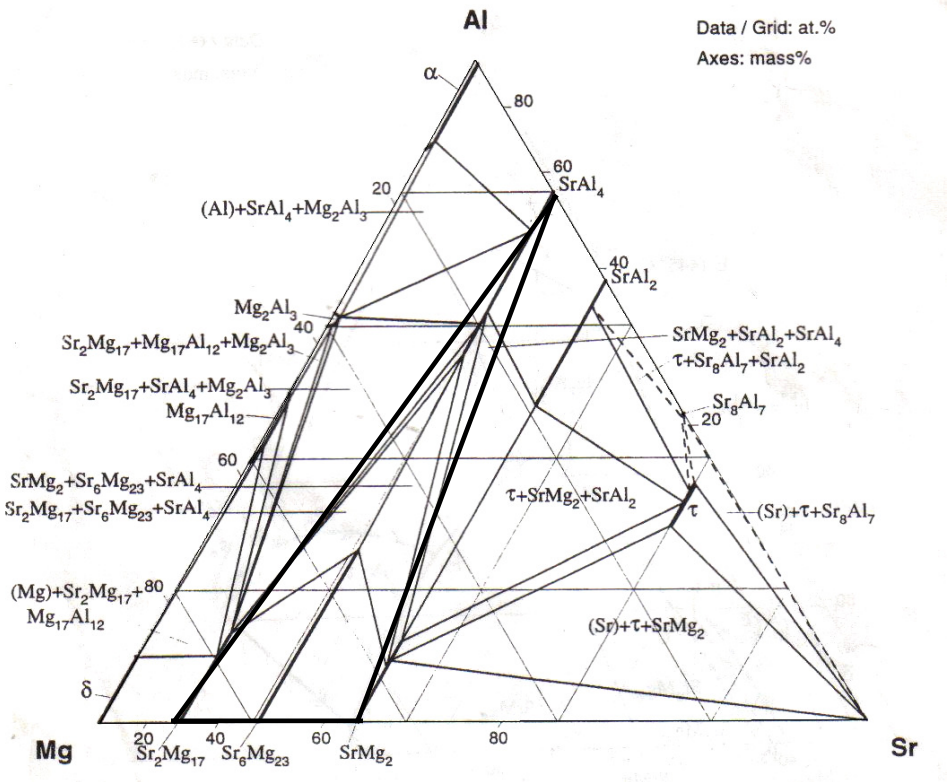

Figure 2-9: Experimental phase diagram (isothermal section at 400°C) in weight percent [18].

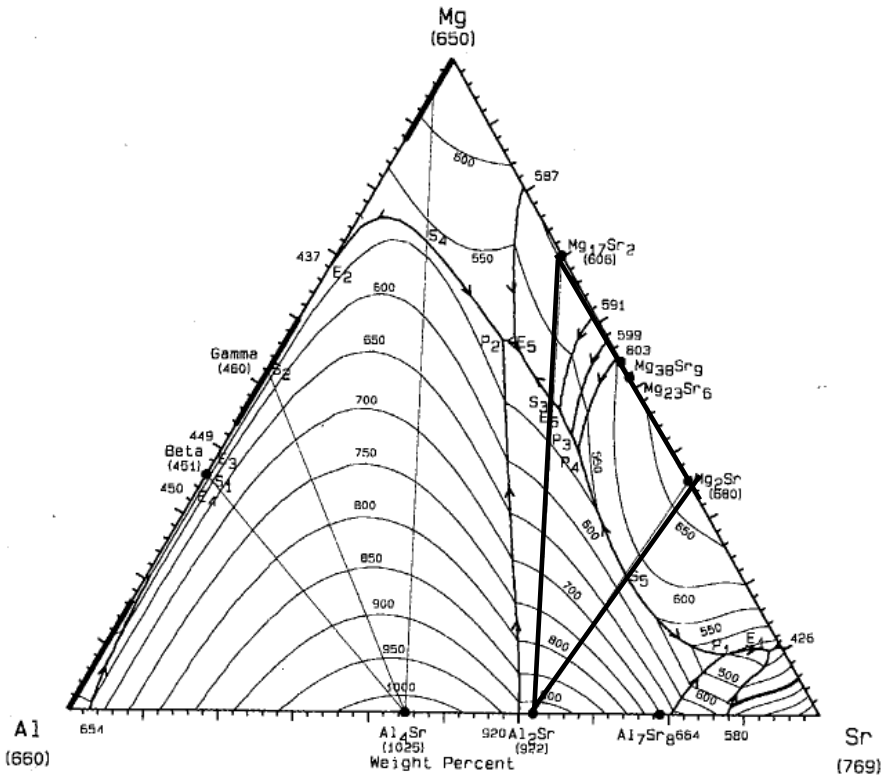

Figure 2-10: Calculated phase diagram in weight percent [23].

2.6 Thermal Analysis

Thermal analysis measures the change in physical properties of a substance as a function of temperature. Techniques include Differential Scanning Calorimetry (DSC), Diffrential Thermal Analysis (DTA), Thermogravimetry (TG), Thermomechanical Analysis (TMA). Phase equilibria of Mg-Al based system have been investigated by several techniques such as thermal analysis, X-ray diffraction, metallographic examinations, and electron microprobe [17,21,33,34].

Though most of the thermal analysis on metal systems were made using DTA, DSC will be used in this investigation in order to improve the accuracy of measurement. In DTA, difference in temperature is measured as a function of time or temperature whereas in DSC the variation of heat flow is measured. In recent times modified DTA can also work as DSC and named as heat-flow DSC. The thermal analysis of Mg alloys is difficult since they are highly reactive and evaporative especially in the liquid state. In addition, the highly reactive Mg-alloys oxidize easily in solid state. So the selection of crucibles, the dimensions of the samples as well as heating and cooling rates are important [50,51]. Besides, a high purity inert gas atmosphere is necessary to prevent oxidation. The information of using DSC/DTA to study Mg alloys is very scarce.

Lindemann *et al.* [52] determined different thermophysical properties of Mg alloys: density, specific heat capacity, melting ranges and enthalpy of melting using DSC. They used TG/DTA equipment and found a good consistency of the onset temperature determined by two different devices. They used platinum, alumina and graphite crucibles. They found Mg samples are highly reactive with platinum crucibles and also affected the internal alumina crucibles. Graphite crucibles showed better results in preventing the chemical reactions with Mg vapors, hence they are used in the current research.

Gröbner *et al.* [10] used DTA to investigate the Mg-Al-Ca system. The pre-molten sample was sealed under argon by welding in tantalum crucible to avoid oxidation and evaporation. The DTA measurement was carried out under vaccum with heating/cooling rates of 5 and 1 K/min. Some thermal effects showed large undercooling. DTA provided transformation temperatures that were later compared with the

thermodynamic calculations. Gröbner *et al.* [53] also used DTA to study the Al-Li-Si system and provided extremely important information for the analysis of the DSC results. In this analysis, they considered the onset signals during cooling and onset and peak temperature during heating for different transformations. This is followed in the current study.

Tkachenko *et al.* [54] used DTA to construct the isotherms on the projection of the liquidus surface in the Mg-Al-Ca system. They also determined the position and temperature of invariant points in the investigated composition.

Graham *et al.* [55] investigated the extruded Al-Si-Mg alloys with different heat treatment conditions by DSC. The thermograms generated from DSC showed the precipitation events clearly. DSC was also used to heat the sample to selected temperature to allow precipitates to develop to various stages for investigation by TEM. Whereas, Ogawa *et al.* [56] used DTA for the Mg-Zn-Sn system to determine the liquidus and eutectic temperatures.

In 1940, Brown [47] investigated the Mg-Sr system using DTA. He used iron crucible for this system and argon atmosphere. Ray according to Nayeb-Hashemi *et al.* [45] also used DTA to determine the Sr solidus. Tomassz *et al.* [32] investigated the Mg-Al system using DSC. But they did not provide any information regarding crucible selection and possible reaction with Mg vapors. Makhmudov *et al.* [17] used DTA in their investigation of the phase equilibria of Mg-Al-Sr system.

The interpretation of a DSC measurement requires a considerable amount of experience in thermal analysis especially for the ternary metal system. Information reported for different systems [57-71] such as polymer and ceramic along with other metal alloy systems have been used to understand the interpretation of the DSC curves. This information includes the determination of: knowledge of onset temperature, melting temperature, liquidus temperature, enthalpy of melting and invariant and univariant reactions.

2.6.1 Principle of DSC

DSC is a technique, which determines the variation in the heat flow given out or taken in by a sample when it undergoes temperature scanning in a controlled atmosphere. DSC monitors heat effects associated with phase transitions and chemical reactions as a function of temperature. Two types of DSC exist: heat flux and power compensation. In power compensated DSC, the sample and the reference are heated separately by individual heaters. In general, power compensated DSC yield the most precise and accurate heat capacity. However, heat flux DSC is simple, inexpensive and widely used. In this investigation a heat flux DSC has been used.

2.6.1.1 Theory of Heat Flux DSC

Temperature is measured in thin plates in contact with the reference and sample, thereby measuring the difference in heat flow from crucibles. The differential temperature between the sample and reference is converted to differential heat flow in a

way that is analogous to current flow in Ohms law. This gives a signal proportional to the difference in heat capacities between the sample and the reference. This heat flow difference is quantitative and output as a y-axis signal for the DSC scan. Both sample and reference pans are heated in a common block in the heat flux DSC as shown in Figure 2-11.

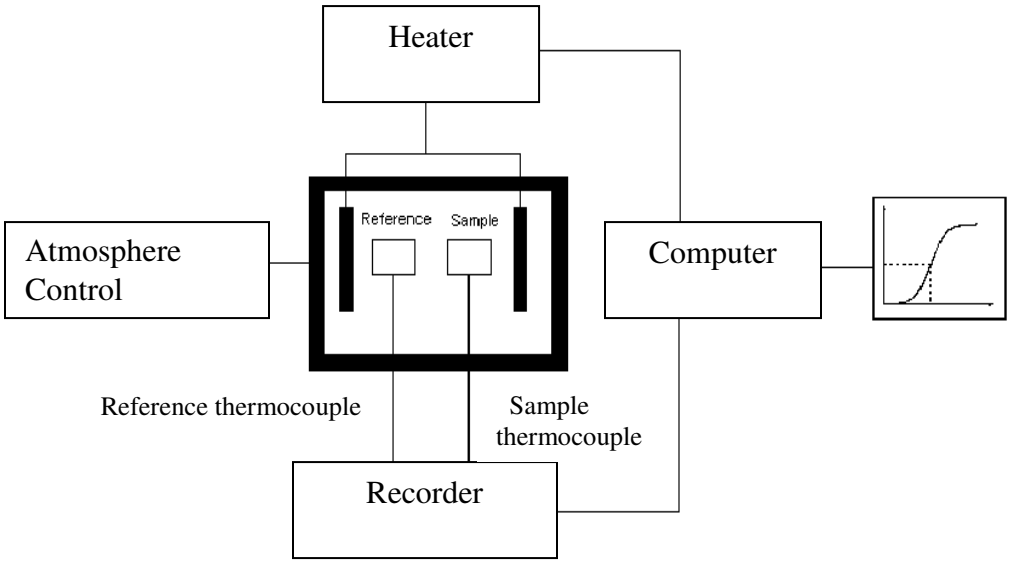

Figure 2-11: Heat Flux DSC.

2.7 X-ray Diffraction Technique

X-ray diffractometry is used to determine the phase content in many minerals and materials. A schematic diagram of an X-ray diffractometer is shown in Figure 2-12. The instrument consists of three basic parts: a source of X-ray radiation, specimen and the detector. The machine used filtered CuKα radiation. Each component wavelength of a polychromatic beam of radiation falling onto a single crystal will be diffracted at a discrete angle, in accordance with Bragg's law. Diffraction can occur whenever Bragg's

law, equation 2-1, is satisfied. For powder diffractometry monochromatic X-rays are needed.

$$\sin 2\theta = \frac{\lambda}{2d} \qquad \text{..... 2-1}$$

Where, θ is the peak position, λ is the wavelength and *d* is lattice spacing.

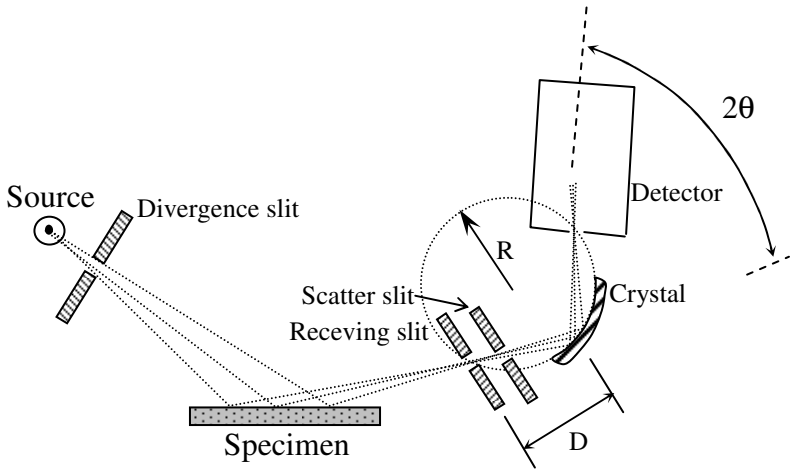

Figure 2-12: X-ray Diffractometer configuration.

XRD was used in several investigations of the phase equilibria. For instance, Gröbner *et al.* [10] studied Mg-Al-Ca system by XRD, and used all the samples in powdered form. They also reported that the ternary solid solubilities do not vary substantially with temperature. This is confirmed not only by the comparison of the as-cast versus heat treated samples but also XRD analysis of lattice parameter variation in the as-cast versus post-DTA samples. The identification of the binary phases by XRD is complicated by their large solubilities and the resulting large variations of their lattice parameters. Koray [24] used XRD to identify the phases as well as their crystal structure in the Mg-Al-Ca system. Measurements performed using XRD by Landriault Emmanuelle [22] showed the presence of two phases in Mg-matrix of the Mg-Al-Sr

system. She did not indicate any variation of the lattice parameters with time. Baril *et al.* [21] used XRD and electron diffraction to confirm the phase identification in Mg-Al-Sr system. They used the samples in the as-cast condition. Additional distinct peaks associated with Al_4Sr phase were observed in the XRD pattern of one of the five magnesium alloys and the phase was tentatively named as $Al_3Mg_{13}Sr$. They also used the XRD analysis to measure the lattice parameters of (Mg). Makhmudov *et al.* [16,17] identified a ternary compound $Mg_6Al_{34}Sr_{60}$ by using X-ray phase analysis of Mg-Al-Sr system.

2.8 Microstructural Characterization

Microscopic examination of a properly prepared specimen will clearly reveal the structural characteristics such as grain size, the shape, size and distribution of the phases and inclusions that are present. Microstructural observations were made in different Mg-based system using optical and scanning microscopes by several investigators [10,16,21-24]. Preparation of magnesium and its alloys is rather difficult due to the low matrix hardness and the higher hardness of precipitate phases that lead to relief problems, and from the reactivity of the metal. Pure magnesium is attacked slowly by water while Mg alloys may exhibit much higher attack rates.

Etchants are very important to reveal grain boundaries and grain size. And in Mg alloy it is very important as Mg grains dissolve very quickly on contact with the etchant comparing with the second phase. Koray *et al*. [24,72] used 4 vol% Nital solution (HNO_3 in ethanol) as etchant and applied it on the surface for a short period of time (~10 s). The prolonged etching (~20 S) was performed by dipping the samples in the etchant to

increase the surface area of the intermetallic precipitates on X-ray spectrum. The samples were cut from the as-cast by lab scale diamond saw. A comparison was made with the micrographs in the as-cast and heat treated condition. The quantitative chemical analysis of the individual phases was observed using X-ray spectroscopy-EDS technique.

Gröbner *et al.* [10] examined different Mg-Al-Ca alloys by optical and scanning electron microscopes. The samples were ground and polished under alcohol to avoid reaction with water. Etching was not necessary as alcohol already etched the surface of the polished samples. Ca-rich alloy immediately corroded after reacted fast with oxygen and the corrosion intensified the contrast in the microstructure.

Baril *et al.* [21] examined Mg-Al-Sr-based alloys via optical and field emission gun-scanning electron microscopes (FEG-SEM) coupled with an x-ray energy dispersive spectrometer (EDX). The second phase particle was not observed using SEM-EDX as it remained in very small amount in the die-cast.

2.9 Calculation of Phase Diagram

Computational thermodynamics often referred to as Calculation of Phase Diagram (CALPHAD) is one of the essential components to understand the existing alloys and to develop new ones. It relies on the Gibbs energies of the individual phases stored in the databases. Once the databases are completed, a computer program can be used to minimize the Gibbs energy. Computational thermodynamics is not able to predict the existence of new phases, however, the First-Principles calculations can provide necessary information of such phases. Chartrand and Pelton [23] and Koray [24] carried out the

thermodynamic calculation of the ternary Mg-Al-Sr phase equilibria. As indicated earlier, both works reported similar phase diagrams, and since the database of Chartrand and Pelton [23] is available, it will be used to calculate the relevant diagrams and for the comparison with the current results.

CHAPTER 3

Methodology

3.1 Experimental Approaches

As the main focus of this research is to investigate Mg-Al-Sr system, experimentally DSC, XRD and optical microscopy were used. This section explains in details the alloy preparation, thermal analysis by DSC, phase identification using XRD and metallography.

3.1.1 Alloy Preparation

Twenty-two samples were chosen by critical assessment of the experimental and thermodynamic datasets that are available in the literature. Table 3-1 shows the group with number of samples and their predicted phase fields by thermodynamics. Special attention was focused on the Mg-rich corner because of the interest in the Mg alloys. Since Al_4Sr gives the thermodynamic stability to Mg-Al-Sr-based alloys, samples containing this phase were also chosen. This will help in determining the extent of the Al_4Sr phase field. In addition, two samples at the eutectic points reported by Makhmudov *et al.* [17] were prepared.

Table 3-1: Samples in different phase fields

Group	Sample Nos.	Predicted phases
#1	1, 2,3,4,5,6,7,8,9	(Mg)+Al_4Sr+γ
#2	10,11,12,13,14	(Mg)+Al_2Sr+Al_4Sr
#3	15,16,17	Al_4Sr+γ+β
#4	18,19,20	(Al)+Al_4Sr+β
#5	21,22	(Mg)+Al_2Sr+$Mg_{17}Sr_2$

Mg-Al-Sr ternary diagram with the investigated compositions in weight and atomic percentage are given in Figures 3-1 and 3-2 respectively. The actual composition was determined by chemical analysis for twelve samples at CANMET-MTL. The nominal sample compositions remained in very close proximity with the actual composition. Moreover, the thermodynamic prediction of the liquidus temperature for the nominal and actual compositions was almost the same for most of the samples.

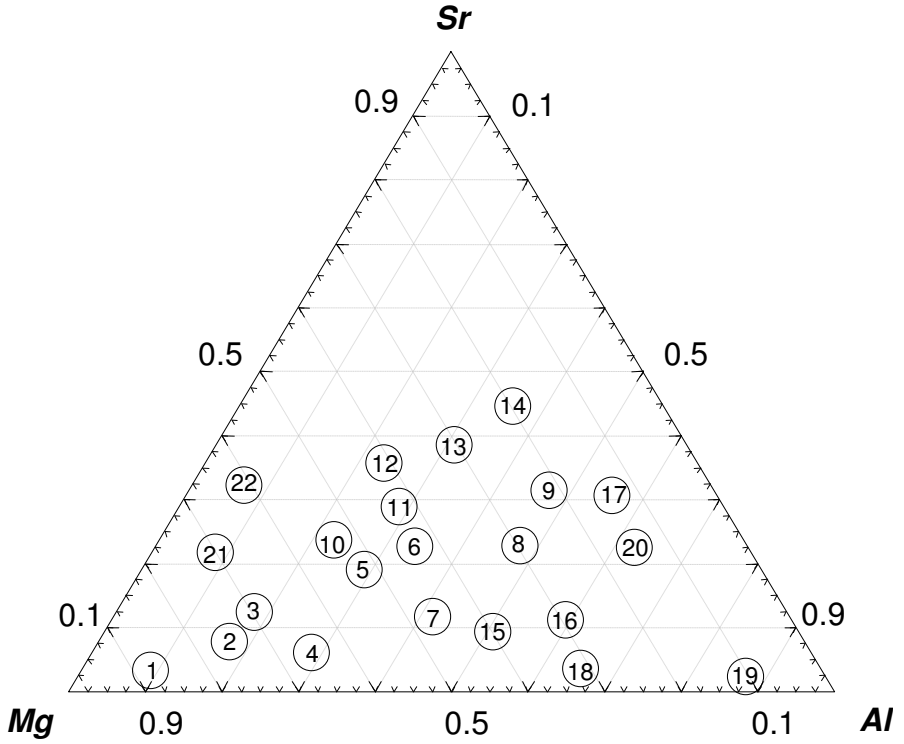

Figure 3-1: Ternary diagram showing investigated compositions in wt.%.

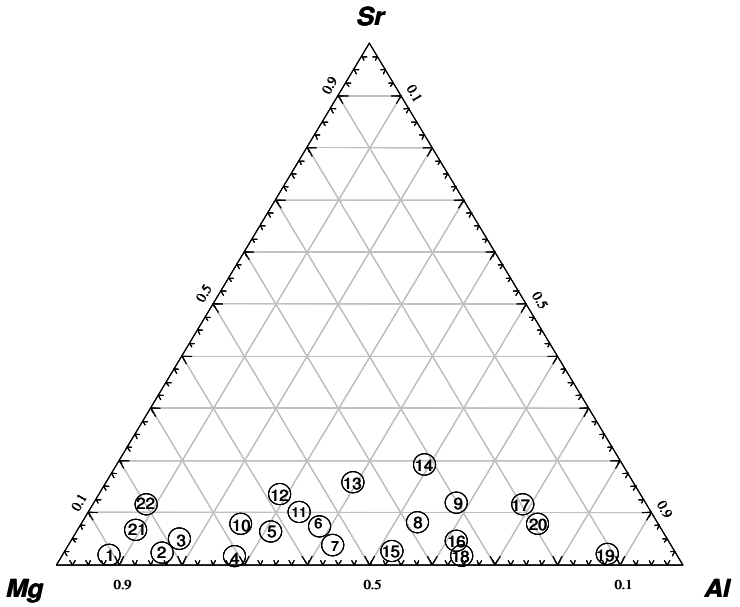

Figure 3-2: Ternary diagram showing investigated compositions in at.%.

The alloys were of high purity with the nominal compositions of the studied alloys and the actual compositions of the 12 alloys are given in Table 3-2. In preparing the Mg-Al-Sr-based alloys, magnesium of 99.8 wt.%, aluminum of 99.9 wt.% and strontium of 99 wt.% were used. The alloys were prepared at CANMET-MTL, Ottawa. The charge was melted in a graphite crucible in an induction-melting furnace under argon with 1%SF6 to protect the melt from oxidation. The actual chemical composition was measured quantitatively by atomic absorption spectroscopy. The loss in total mass was below 2% for most of the samples.

*Table 3-2: Sample composition in wt.% percent (**N**: Nominal and **A**: Actual)*

Sample No.		Sr	Mg	Al
1	N	3.5	88.5	8
	A	**3.32**	**87.29**	**9.39**
2	N	9	75.5	15.5
	A	**8.65**	**76.15**	**15.20**
3	N	13	70	17
	A	**7.09**	**74.82**	**18.09**
4	N	6.66	65.64	27.7
	A	**6.88**	**65.45**	**27.67**
5	N	20	52	28
	A	**22.48**	**48.57**	**28.95**
6	N	22.59	43.79	33.62
	A	**22.53**	**43.75**	**9.39**
7	N	13.02	46.92	40.06
8	N	24	30	46
9	N	32	22	46
10	N	23.75	53.75	22.5
	A	**22.78**	**54.39**	**22.83**
11	N	29	43	28
	A	**27.83**	**42.89**	**29.28**
12	N	36.16	41.41	22.43
	A	**34.83**	**39.59**	**25.58**
13	N	39.87	30.73	29.4
14	N	45.19	20.19	34.62
	A	**48.30**	**19.26**	**32.44**
15	N	9.5	40	50.5
16	N	11	30	59
17	N	31.18	14.42	54.4
18	N	4.56	31.63	63.81
19	N	2.58	10.74	86.68
	A	**2.04**	**10.80**	**87.16**
20	N	23	15	62
21	N	21.5	70.5	8
	A	19.90	72	8.1
22	N	32.74	60.55	6.71

3.1.2 Thermal Analysis using DSC

Thermal investigation of the systems was performed using a Setaram Setsys DSC-1200 instrument (Figure 3-3). Temperature calibration of the DSC equipment was done using pure Mg and Al. The samples were cut and mechanically polished to remove any possible contaminated surface layers. Afterwards, they were cleaned with acetone and placed in a graphite crucible with a lid cover to contain Mg vapors and protect the apparatus. To avoid oxidation, multiple evacuations followed by rinses with argon were done. The DSC measurements were carried out under flowing argon atmosphere with heating and cooling rates of 5°C/min. Slower heating rates were tried and were not found to reveal any other thermal arrests. The weight of the sample was 40~50 mg. Table 3-3 and Figure 3-4 show the experimental conditions for the determination of the thermophysical properties and the thermograms for each sample respectively. The reproducibility of every measurement was confirmed by collecting the data during three heating and cooling cycles. The estimated error between the repetitive heating and cooling is ±1°C or less. Furthermore, difference between heating and cooling peaks was in most cases lower than 15°C. Temperatures along with enthalpies corresponding to various thermal events were obtained from the analysis of the DSC curves during heating and cooling runs. However, the solidification behavior can be revealed much better with the cooling scans.

Figure 3-3: Setaram DSC.

Table 3-3: Experimental conditions for the determination of thermophysical properties.

Item	Conditions
Heating rate	5°C/min
Cooling rate	5°C/min
Temperature range	25~800
Atmosphere	Flowing argon, 1 atm.
Weight of sample	40~50 (mg)

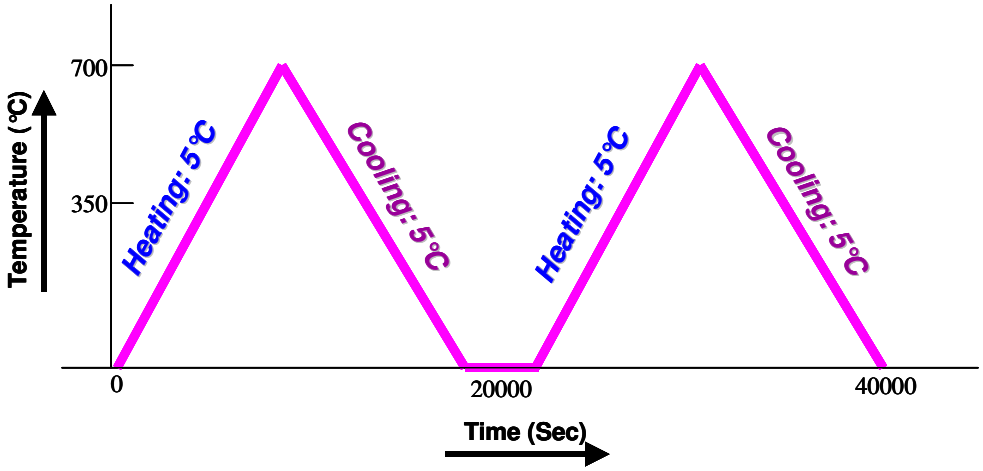

Figure 3-4: Thermogram showing experimental procedure.

Figure 3-5 shows a typical DSC curve for pure Mg. It shows a sharp melting at 656°C, which is close to the melting point of pure Mg at 650°C. In the samples that show melting range, onset temperature for the melting was obtained from the points of intersection of the extrapolated baseline and the line of maximum slope. The highest temperature at which the DSC signal returned to the baseline corresponds to the liquidus temperature. The sharp and narrow peak represents an isothermal transition where the heat capacity is close to infinity. Lower and broader peak indicates univariant transition. A single endothermic peak without any tail indicates the characteristics of a congruently melting phase. To facilitate, the calculation of the peaks that overlap, by horizontal plot, baseline was subtracted. The onset temperature was calculated either before or after the subtraction of the baseline. The total values of enthalpy before and after the subtraction were similar. The baseline was obtained using the empty crucibles in sample and reference pan. On heating, onset temperature was used for invariant reactions while peak maximum was used for phase field boundaries. On cooling, onset temperature was used for both the invariant reactions and the phase field boundaries.

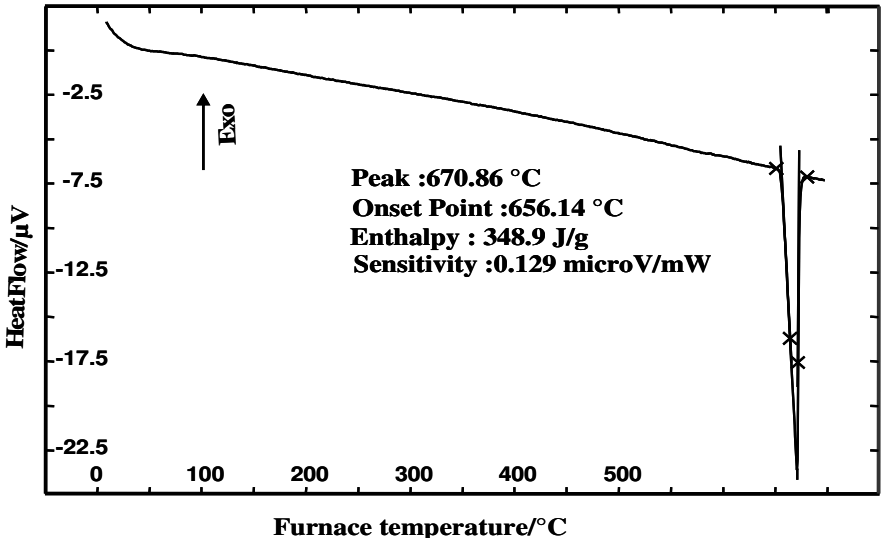

Figure 3-5: Typical DSC curve for pure Mg.

3.1.3 Phase Identification using XRD

Phase identification was carried out by X-ray diffraction (XRD). All the twenty-two samples were investigated in the powder form in the as-cast condition. The measurement was performed with a Philips diffractometer (Cu*K*α radiation) equipped with a PW 1050/25 focusing gonimometer with steps 0.02° of 2θ diffraction angle and 1s exposure time. The diffraction patterns were obtained at room temperature. For the calibration of the X-ray diffractometer, powder was made from pure Mg supplied by Noranda and diffraction patterns were obtained and compared with the literature. The relative peak intensity and the position matched completely. PowderCell 2.3 [73] was used to calculate the diffraction patterns for different phases and to identify their peaks [74,75]. The patterns were checked for known oxide phases such as MgO, Al_2O_3 and $MgAl_2O_4$ for any possible oxide formation.

3.1.3.1 Calculation of X-ray Diffraction Pattern

The crystal structure and the atoms positions in the unit cell must be known in order to calculate a diffraction pattern. The intensity of a diffracted beam depends on the structure factor, which is determined by the arrangement of atoms within a unit cell (Wyckoff position). Calculation of the XRD pattern of Al_4Sr is presented in this section as an example. Crystal structure and lattice parameters of Al_4Sr are listed in Table 3-4. The positions of the atoms in the unit cell of Al_4Sr are listed in Table 3-5.

Table 3-4: Crystal Structure data of Al_4Sr [76].

Structure	Tetragonal		
Spacegroup	*I4/mmm*		
Spacegroup number	139		
Lattice parameter (Å)	a	b	c
	4.4590		11.0700
Angles	α	β	γ
	90.00	90.00	120.00
Atoms in unit cell	6		

Table 3-6: Atoms positions in the unit cell of Al_4Sr [76].

Atom	Wyckoff position	x	y	z
Al	4e	0	0	0.3800
Sr	2a	0	0	0

After gathering the required information from the literature [76], the diffraction patterns were calculated using the "PowderCell 2.3" program. The unit cell and XRD pattern of Al_4Sr is shown in Figure 3-6 and Figure 3-7 respectively. The crystal structure, the atoms positions and the corresponding XRD patterns for the known phases in Mg-Al-Sr system are provided in Appendix A.

Error!

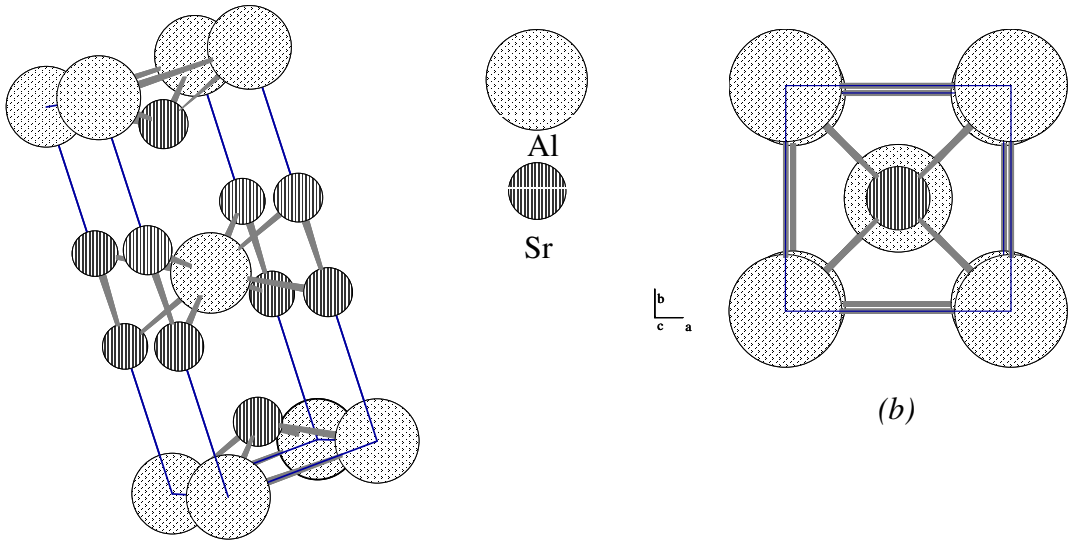

Figure 3-6: (a) Al_4Sr unit cell, (b) (001) projection.

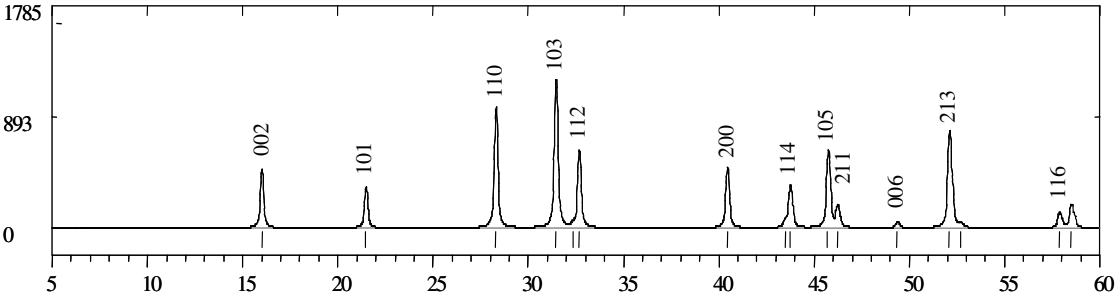

Figure 3-7: Calculated XRD diffraction pattern for Al_4Sr.

3.1.4 Metallography

Microstructural observations were made using optical microscope (Olympus BX60M). The samples were polished with 1 μm α-Al_2O_3 suspension. The samples were etched using 1vol% nital solution (HNO_3 in ethanol). Etching was performed only by applying the etchant on the surface for a short period of time (~ 5s) to prevent dissolving of the Mg grains. The change in the morphology of the samples after the DSC experiment was observed for two samples and compared with the as-cast condition.

3.2 Thermodynamic Calculation

Phase assemblage diagrams and vertical sections have been drawn from the database provided by Chartrand and Pelton [23]. Phase assemblage diagram that shows the relative amount of each phase and formation and decomposition temperature can be drawn from this thermodynamic database. The proportion of different phases at any temperature of interest can be read from this diagram. Vertical sections are calculated and will be used to obtain the phase boundaries and the associated temperatures, which can be compared with the DSC signals. These diagrams are two-dimensional representations of the crystallization paths for a series of points that lie along a chosen line on a ternary phase diagram.

CHAPTER 4

Result and Discussions

4.1 Samples in (Mg)+Al_4Sr+γ phase field

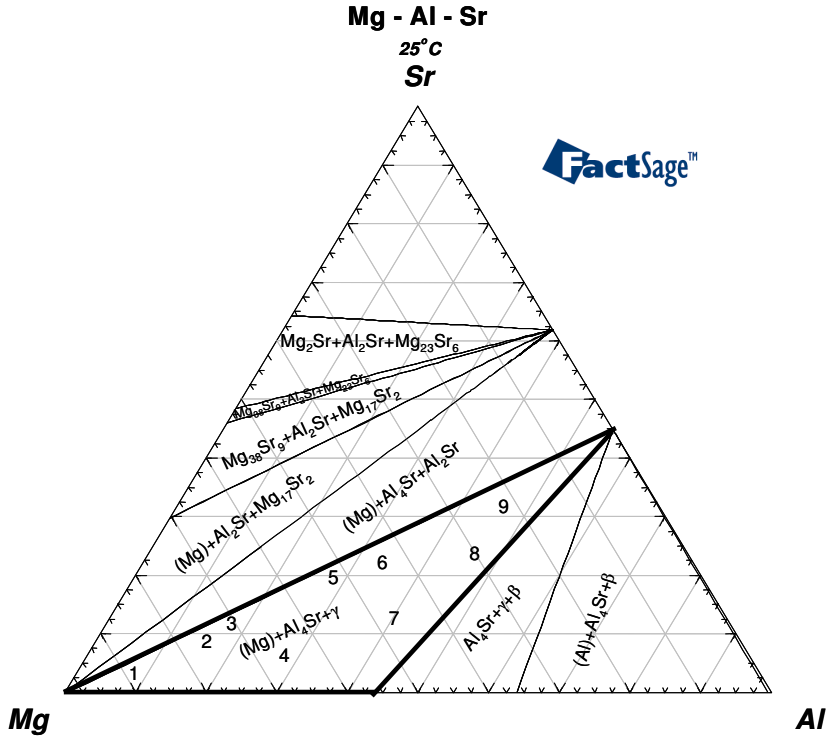

Figure 4-1: Isothermal section at 25°C showing samples in (Mg)+Al_4Sr+γ phase field.

There are nine samples in the (Mg)+Al_4Sr+γ phase field that have been studied using DSC, XRD and metallography. DSC spectra of sample 1 with heating and cooling runs are shown in Figure 4-2. The onset temperature, peak temperature, melting temperature and the melting enthalpy were registered. There are two peaks during heating that reoccurred during cooling. Similar results were observed in all three heating and cooling cycles. It can be seen from this figure that there is a temperature difference

between the heating and cooling patterns, however the maximum temperature difference of the observed signals between two repetitive heating or cooling runs were below 3°C. On heating, onset temperature was used for invariant reactions while peak maximum temperature was used for phase field boundaries. On cooling, onset temperature was used for both the invariant reactions and the phase field boundaries. The enthalpy and onset temperatures were determined after the subtraction of the baseline.

During heating of this sample, two thermal arrests, corresponding to the invariant reaction at 527°C and the univariant reaction at 605°C are observed. The 1st peak is high and sharp and resembles a δ function. So it denotes the peak of eutectic melting. The second peak is a non-isothermal transition (univariant) because it exhibits a lower and broader peak. For this sample, the liquidus temperature is observed during cooling which is 609°C.

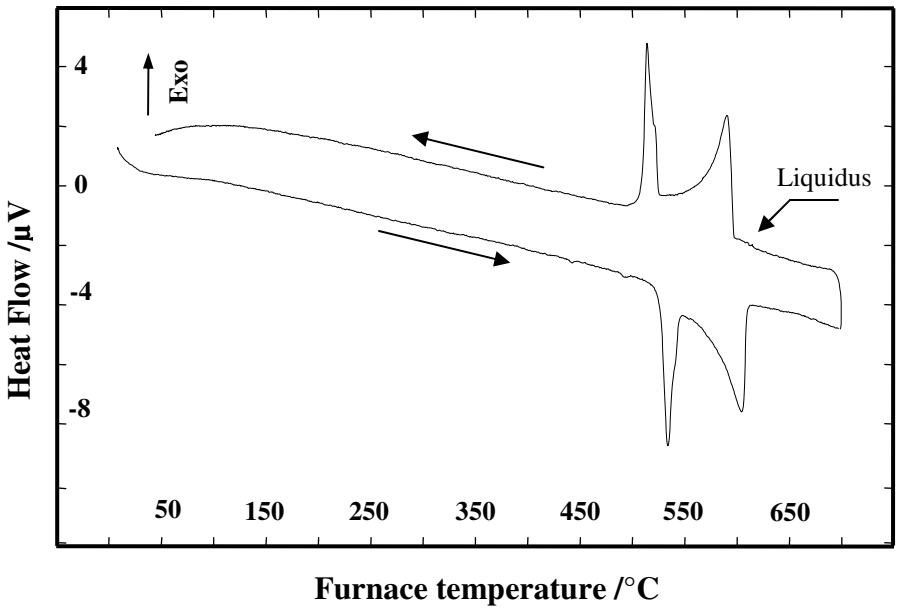

Figure 4-2: DSC spectra of sample 1 (3.32/87.29/9.39 Sr/Mg/Al wt.%) during heating and cooling.

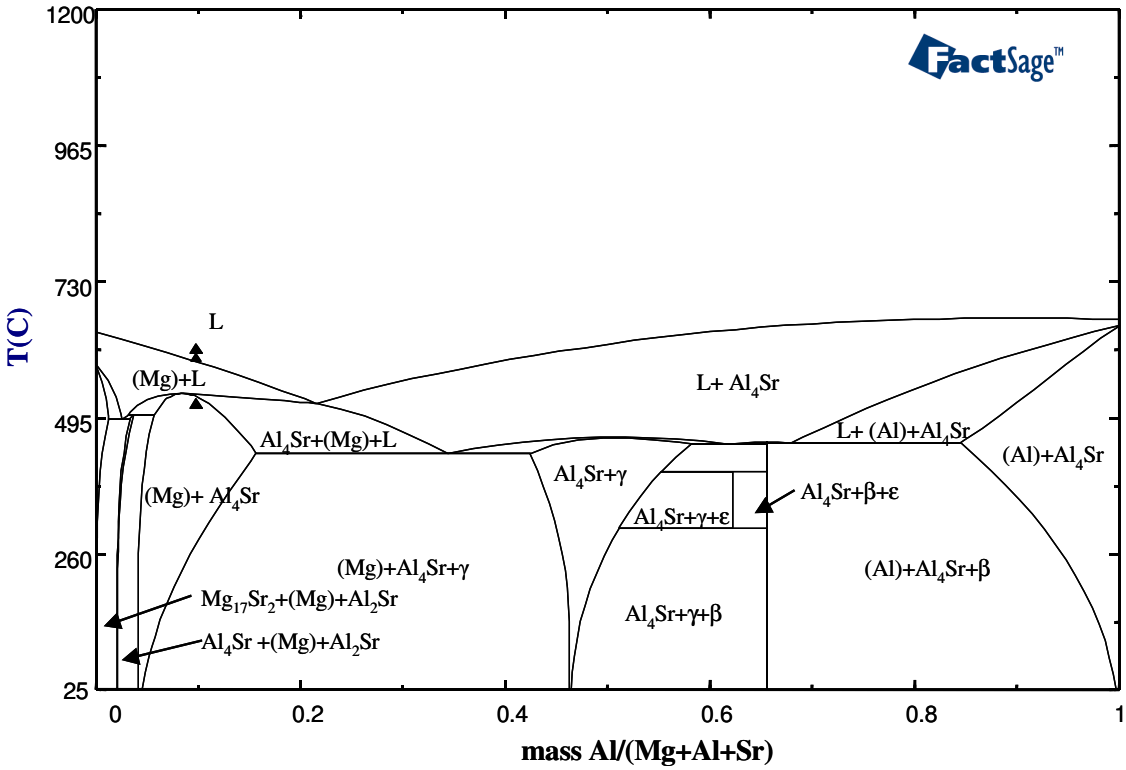

Figure 4-3: Calculated vertical section at constant 3.32 wt.% Sr with DSC signals from cooling curve of sample 1.

The experimental results were compared with the thermodynamic calculations to confirm the transformation temperature along with the associated reaction. For this purpose, the vertical section was calculated using FactSage [14] and the database developed by Chartrand and Pelton [23]. Figure 4-3 shows the calculated vertical section of sample 1 (3.32 wt.% Sr, 87.29 wt.% Mg and 9.39 wt.% Al) with DSC signals from the cooling curve. This vertical section has been calculated for the actual composition. It can be observed that the liquidus temperature matched very well with the experimental values. However, the transformation temperature predicted by the thermodynamic modeling at 222°C was not observed in the DSC signals. Slower heating rate at 2°C/min also did not reveal any signal at this temperature.

XRD was used to identify the phases in the studied samples at room temperature. The peaks are identified by markers given in the legend of each figure. In sample 1, three phases were identified in the diffraction pattern. It can be seen from Figure 4-4 that this sample is composed of (Mg), Al_4Sr and γ at room temperature. (Mg) peaks are identified as a hexagonal unit cell (space group $P6_3/mmc$, a = 3.1210Å and c = 5.1581Å), while Al_4Sr and γ were identified using a tetragonal and cubic unit cell (space group I4/mmm, a = 4.459Å and c=11.0700 Å) and (space group I43m, a = 10.5438 Å), respectively. The presence of known oxide phases such as MgO, Al_2O_3 and $MgAl_2O_4$ was also checked out and the XRD pattern showed no trace of these compounds. Baril *et al.* [21] reported that the γ phase was not observed in an alloy with the chemical composition of 2.4 wt.% of Sr, 91.6 wt.% of Mg and 6.0 wt.% of Al, which is close to this sample. This information along with some more experimental data with different samples in this Mg-rich region can be used to setup a window to identify the possible creep resistant alloy for the end user. Because it is very important for the developed Mg alloys not to have traces of the γ phase, which is detrimental to tensile strength, creep and ductility.

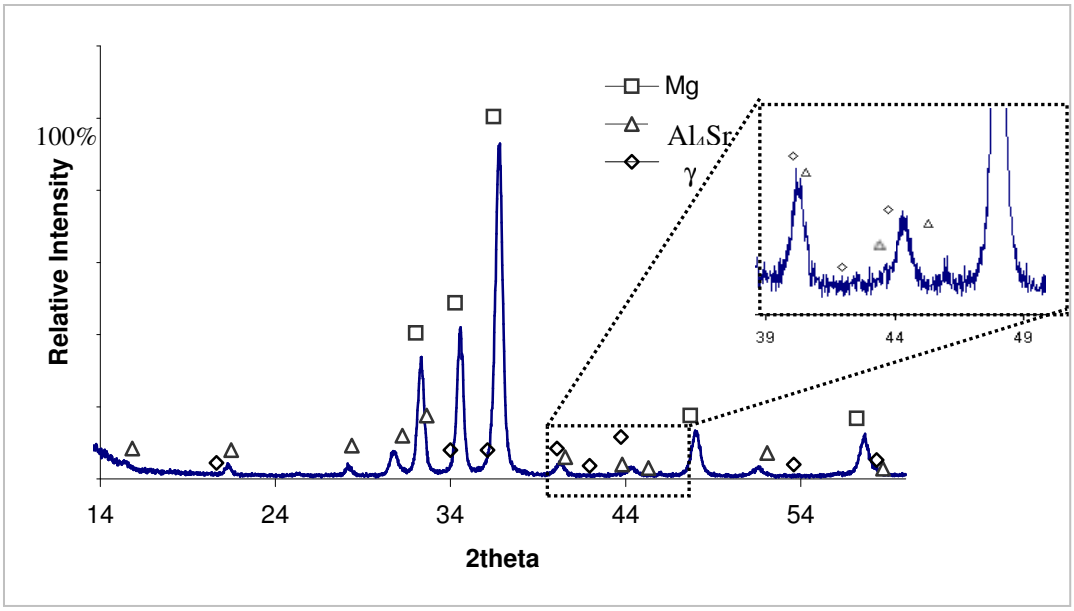

Figure 4-4: XRD pattern of sample 14 (3.32/87.29/9.39 Sr/Mg/Al wt.%).

Figure 4-5 shows the phase assemblage diagram of sample 1 (3.32 wt.% Sr, 87.29 wt.% Mg and 9.39 wt.% Al), where the relative mass versus temperature is calculated. The proportion of each phase at any temperature of interest can easily be interpreted from this figure. For instance, at 25°C, 100 g of the overall material consists of 7.5g of Al_4Sr, 4.5g of γ and 88g of (Mg). The proportion of each phase for this sample has been reflected in terms of peak intensity in the diffraction pattern. Moreover Figure 4-5 shows that while cooling this sample from the melt, (Mg) solidifies first, followed by Al_4Sr and then γ.

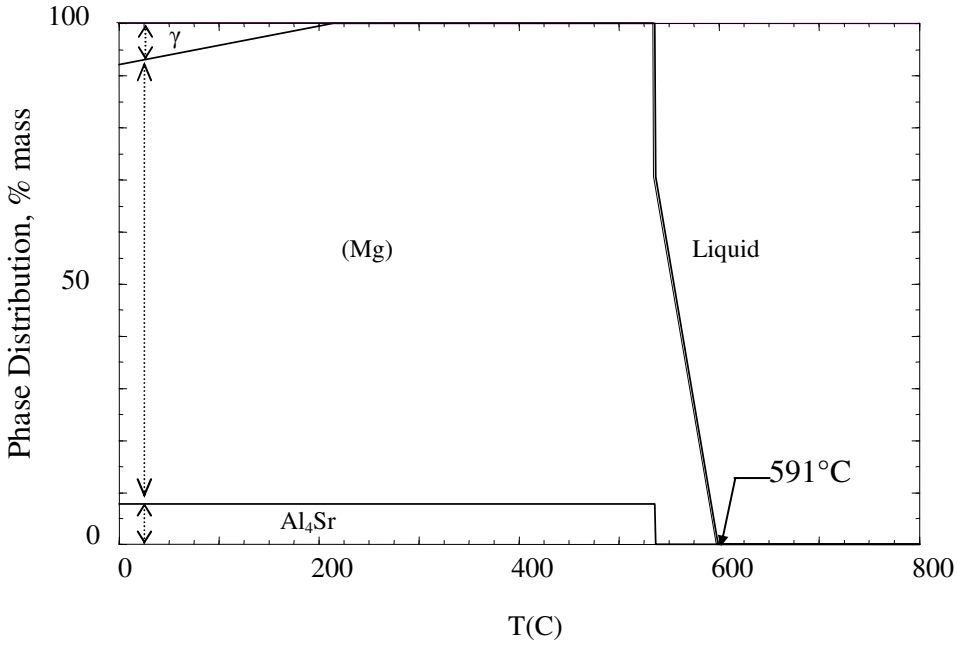

Figure 4-5: Phase assemblage diagram of sample 1.

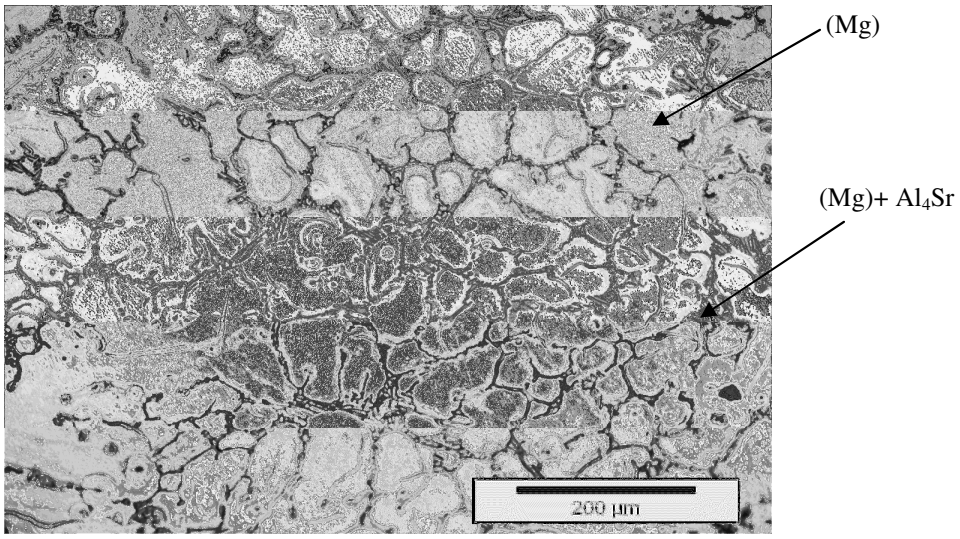

Figure 4-6: Optical micrograph of sample 1.

Figure 4-6 shows the optical micrograph of sample 1. The solidification nature can be understood using the phase assemblage diagram. The primary (Mg) grains are

surrounded by the interconnected network of the grain boundary phase in the as-cast state. The grain boundary phase is formed during the eutectic solidification process and thus having a lamellar type morphology. Baril *et al.* [21] found Al_4Sr in the lamellar eutectic morphology in the alloy quite close to this sample, which indicates that Al_4Sr is in the grain boundary phase. However, γ phase is difficult to reveal by the micrograph because of its small relative amount.

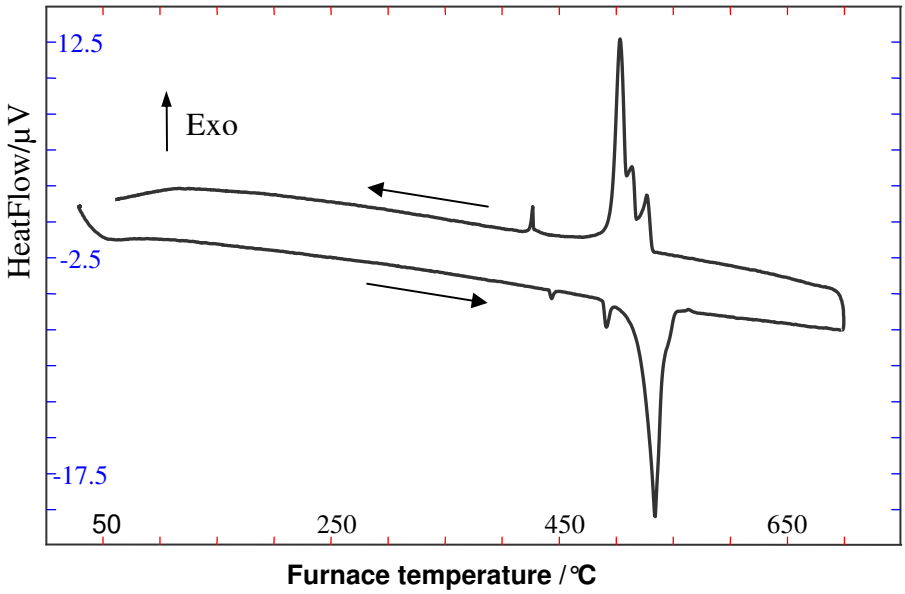

Figure 4-7: DSC spectra of sample 2 (8.65 wt.% Sr, 76.15 wt.% Mg and 15.20 wt.% Al) during heating and cooling.

Figure 4-7 shows the DSC spectra of sample 2 (8.65 wt.% Sr, 76.15 wt.% Mg and 15.20 wt.% Al). It shows three peaks during heating and four peaks during cooling. In this sample, the endothermic peak during heating begins at 440°C. On cooling, the onset temperatures of the exothermic peaks are observed at 427°C, 510°C, 515°C, and 531°C. The liquidus temperature was registered at 563°C.

Figure 4-8 shows the calculated vertical section of sample 2 with DSC signals from the cooling curve. The calculated liquidus temperature was observed 14°C below the experimental results. However the lower transformation temperature cannot be obtained through DSC signals.

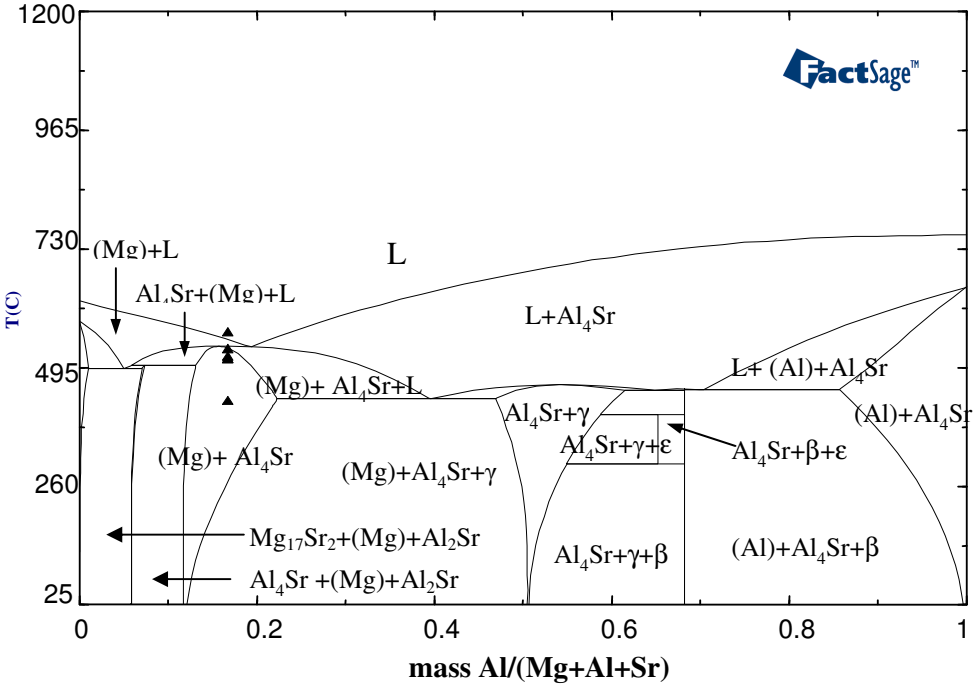

Figure 4-8: Calculated vertical section at constant 8.65 wt.% Sr with DSC signals from cooling curve of sample 2.

Three phases were identified positively in the diffraction pattern (Figure 4-9). They are Al_4Sr, γ and (Mg). Figure 4-10 shows the phase assemblage diagram of this sample. Thermodynamic predictions show that γ decomposes completely above 262°C. However, Figure 4-10 shows that Al_4Sr, γ and (Mg) are stable phases at room temperature. The identified phases by XRD agree well with the thermodynamic findings.

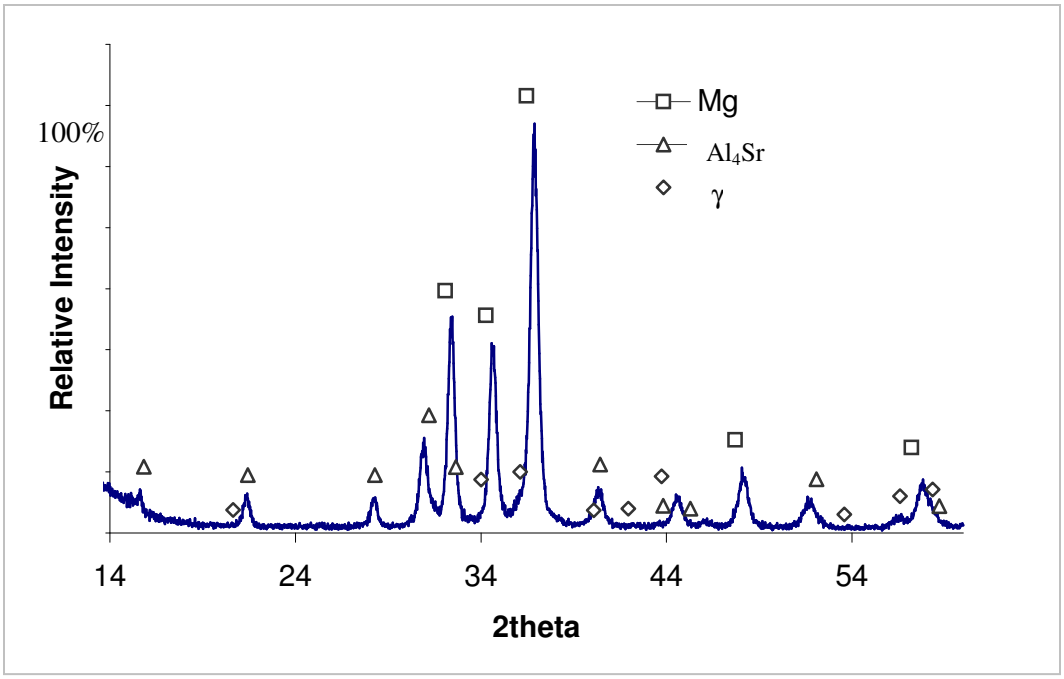

Figure 4-9: XRD pattern of sample 2 (8.65/76.15/15.20 Sr/Mg/Al wt.%).

Figure 4-11 shows the optical micrograph of sample 2. It can be seen from this micrograph that the eutectic morphology is different than sample 1, although they have the similar phases. It is to be noted that sample 2 is much closer to the eutectic point than sample 1 so that the eutectic morphology is more pronounced in sample 2. The increase in content of Al_4Sr has been reflected in the XRD pattern.

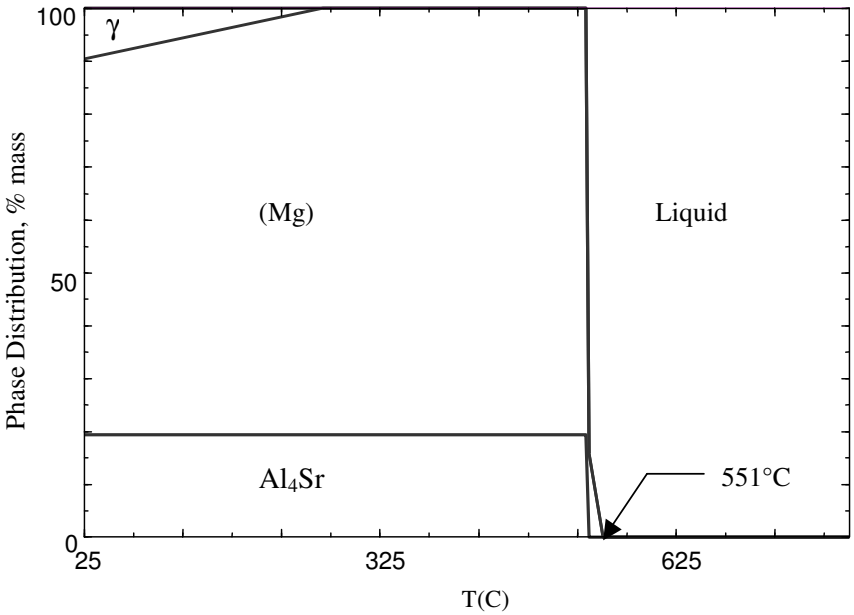

Figure 4-10: Phase assemblage diagram of sample 15.

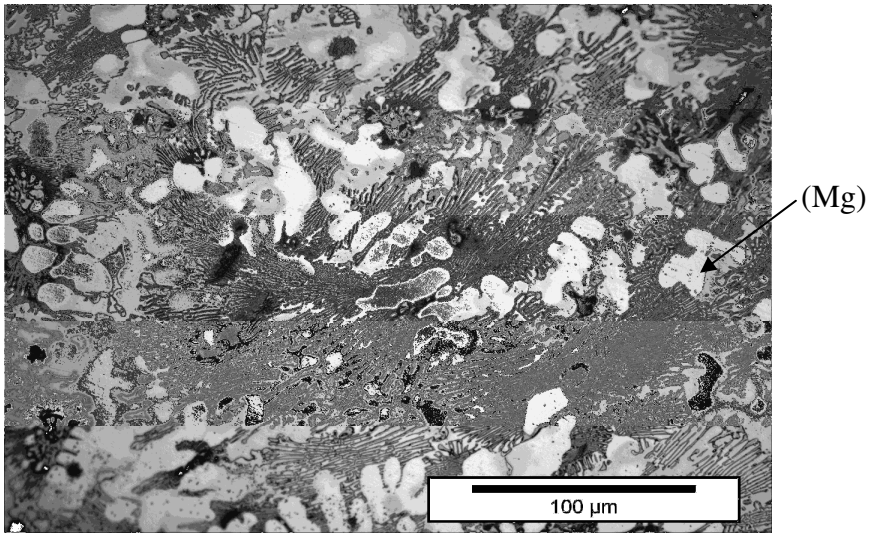

Figure 4-11: Optical micrograph of sample 15.

Sample 3 (7.09 wt.% Sr, 74.82 wt.% Mg and 18.09 wt.% Al), sample 4 (6.88 wt.% Sr, 65.45 wt.% Mg and 27.67 wt.% Al, sample 5 (22.48 wt.% Sr, 48.57 wt.% Mg and 28.95 wt.% Al), sample 6 (22.53 wt.% Sr, 43.75 wt.% Mg and 33.72 wt.% Al, and also have been identified positively with three phases (Mg), Al_4Sr and γ. This is consistent with the thermodynamic calculation. Figure 4-12 to 4-15 show the DSC spectra, phase assemblage diagram, XRD pattern and microstructure of these samples. It can be seen from Figures 4-13 and 4-14 that an increase in the content of Al_4Sr predicted by the thermodynamics has been reflected in the micrograph for sample 4 and sample 5. An understanding of the reactions that take place in samples 4 and 5 from their melting point to room temperature was established using the phase assemblage diagrams and the micrographs. In sample 4 and 5, Al_4Sr precipitated 1st at 591°C and 648°C when cooling from melt. The liquidus temperature of sample 5 is consistent with the calculated temperature. Furthermore, sample 4 was reported as a ternary eutectic by Makhmudov *et al.* [19]. However, the DSC spectra and phase assemblage diagram show that this sample is not eutectic. If it were eutectic, all the three phases should have precipitated at the same temperature and DSC spectra should have been registered with a single peak. It can be seen from the micrographs (Figures 4-13 (d) and 4-14 (d)) that Al_4Sr is the primary phase. In sample 4 and and 6, the smaller lighter phase as seen in Figures 4-13 (d) and 4-15 (d), has been tentatively designated as γ phase. It is not possible to identify the phases of sample 3, as shown in Figure 4-12(d), due to the very fine structure which requires higher magnification than the optical microscope.

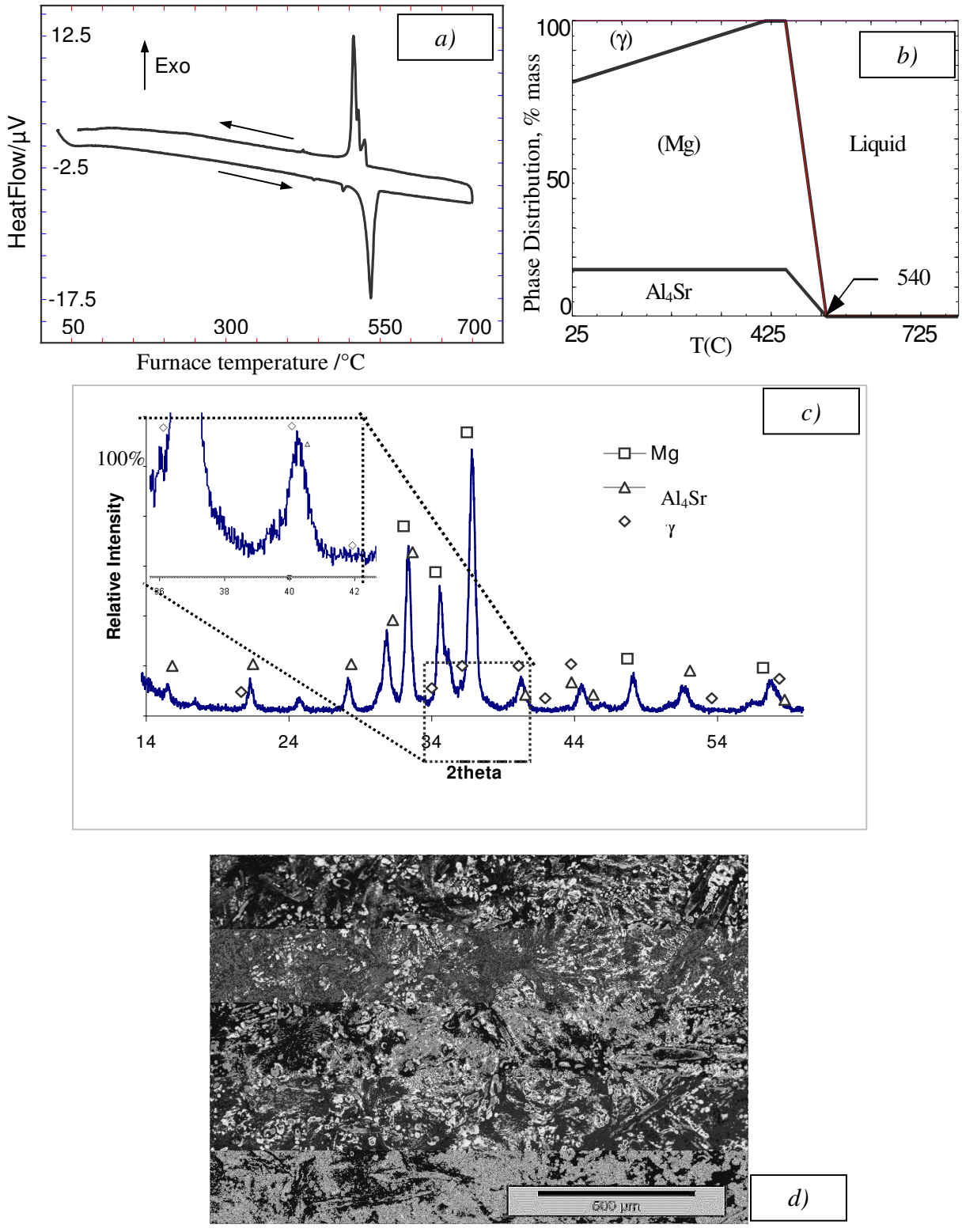

Figure 4-12: a) DSC spectra, b) phase assemblage diagram, c) XRD pattern and d) optical micrograph of sample 3.

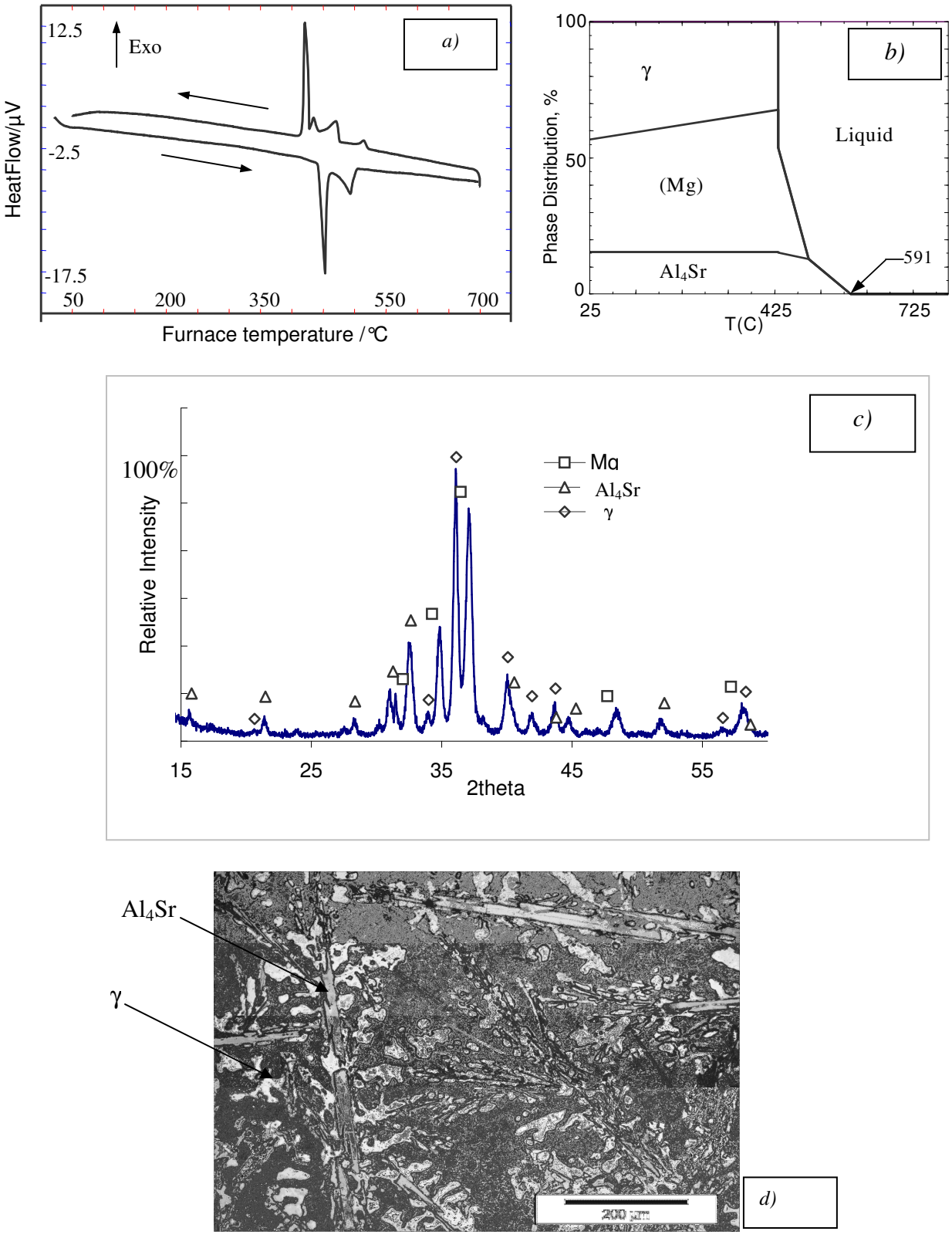

Figure 4-13: a) DSC spectra, b) phase assemblage diagram, c) XRD pattern and d) optical micrograph of sample 4.

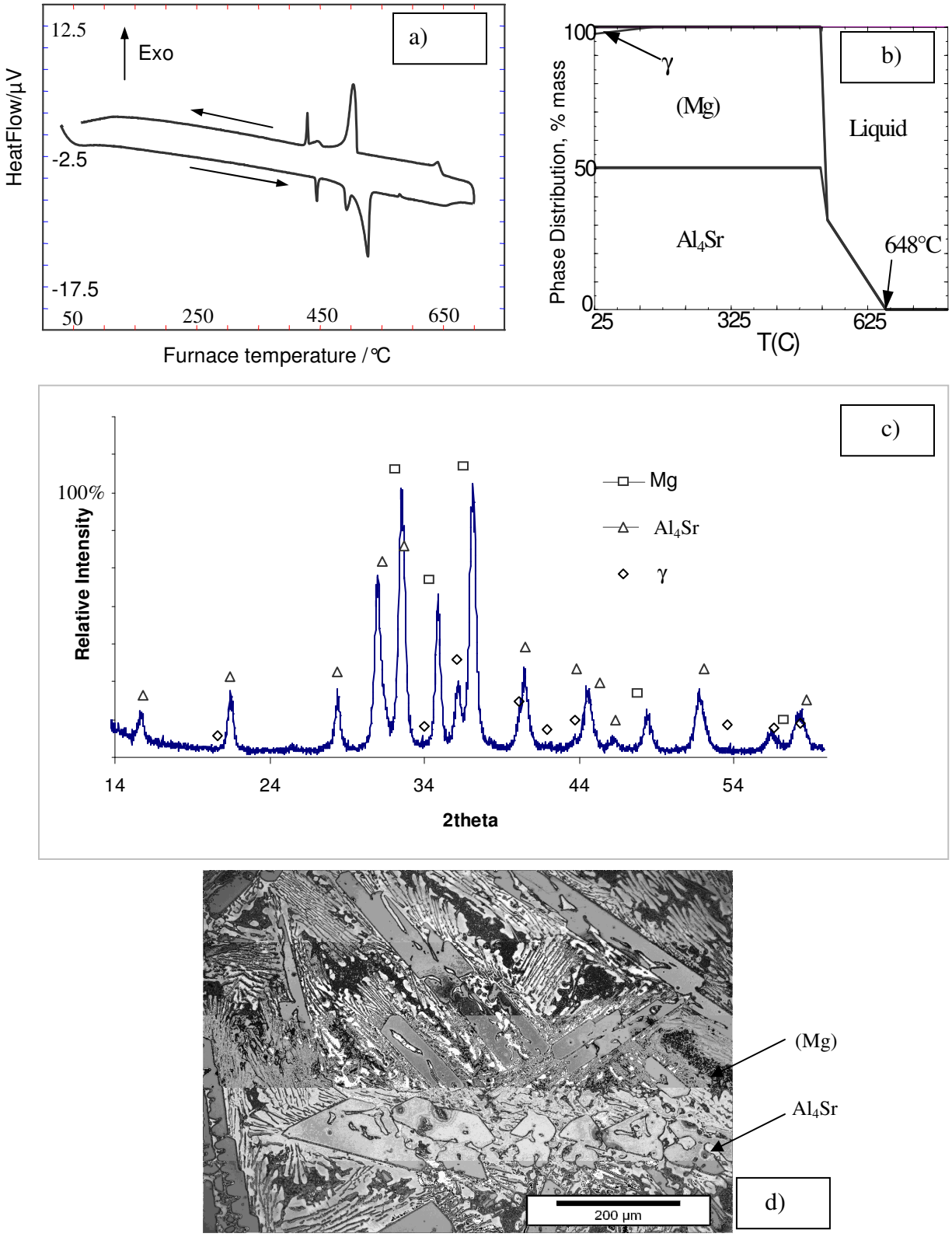

Figure 4-14: a) DSC spectra, b) phase assemblage diagram, c) XRD pattern and d) optical micrograph of sample 5.

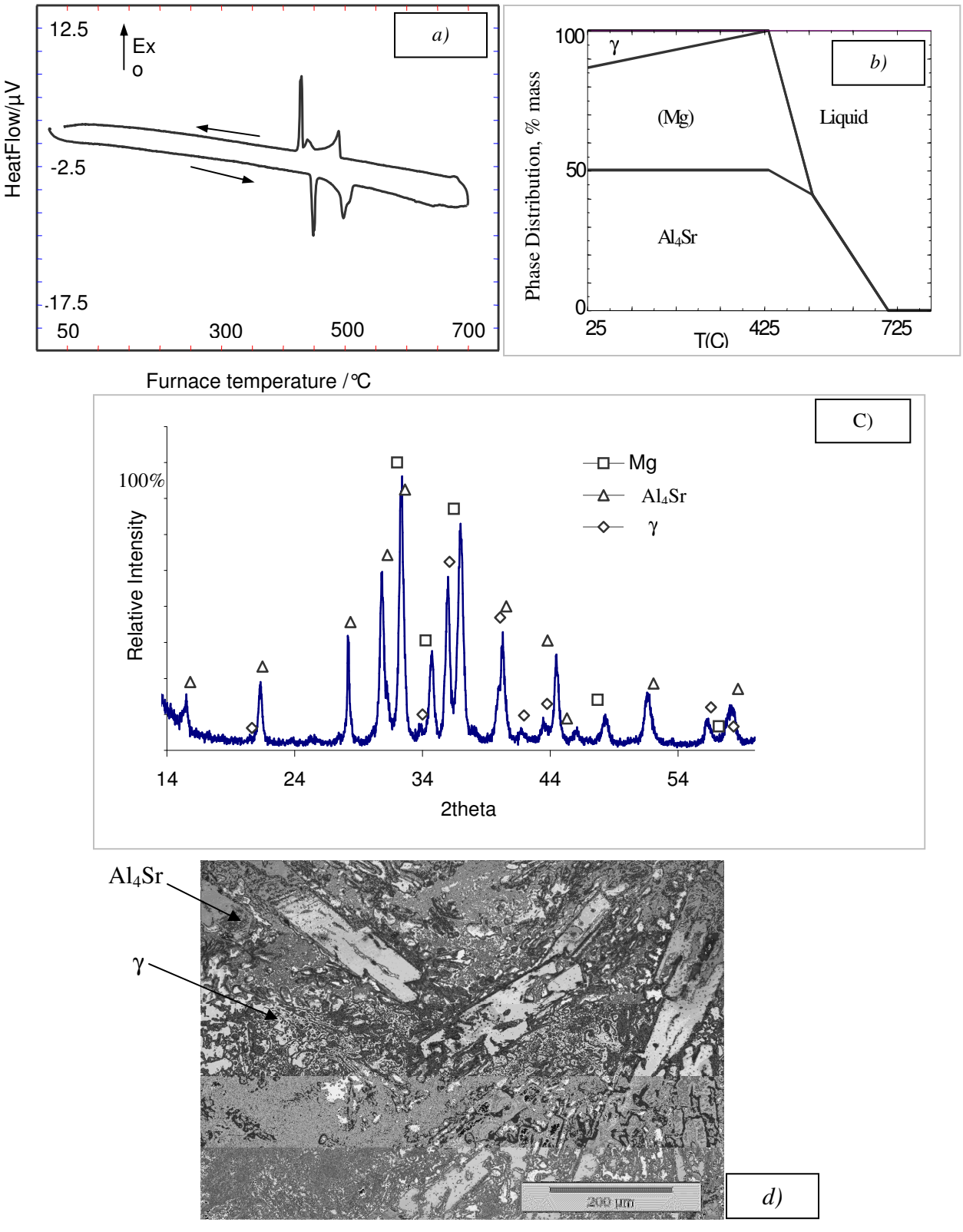

Figure 4-15: a) DSC spectra, b) phase assemblage diagram, c) XRD pattern and d) optical micrograph of sample 6.

DSC measurements and calculated thermal arrests for the samples 1,2,3,4,5 and 6 are presented in Table 4-1 to check the temperatures of liquidus and reactions between the phases. It can be seen from this table that the thermodynamic calculation could not accurately predict all the transformations that have been measured by the DSC. Besides, DSC was not able to registrar the lower temperature transformation although the samples were investigated at lower scanning rate. Figure 4-16 shows the comparison between the measured liquidus temperature obtained by experimental and predicted by the thermodynamics, which shows good agreement except for samples 4 and 6.

Table 4-1: DSC measurements with thermodynamic analysis of Mg-Al-Sr alloys (h: denotes heating and c: denotes cooling).

Sample	DSC Thermal Signals (°C)	Thermodynamic calculation based on the database reported in [23]	
		Temp.	Reaction or phase boundary
1	609c/	591	L/ L+ (Mg)
	596c/605h		
	517c/535h	535	L+ (Mg) / (Mg)+Al_4Sr
		222	(Mg)+Al_4Sr / (Mg)+Al_4Sr+γ
2	563h	551	L/ L+ (Mg)
	531c	533	L+ (Mg) / (Mg)+Al_4Sr
	516c/536h	525	
	510c/491h		
	427c/441h		
		282	(Mg)+Al_4Sr / (Mg)+Al_4Sr+γ
3	531c	540	L/ L+ (Mg)+Al_4Sr
	528c	530	L+ (Mg)+Al_4Sr/ (Mg)+Al_4Sr
	516c/523h		
	487c/510h	460	
	427c/442h		
		398	(Mg)+Al_4Sr / (Mg)+Al_4Sr+γ
4	524	591	L/ L+ Al_4Sr
	514c		
	472c		

	435c/494h	496	L+ Al_4Sr / L+(Mg)+Al_4Sr
	422c/442	429	L+(Mg)+Al_4Sr/(Mg)+Al_4Sr+γ
5	652	648	L/ L+ Al_4Sr
	647c	535	L+ Al_4Sr / L+(Mg)+Al_4Sr
	510c/513h	525	L+(Mg)+Al_4Sr/ (Mg)+Al_4Sr
	453c/489h		
	431c/445h		
		318	(Mg)+Al_4Sr / (Mg)+Al_4Sr+γ
6	499c/490h	703	L/ L+ Al_4Sr
	448c/449h	532	L+ Al_4Sr / L+(Mg)+Al_4Sr
	432c	433	L+(Mg)+Al_4Sr / (Mg)+Al_4Sr+γ

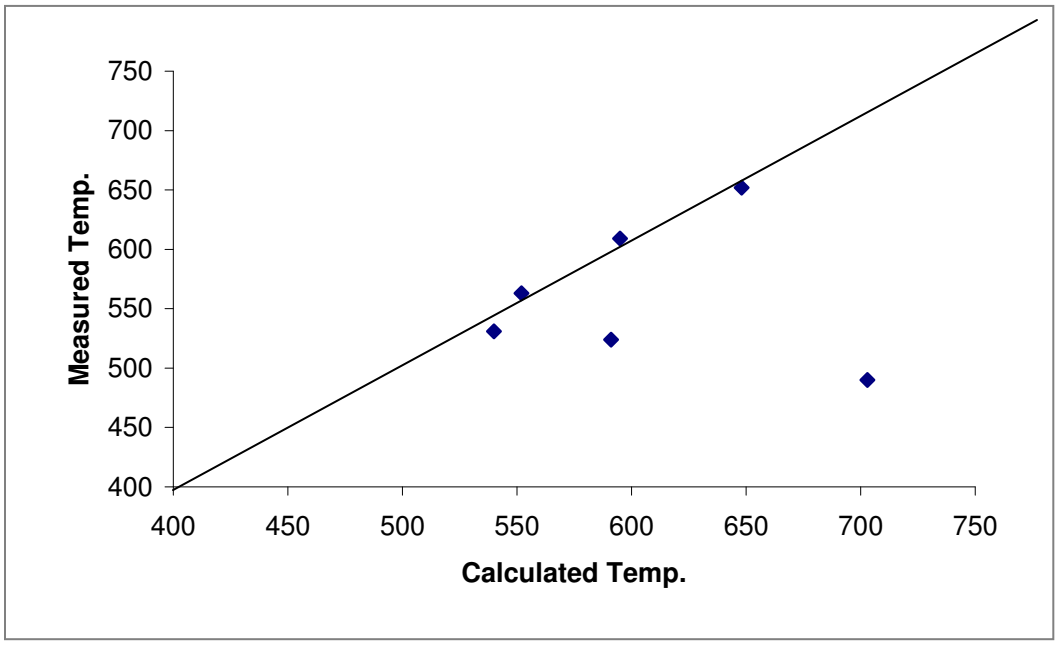

Figure 4-16: Comparison between calculated and experimental DSC data.

In this phase field, samples 7, 8 and 9 were identified positively with Al_4Sr and γ. Some other distinct peaks that are not associated with the known phases in the Mg-Al-Sr system have been observed. There is no information regarding any stable ternary compounds available in the literature. Some of the peaks of the XRD pattern for these samples did match well with a ternary compound tentatively designated as $Al_3Mg_{13}Sr$ and

reported by Baril *et al.* [21]. However, the crystal structure of $Al_3Mg_{13}Sr$ is still unknown. Therefore, these peaks were tentatively designated as $T_{Sr}1$. It may be a new ternary compound or a ternary solid solution. It is very important to note that these distinct peaks appear in the XRD patterns of these samples in a similar fashion (Figure 4-17 to Figure 4-19). It should be noted that large solubilities may cause large peak shifting, for instance Koray *et al.* [24] reported a ternary solid solution phase $(Mg,Al)_2Ca$ in Mg-Al-Ca system that occurs through the substitution of Al atoms in Mg_2Ca structure. In the phase field of (Mg)+Al_4Sr+γ, Al_4Sr was found to be the dominating phase for most of the samples.

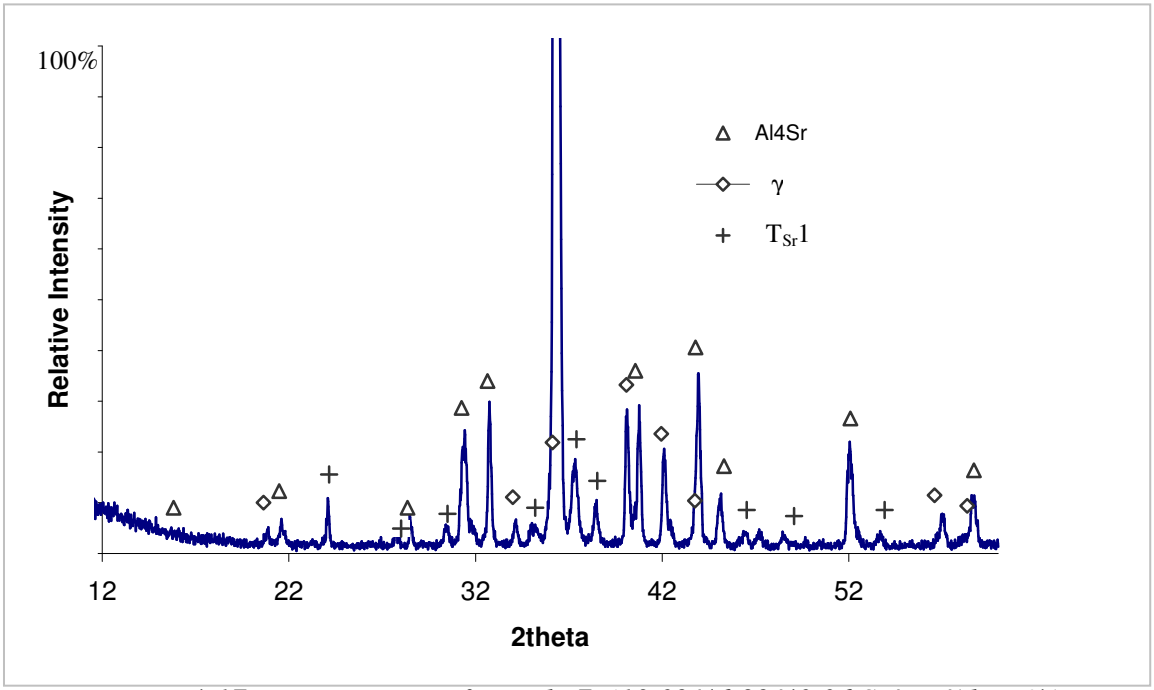

Figure 4-17: XRD pattern of sample 7 (13.02/46.92/40.06 Sr/Mg/Al wt.%).

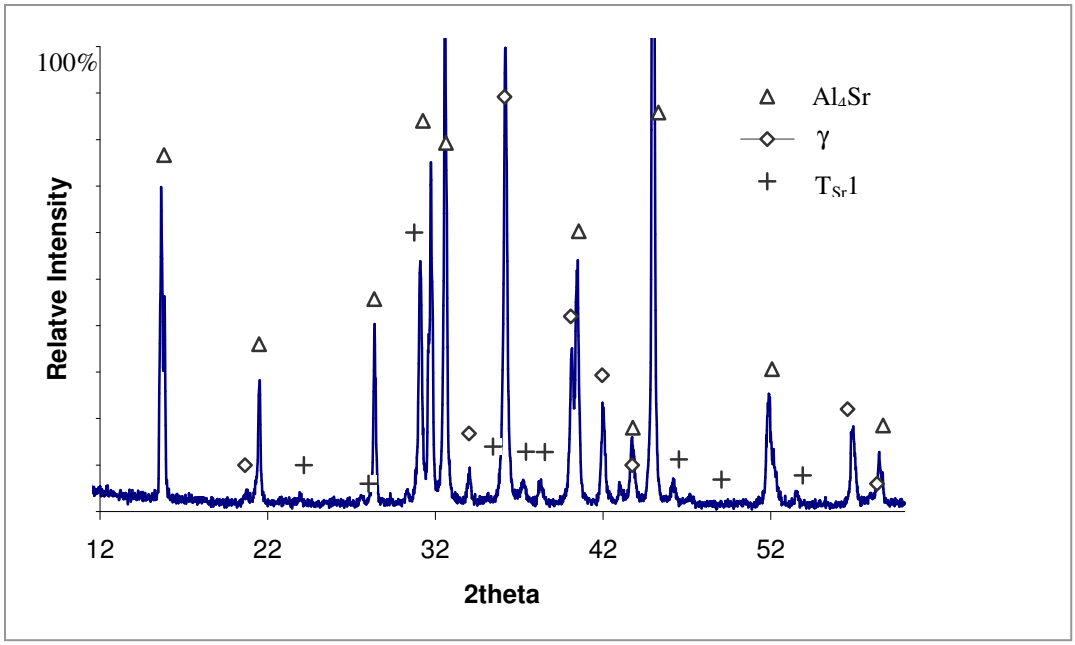

Figure 4-18: XRD pattern of sample 8 (24/30/46 Sr/Mg/Al wt.%).

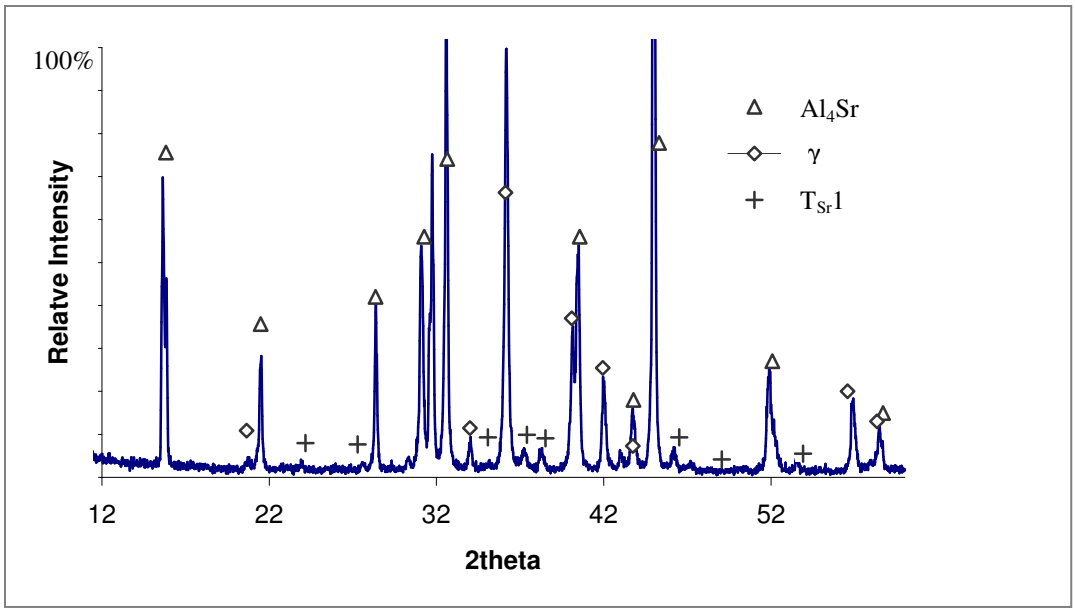

Figure 4-19: X-ray diffraction pattern of sample 9 (32/22/46 Sr/Mg/Al wt.%).

Table 4-2 summarizes the DSC measurements in relation to the results from thermodynamic modeling. The thermodynamic calculation was made to check the

temperature of liquidus and the reaction between the phases. It is evident from the analysis that the calculated liquidus temperatures do not agree well with the experimental results except for sample 7. This is due to the fact that in sample 7, 8 and 9 there is an indication of new ternary compounds or solid solution which may alter the reactions between the phases and hence the liquidus temperature. Figures 4-20 to 4-22 show the DSC spectra and phase assemblage diagram of sample 7, 8 and 9. In all the three samples, the exothermic reaction starts at similar temperature 444~445°C. It can be seen from the phase assemblage diagram that the samples are mainly composed of γ and Al_4Sr, which have been identified positively by XRD. However, the phase assemblage diagram of these samples show that at room temperature there is 10 to17 g of (Mg) out of 100 g and this was detected in the XRD patterns.

Table 4-2: DSC measurements with thermodynamic analysis of Mg-Al-Sr alloys (h: denotes heating and c: denotes cooling).

Sample	DSC Thermal Signals (°C)	Thermodynamic calculation based on the database reported in [23]	
		Temp.	Reactions or phase boundary
7	676	703	L/ L+ Al_4Sr
	510h	443	L+ Al_4Sr/ L+Al_4Sr+γ
	444c/466h	429	L+Al_4Sr+γ/(Mg)+Al_4Sr+γ
8	522	802	L/ L+ Al_4Sr
	507h		
	489h		
	445c/457h	446	L+ Al_4Sr/ L+Al_4Sr+γ
		427	L+Al_4Sr+γ/(Mg)+Al_4Sr+γ
9	519	846	L/ L+ Al_4Sr
	506h	501	L/ L+ Al_4Sr/ L+Al_4Sr+(Mg)
	445c/457h	429	L+Al_4Sr+(Mg) /(Mg)+Al_4Sr+γ

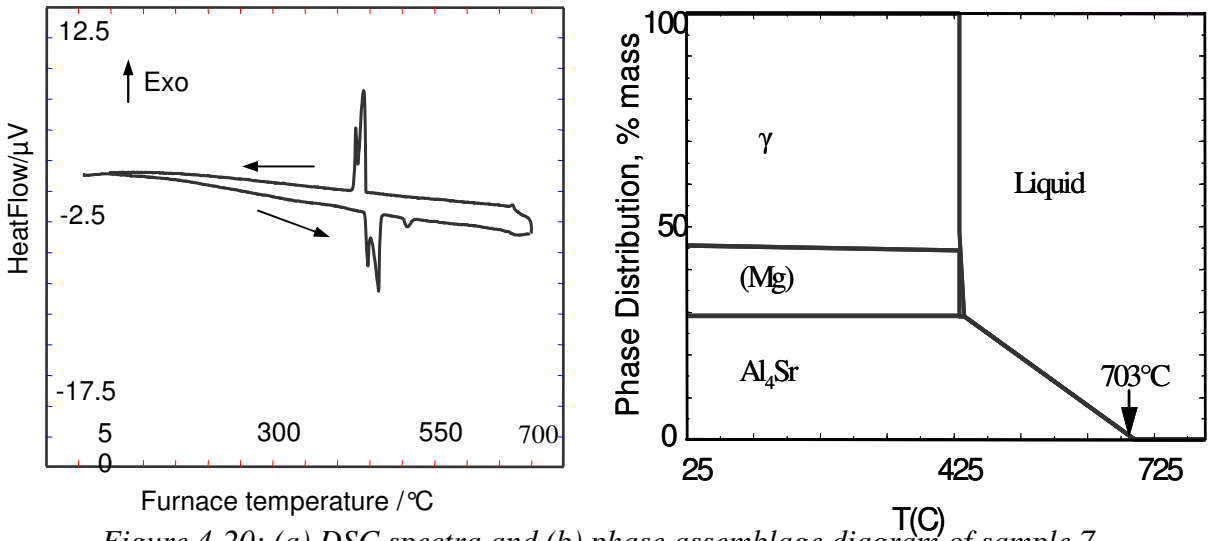

Figure 4-20: (a) DSC spectra and (b) phase assemblage diagram of sample 7.

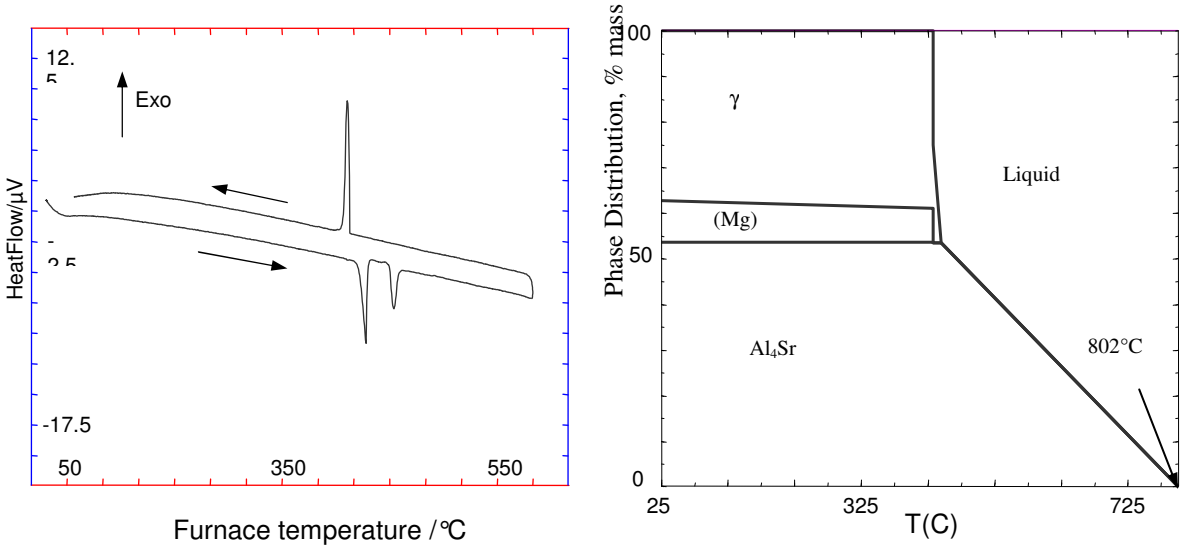

Figure 4-21: (a) DSC spectra and (b) phase assemblage diagram of sample 8.

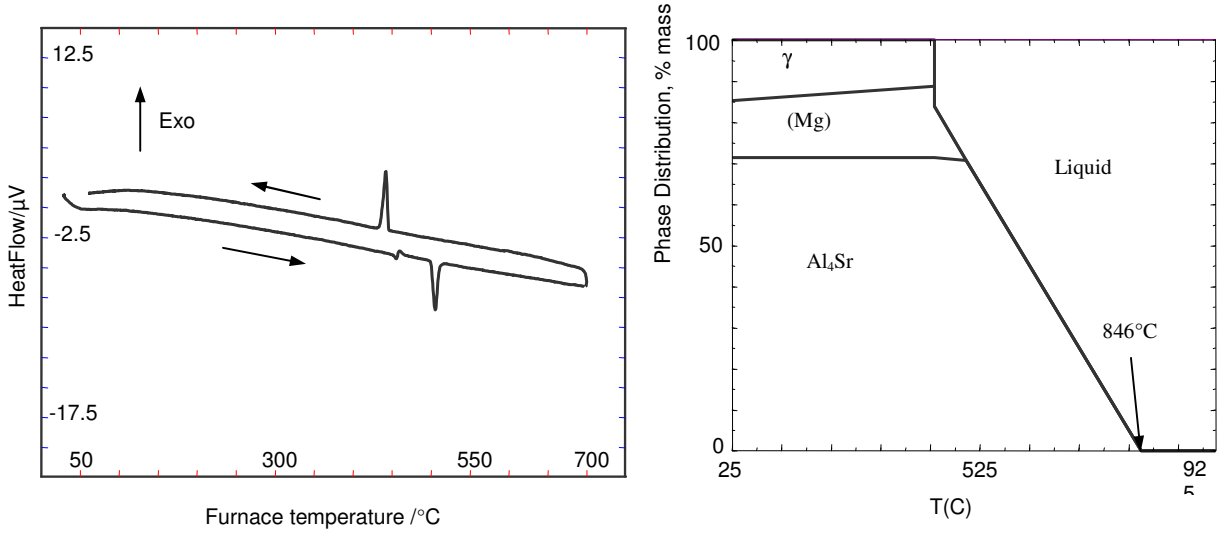

Figure 4-22: (a) DSC spectra and (b) phase assemblage diagram of sample 9.

Figure 4-23 shows the isothermal section at 25°C with optical microscopic images of the microstructure of sample 7, 8 and 9. The micrographs led to the conclusion that these remarkable plate-like crystals are Al_4Sr as it is the primary phase in these alloys as supported by the phase assemblage diagrams (Figures 4-20 (b) to 4-22 (b)) and the XRD patterns (Figures 4-17 to 4-19).

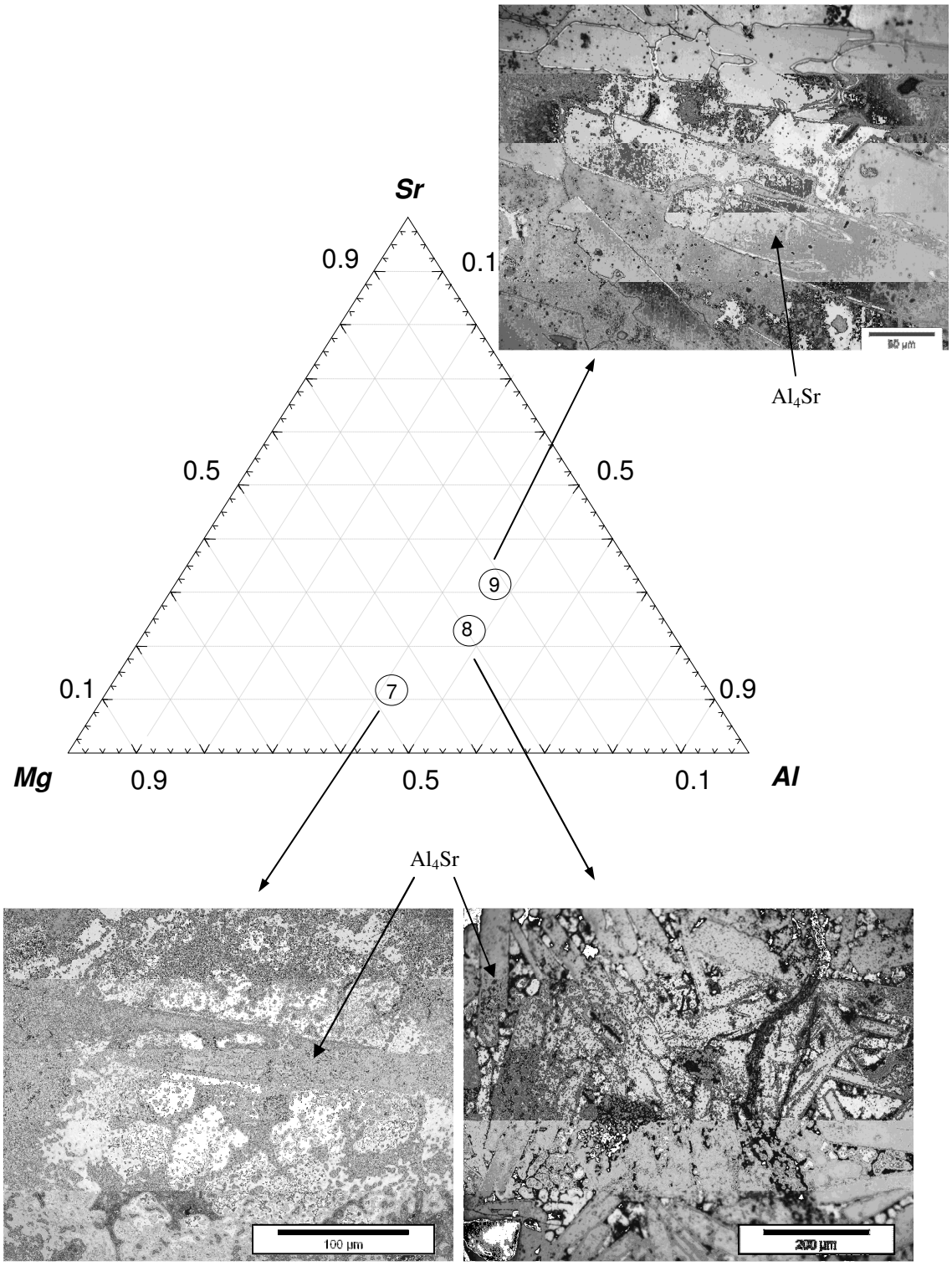

Figure 4-23: Isothermal section at 25°C with optical microscopic images.

4.2 Samples in (Mg)+Al_2Sr+Al_4Sr phase field

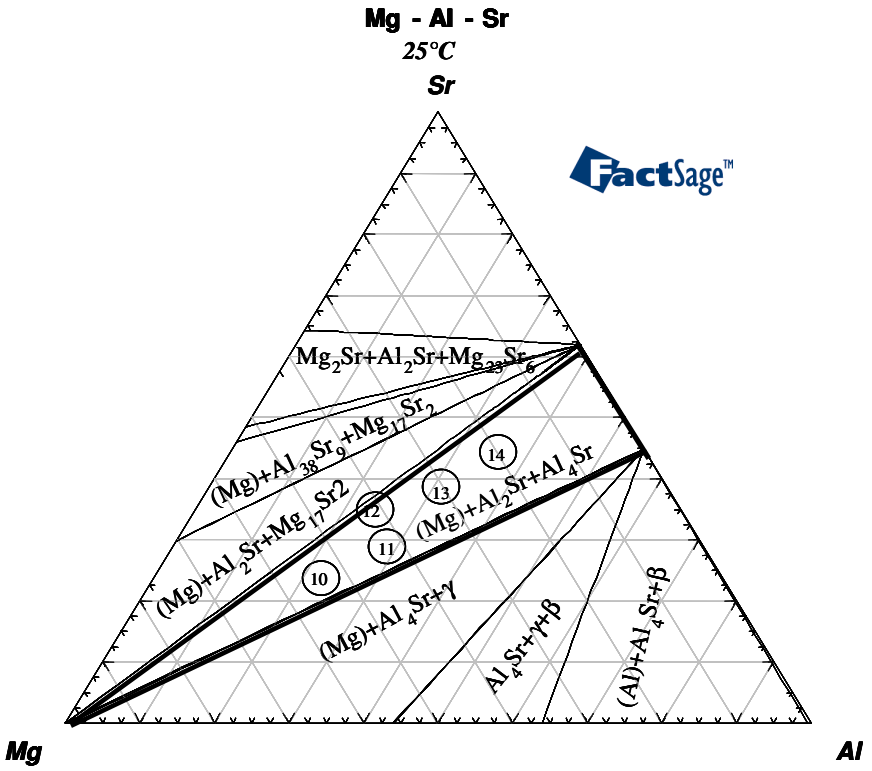

Figure 4-24: Isothermal section at 25°C showing samples in (Mg)+Al_4Sr+Al_2Sr phase field.

Five samples, as shown in Figure 4-24, were studied in this phase fields. In sample 10 and sample 11, (Mg) and Al_4Sr were identified in the diffraction patterns as shown in Figures 4-25 and 4-26, respectively. Figure 4-27 shows the XRD patterns of sample 14 that was identified with Al_2Sr and Al_4Sr. Al_2Sr was identified using a Rhombic unit cell (space group *Fd3m*, a = 8.325(5) Å) [76]. Furthermore, the distinct peaks that are not associated with any of the known phases in Mg-Al-Sr system, appeared identical manner in all the three samples. Samples 10 and 11 are positioned on the edge, which are separating the two three-phase regions. And the new peaks may belong to

ternary compound or solid solution. Hence it indicates that the extent of the field of Al_2Sr is not predicted correctly in the calculated phase diagram. There are also reports of compounds predicted near Al_2Sr stoichiometry but no experimental information is available [44]. This can be clarified by performing SEM-EDS/EDX or microprobe investigation.

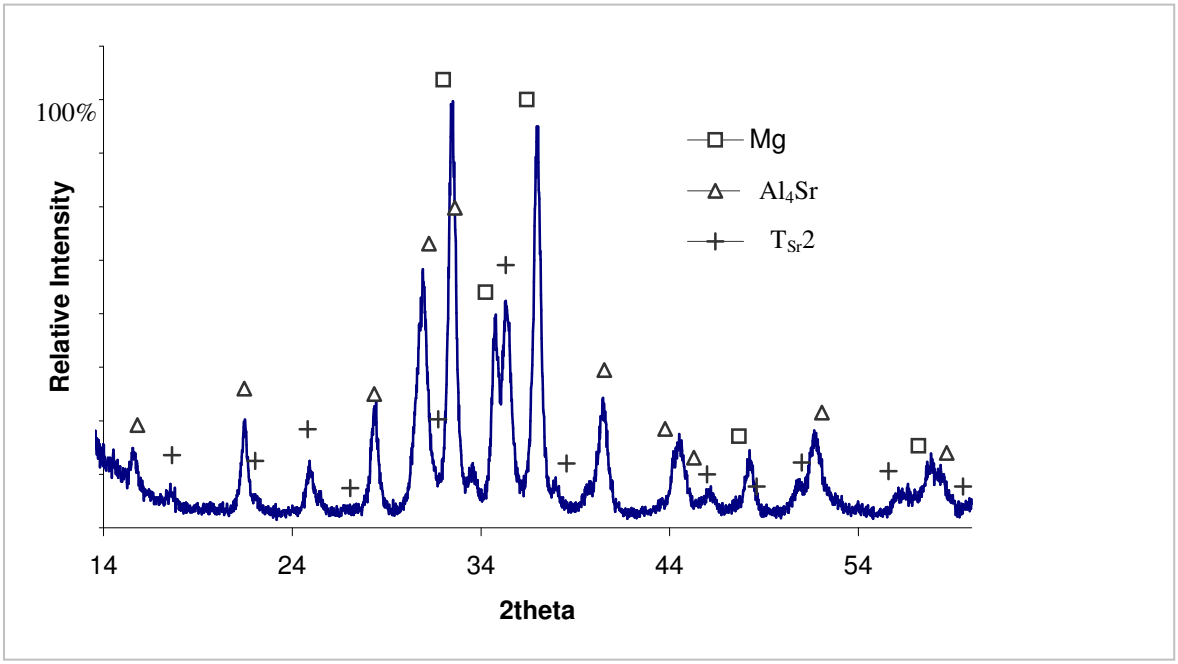

Figure 4-25: X-ray diffraction pattern of sample 10 (22.78/54.39/22.83 Sr/Mg/Al wt.%).

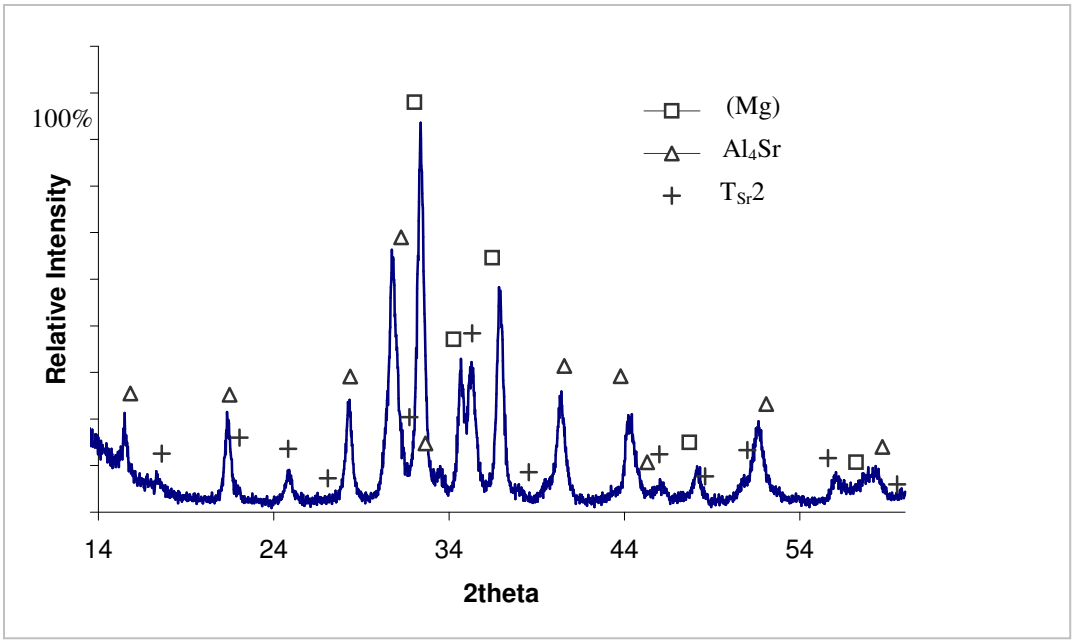

Figure 4-26: X-ray diffraction pattern of sample 11 (27.83/42.89/29.28 Sr/Mg/Al wt.%).

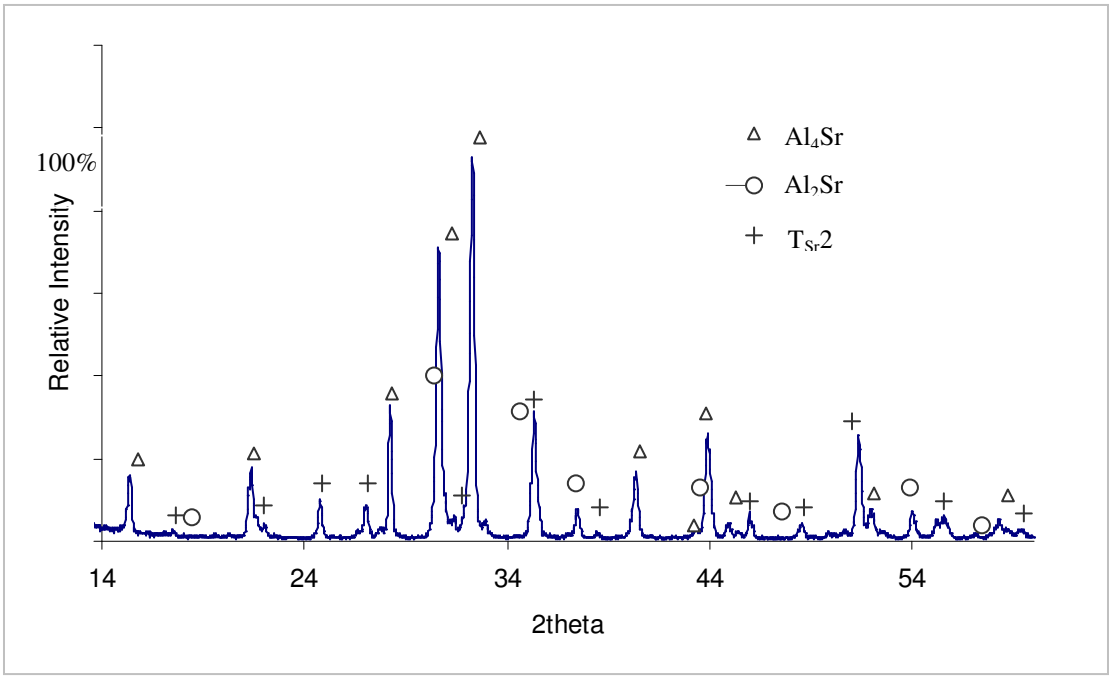

Figure 4-27: X-ray diffraction pattern of sample 14 (48.30 /19.26 /32.44 Sr/Mg/Al wt.%).

Figure 4-28 to 4-30 show the DSC spectra and phase assemblage diagrams of

samples 10, 11 and 14. Figure 4-28 exhibits two peaks during heating and three peaks during cooling. Similar result was observed in all the three heating and cooling cycles. In this sample, the endothermic peak during heating begins at around 500°C. The absence of a single endothermic peak without any tail indicates that this sample does not melt congruently but undergoes a peritectic decomposition at 550°C. Difference between onset temperature between heating and cooling was found 10°C for the invariant reaction. It can be seen from the phase assemblage diagrams (Figures 4-28(b) to 4-30(b)) that if the amount of phase at room temperature is less than 20g, it could not be identified in the XRD patterns. Table 4-3 shows the calculated transformation temperatures, associated reactions with DSC signals of samples 10, 11 and 14. Although the number of transformation predicted by the thermodynamics matched well with the experimental results. However, the transformation temperatures did not agree well.

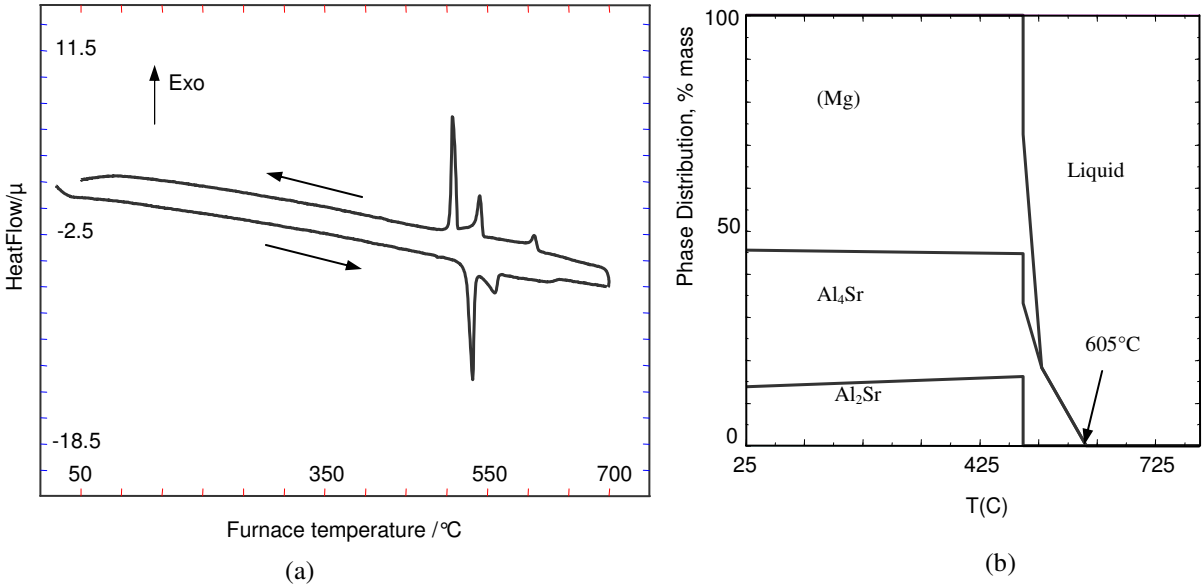

Figure 4-28: (a) DSC spectra and (b) phase assemblage diagram of sample 10.

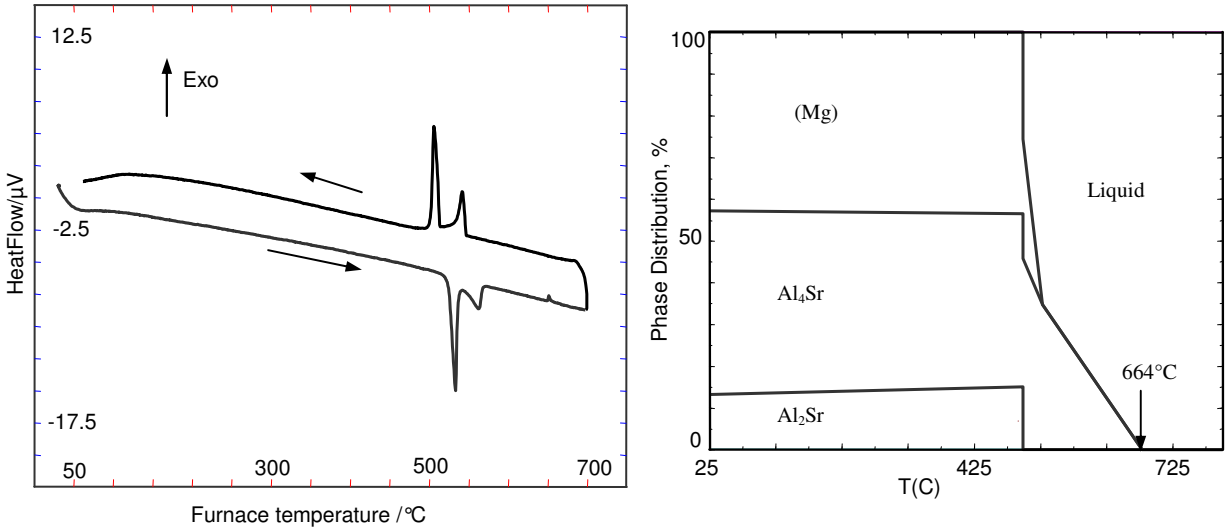

Figure 4-29: DSC spectra and phase assemblage diagram of sample 11.

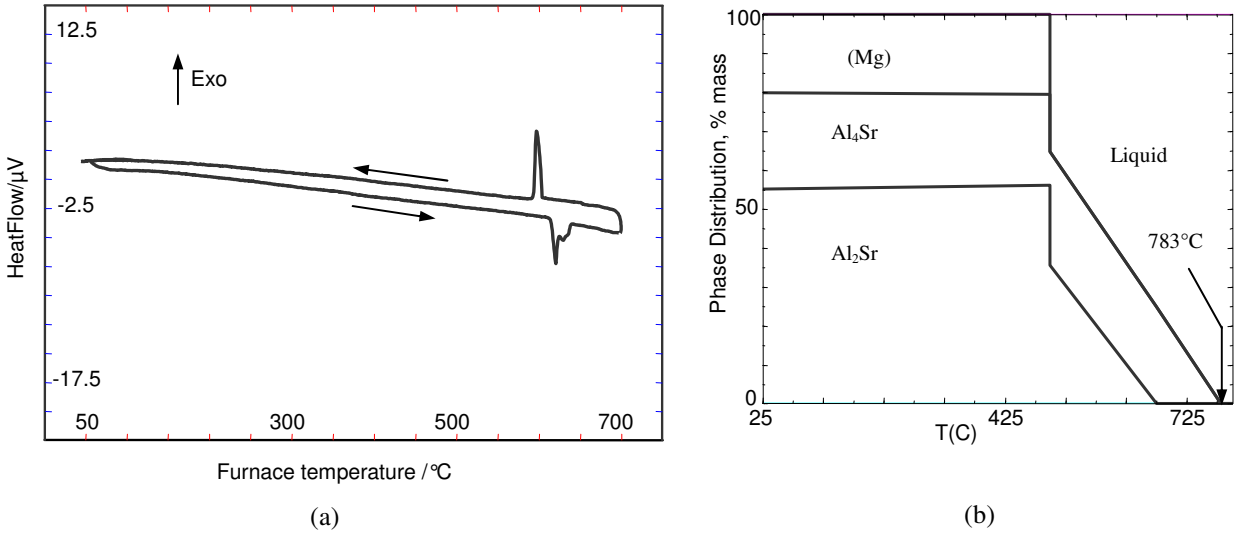

Figure 4-30: DSC spectra and phase assemblage diagram of sample 14.

Table 4-3: DSC measurements with thermodynamic analysis of Mg-Al-Sr alloys (h: denotes heating and c: denotes cooling).

Sample	DSC Thermal Signals (°C)	Thermodynamic calculation based on the database reported in [23]	
		Temp.	Reaction or phase boundary
10	618	605	L/ L+ Al_4Sr
	544c/560h	528	L+ Al_4Sr/ L+Al_4Sr+Mg
	513c/523h	494	L+Al_4Sr+Mg/ Al_2Sr+Al_4Sr+Mg
11	571	664	L/ L+ Al_4Sr
	546c/561h	525	L+ Al_4Sr/ L+Al_4Sr+Mg
	513c/524h	496	L+Al_4Sr+Mg/ Al_2Sr+Al_4Sr+Mg
14	643	783	L/ L+ Al_4Sr
	632h	716	L+ Al_4Sr/ L+Al_4Sr+Mg
	599c/615h	499	L+Al_4Sr+Mg/ Al_2Sr+Al_4Sr+Mg

Figures 4-31 to 4-33 illustrate the microstructure of sample 10, 11 and 14, respectively. Samples 10 and 11 appear to have a similar microstructure. From the analysis of XRD pattern and thermodynamics, it may be concluded that the light gray plat-like phase is Al_4Sr. The relatively long path of dark phase is tentatively designated as Al_2Sr. Figure 4-33 gives a different microstructure. This alloy composition is the far-most alloy from Mg-rich region. The intergrowth of the phases was difficult to be revealed in the micrograph of this sample and requires SEM/EDS system.

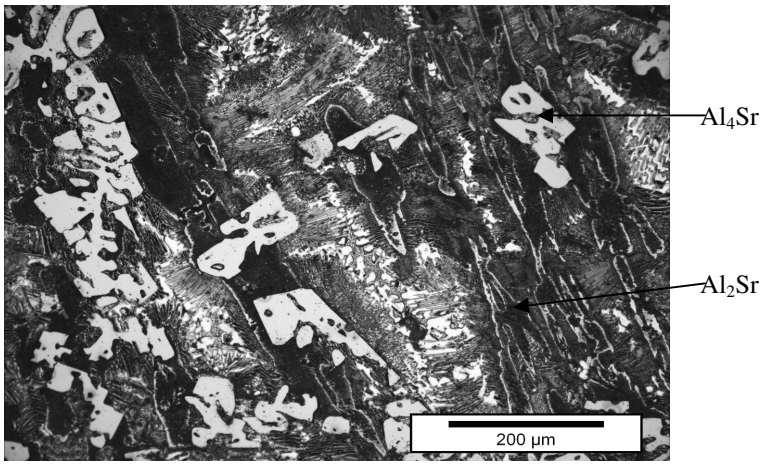

Figure 4-31: Optical micrograph of sample 10.

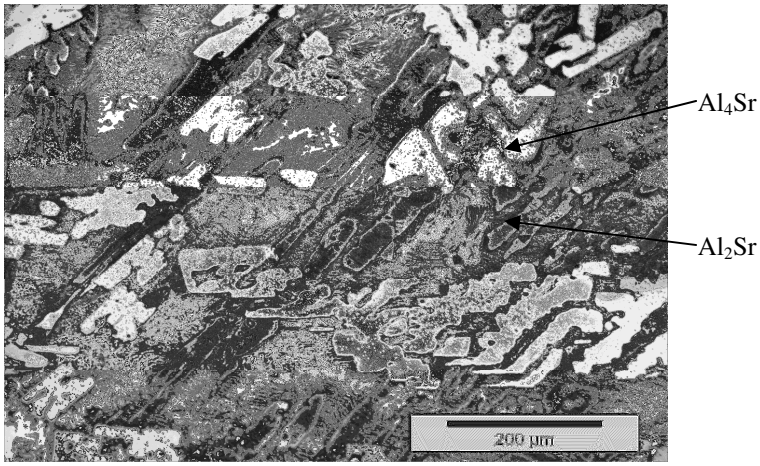

Figure 4-32: Optical micrograph of sample 11.

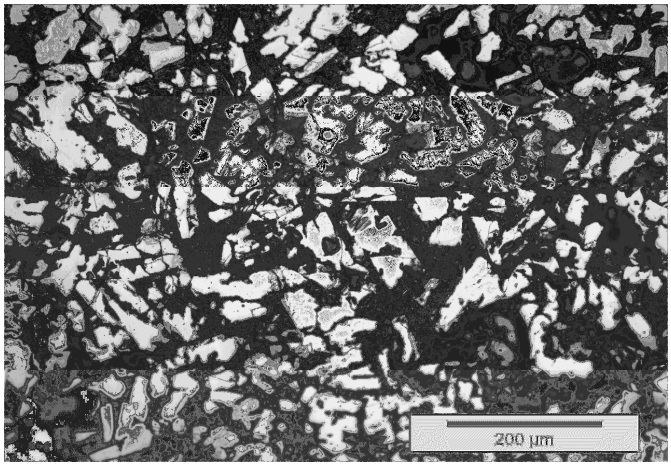

Figure 4-33:Optical micrograph of sample 14.

In the phase field of (Mg)+Al_2Sr+Al_4Sr, sample 12 and sample 13 have been identified positively with Al_2Sr and Al_4Sr along with some distinct unknown peaks. However, the unknown peaks for these two samples appeared in the same manner as shown in Figures 4-34 and 4-35. Sample 12 is chosen on the boundary of two different phase fields while both the samples are far away from the Mg-rich region. In these two samples, Al_2Sr is the primary phase as predicted by the phase assemblage diagram as shown in Figures 4-36(b) and 4-37(b).

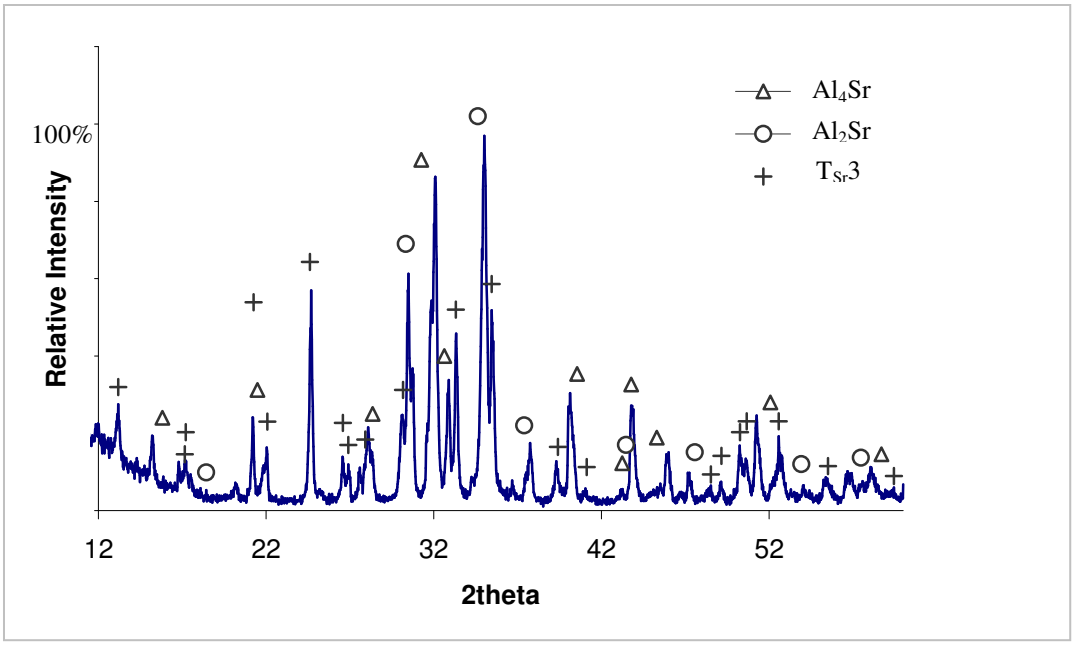

Figure 4-34: *X-ray diffraction pattern of sample 12 (34.83/39.59/25.58 Sr/Mg/Al wt.%).*

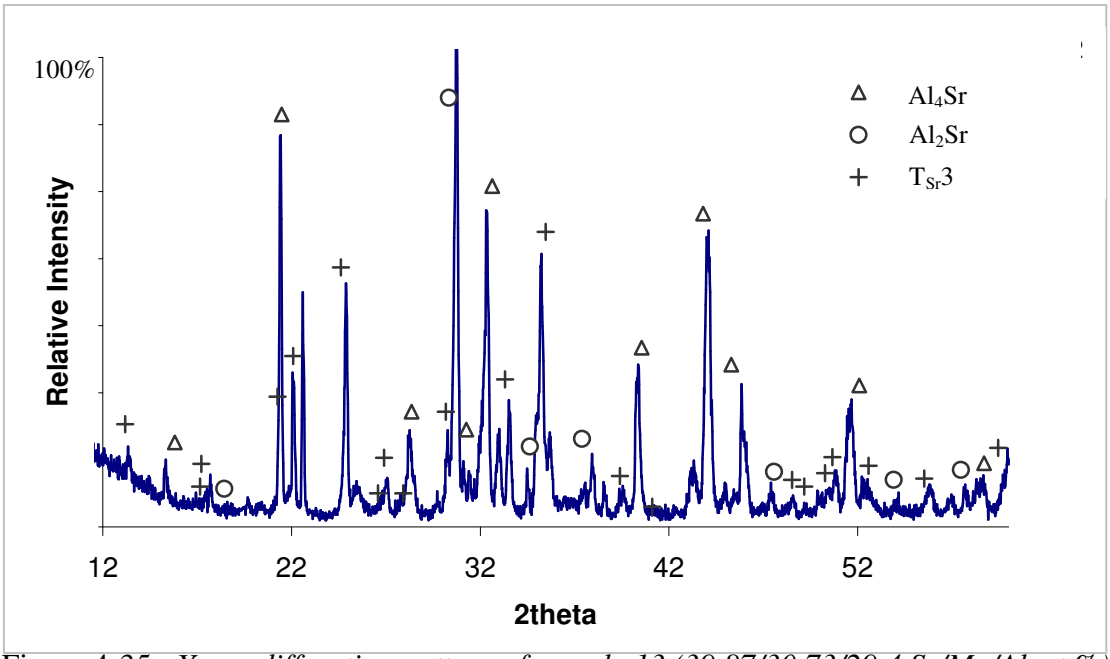

Figure 4-35: *X-ray diffraction pattern of sample 13 (39.87/30.73/29.4 Sr/Mg/Al wt.%).*

DSC spectra and phase assemblage diagram of sample 12 and 23 with heating and cooling runs are shown in Figures 4-36 and 4-37. DSC spectra of sample 23 show two

peaks during heating and three peaks during cooling. For this sample, the liquidus temperature is observed during cooling which is 677°C. The size of the freezing signals is increased due to supercooling.

Figure 4-36: a) DSC spectra, b) phase assemblage diagram of sample 12.

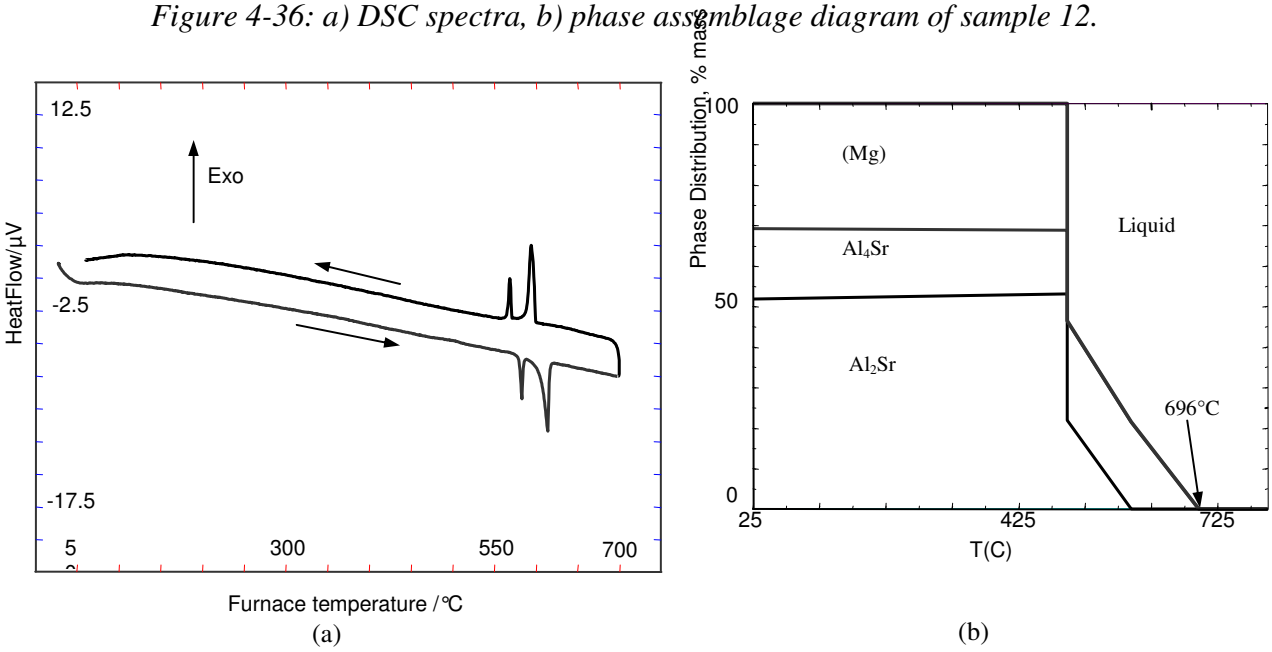

Figure 4-37: (a) DSC spectra and (b) phase assemblage diagram of sample 13.

Figure 4-38 shows the microstructure of sample 12, which is totally different in appearance than all other investigated samples. However, sample 13 was very brittle and became powder and the micrograph was not possible to obtain.

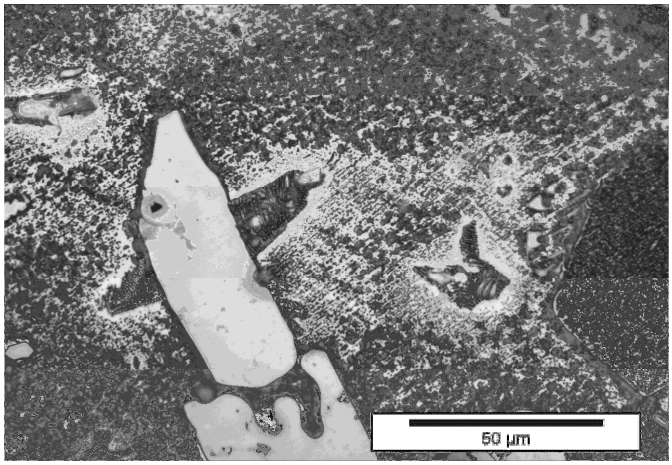

Figure 4-38: Optical micrograph of sample 12

4.3 Samples in Al_4Sr+γ+β phase field

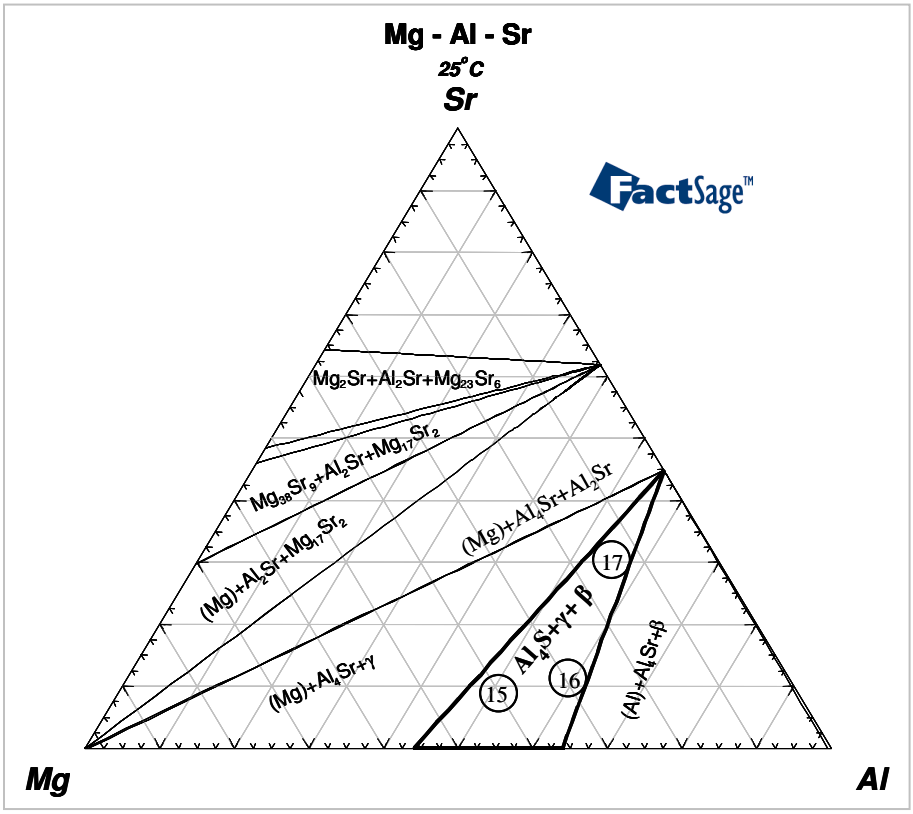

Figure 4-39: Isothermal section at 25°C showing samples in (Mg)+γ+β phase field.

Three alloys in Al_4Sr+γ+β phase field as shown in Figure 4-39 have been investigated. Figure 4-40 shows that the DSC spectra of these three alloys are consistent with a small variation of the thermal arrest of the second peak. Nevertheless the DSC spectra showed that the invariant reaction for these samples occured in quite close temperature at 459°C, 453°C and 452°C, respectively. The liquidus temperature of samples 16 and 17 are 494°C and 495°C, respectively. However, the liquidus temperature of sample 15 was 516°C. Figures 4-41 to 4-43 show the calculated vertical section in comparison with the present DSC result for the samples in this phase field. It can be seen

from Figures 4-41 to 4-43 that the lower transformation temperature was not obtained by the DSC. The enthalpy of invariant reaction for samples 15, 16 and 17 were registered as 316.67 J/g, 390 J/g and 205.34 J/g, respectively. The calculated liquidus temperature of sample 17 as shown in Figure 4-43 is 897°C, however, the liquidus temperature by DSC was registered at 447°C. The thermodynamic model could not predict the correct liquidus temperature when the Sr content is higher.

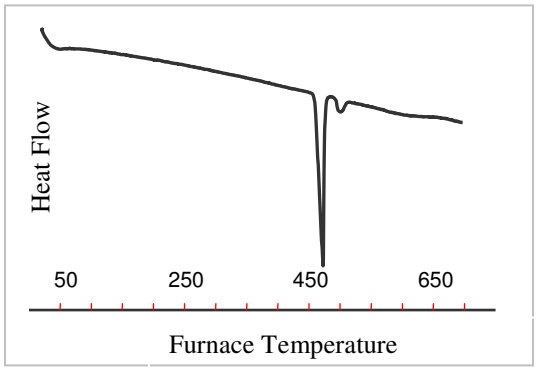

(a)

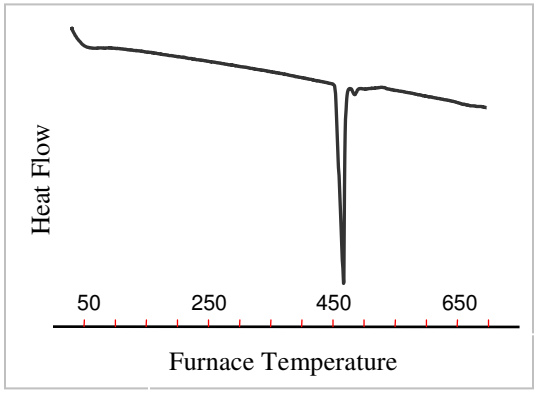

(b)

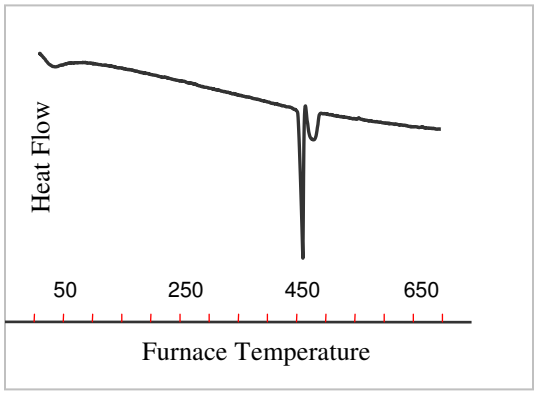

(c)

Figure 4-40: DSC traces of the three samples (a) 15, (b) 16 and (c) 17.

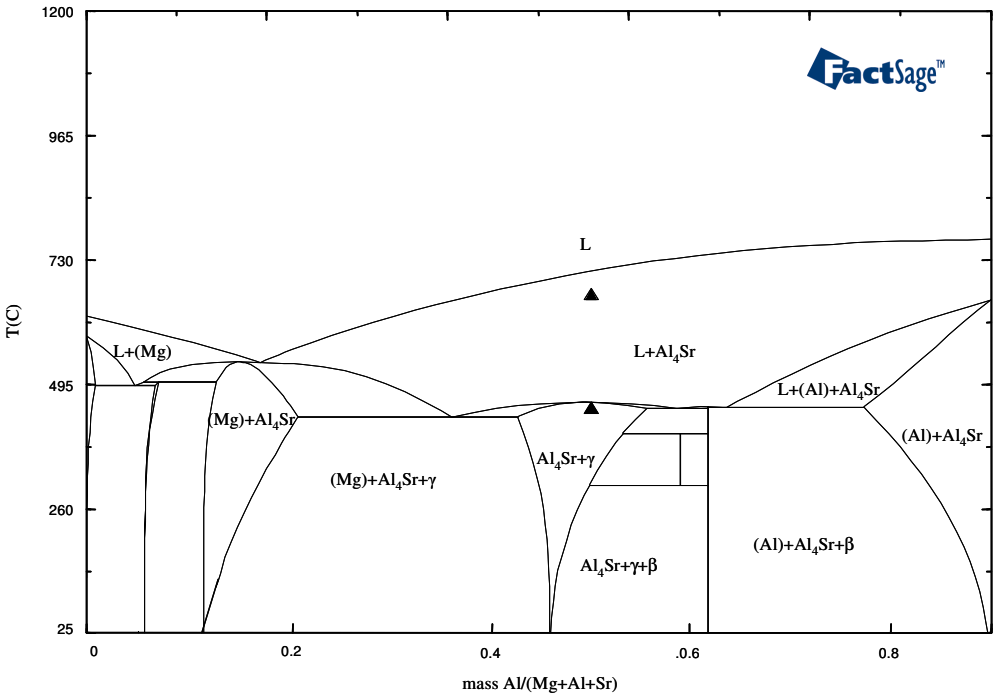

Figure 4-41: Calculated vertical section at constant 9.5 wt.% Sr with DSC signals from cooling curve of sample 15.

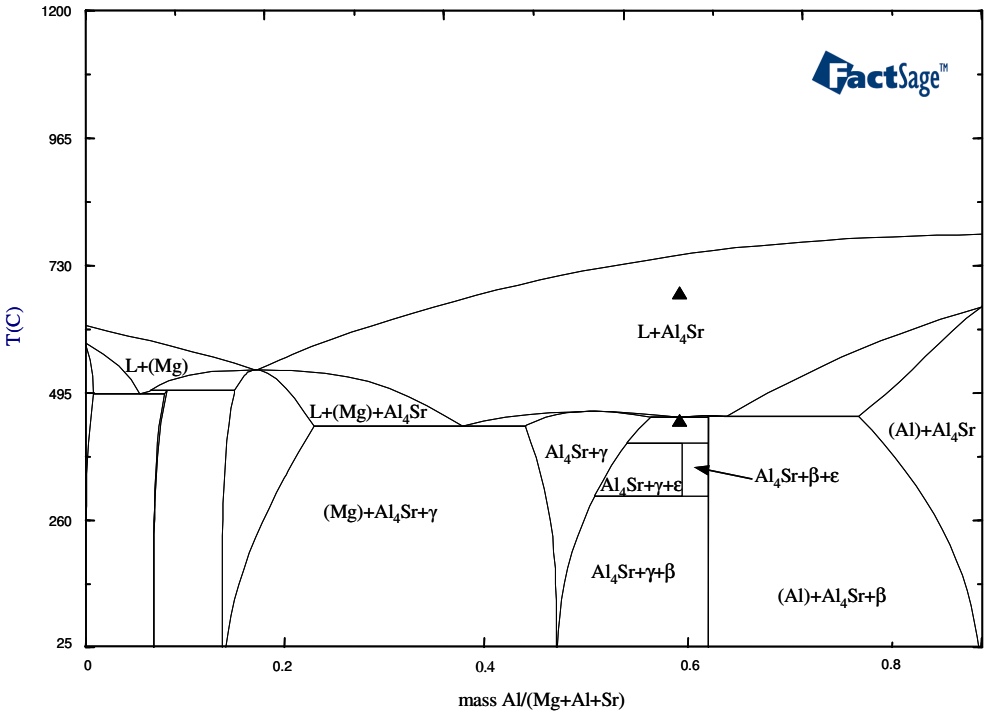

Figure 4-42: Calculated vertical section at constant 11 wt.% Sr with DSC signals from cooling curve of sample 16.

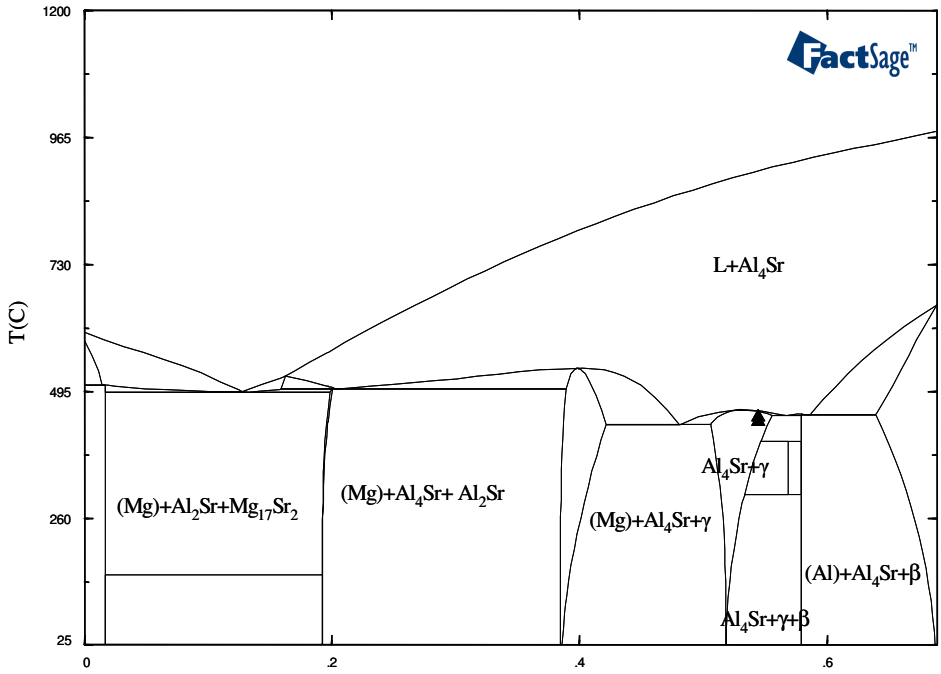

Figure 4-43: Calculated vertical section at constant 31.18 wt.% Sr with DSC signals from cooling curve of sample 17.

It can be seen from Figures 4-44 and 4-45 that sample 15 and16 were identified with all the three phases predicted by the thermodynamics. However, sample 16 as shown in Figure 4-46 was positively identified with Al_4Sr and β. β has a complex cubic unit cell (space group Fm3m, a = 4.2155 Å) [76]. XRD pattern for β has been obtained from the experimental result of Akhtar *et al.* [77]. Distinct peaks not associated with the known phases in the Mg-Al-Sr system were also observed. The peaks did not match with any ternary compound, available in the literature.

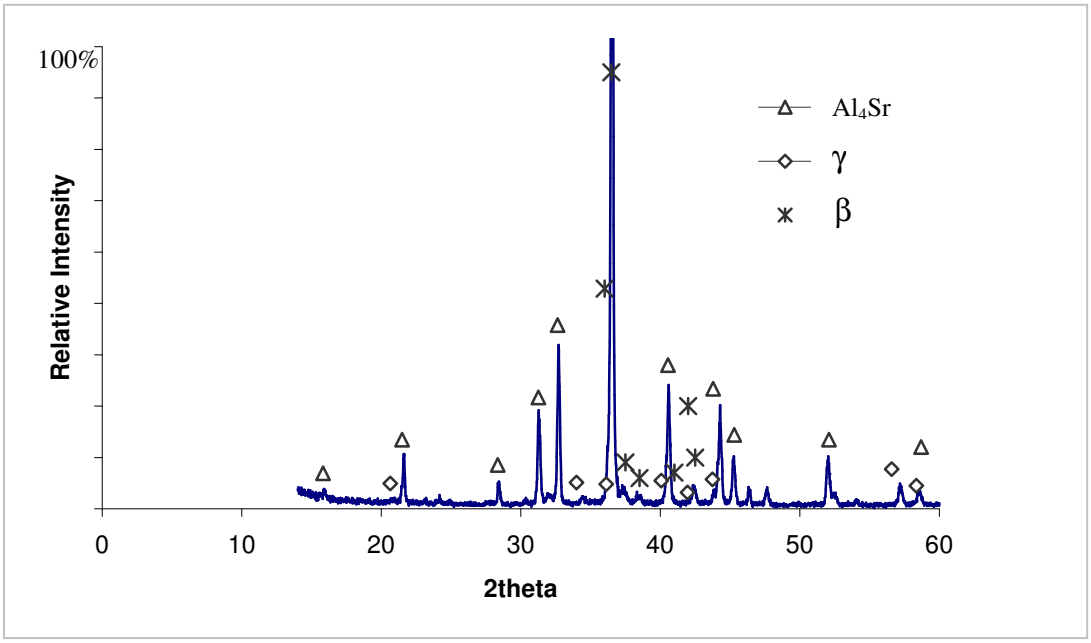

Figure 4-44: XRD pattern of sample 15 (9.5/40/50.5 Sr/Mg/Al wt.%).

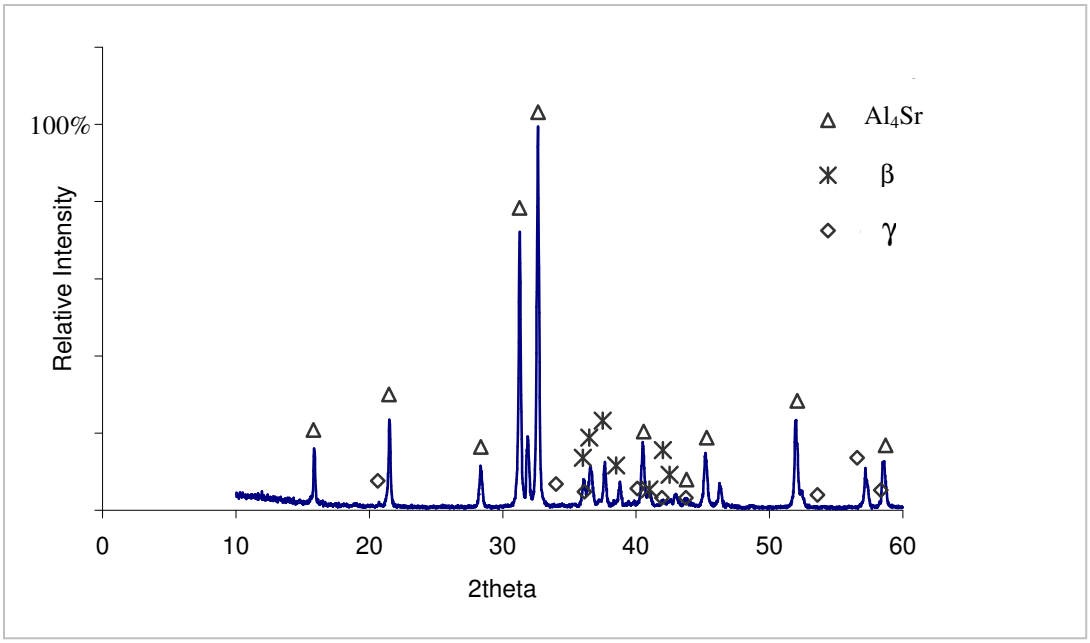

Figure 4-45: XRD pattern of sample 16 (11/30/59 Sr/Mg/Al wt.%).

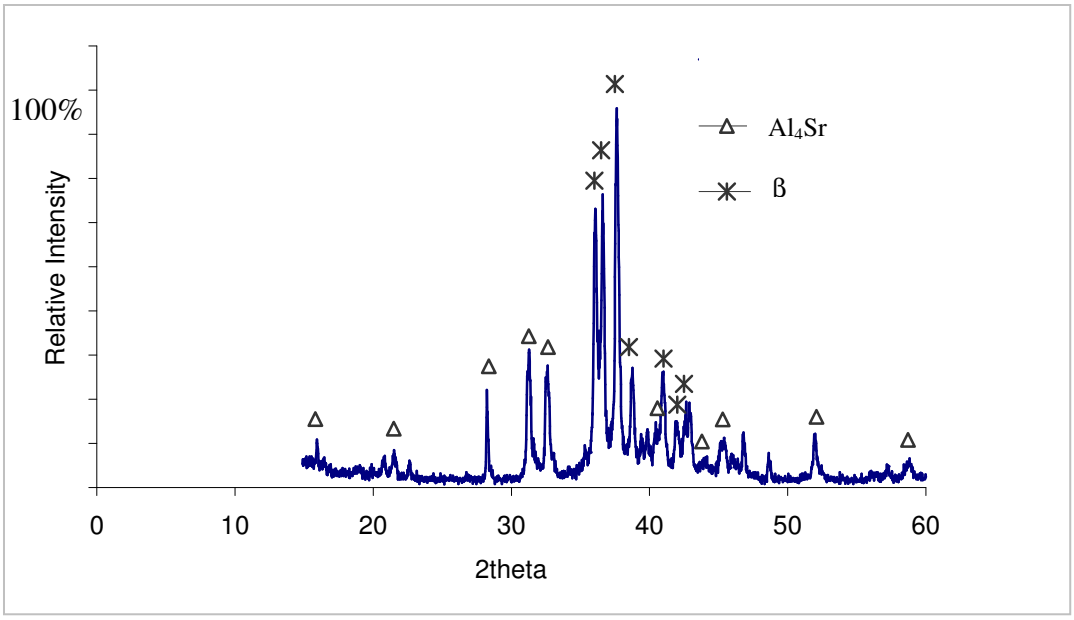

Figure 4-46: XRD pattern of sample 17 (31.18/14.42/54.4 Sr/Mg/Al wt.%).

Figures 4-47 to 4-49 show the optical micrograph of samples 15,16 and 17. All the micrographs show different phase morphologies. Samples 15, 16 and 17 have plate-like structure and designated as Al_4Sr in this investigation. Sample 17 as shown in Figure 4-49 is rich in Al_4Sr.

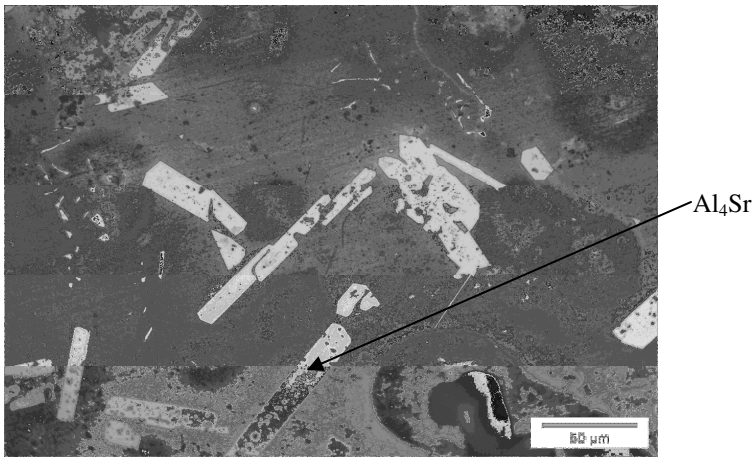

Figure 4-47: Optical micrograph of sample 15.

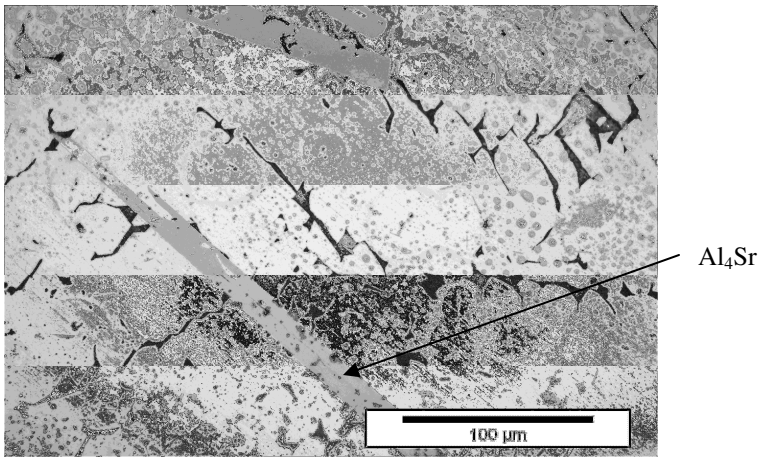

Figure 4-48: Optical micrograph of sample 16.

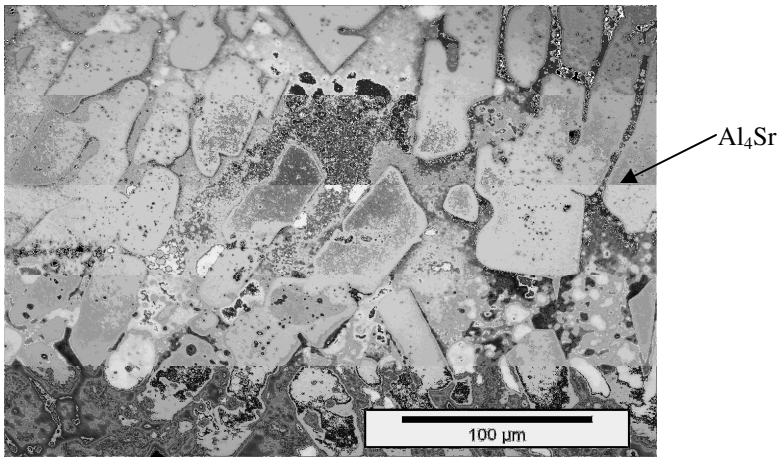

Figure 4-49: Optical micrograph of sample 17.

4.4 Samples in (Al)+Al_4Sr+β phase field

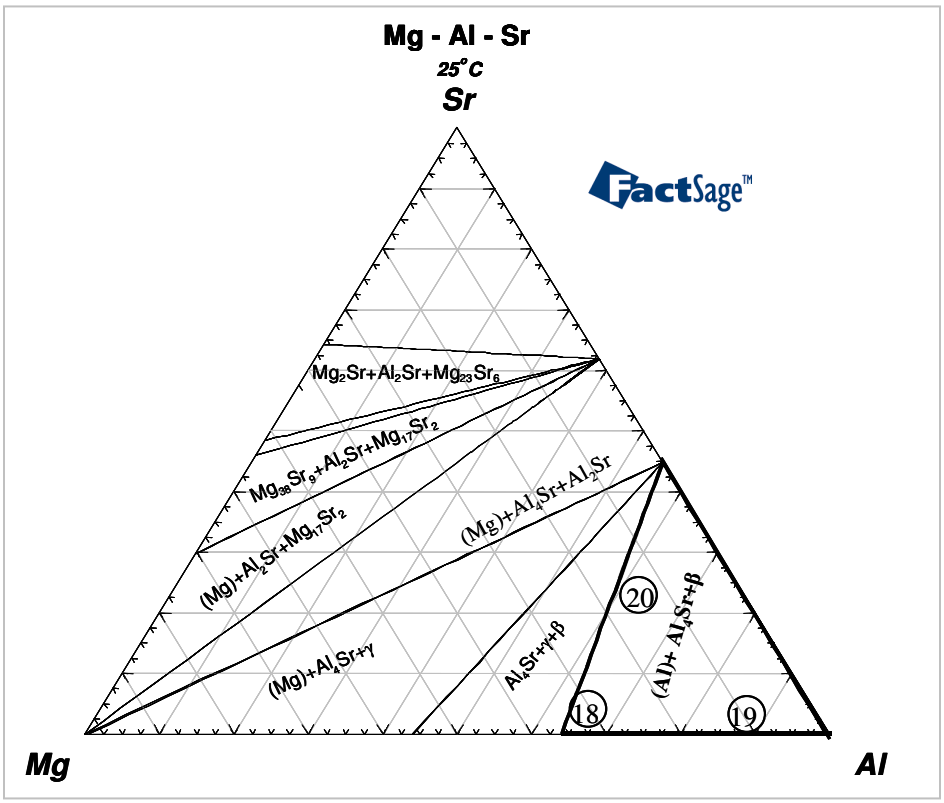

Figure 4-50: Isothermal section at 25°C showing samples in (Al)+ Al_4Srγ+β phase field.

Figure 4-50 shows three samples that have been investigated in (Al)+Al_4Sr+β phase field. A DSC spectrum of sample 18 is shown in Figure 4-51. Two samples reported by Makhmudov *et al.* [19] as ternary eutectic have been prepared. Among these samples only sample 18 (4.56/31.63/63.81 Sr/Mg/Al wt.%) shows eutectic behavior where the DSC heating and cooling run show one single invariant reaction as shown in Figure 4-51. But the thermodynamic calculation of this sample shown in Figure 4-52 did not comply with experimental result. If a ternary eutectic is predicted by thermodynamic calculation then all the three phases should have precipitated at same temperature. Here only (Al) and β precipitated at the same temperature.

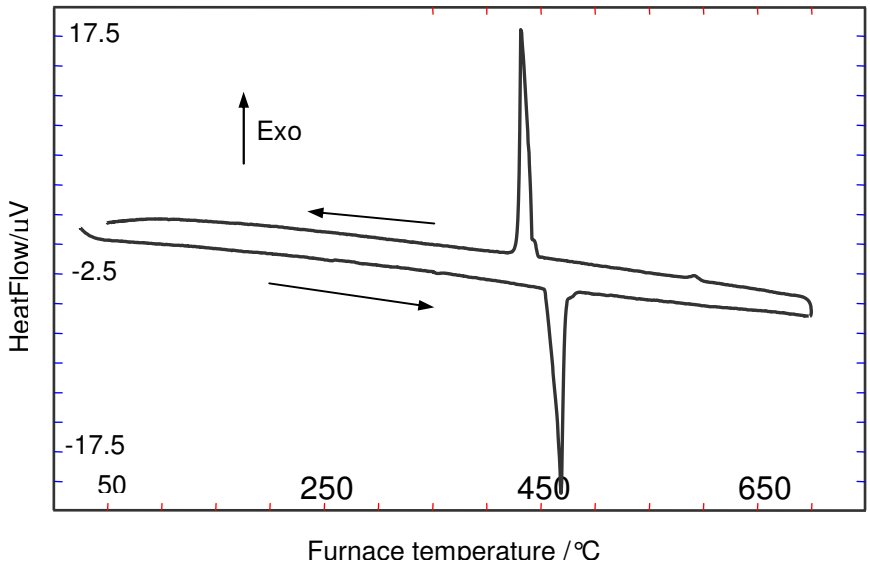

Figure 4-51: DSC spectra of sample 18 (4.56/31.63/63.81 Sr/Mg/Al wt.%) during heating and cooling.

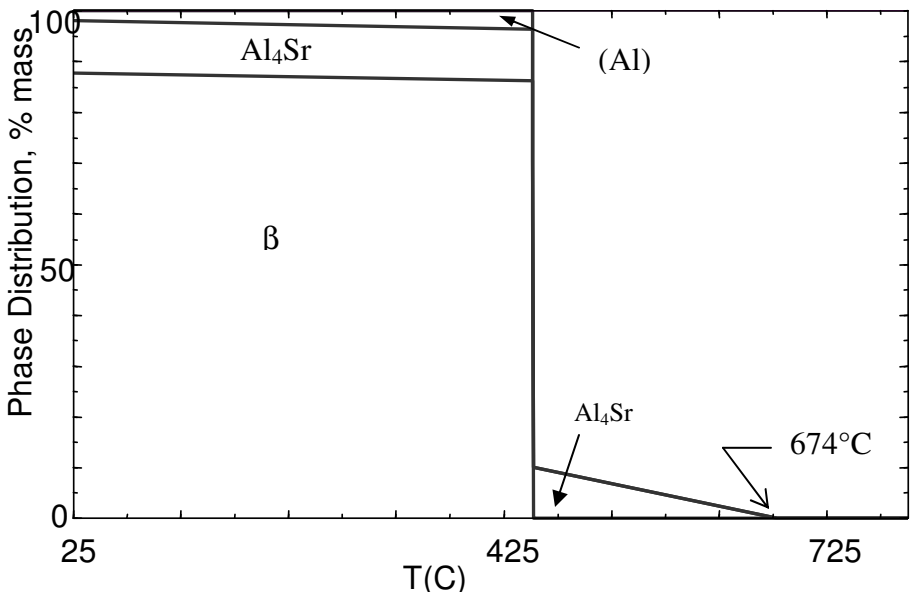

Figure 4-52: Phase assemblage diagram of sample18.

DSC spectra and phase assemblage diagram of samples 19 and 20 are shown in Figures 4-53 and 4-54. The liquidus temperature of sample 19 is quite close to the

calculated temperature whereas, the liquidus temperature of sample 20 did not show good agreement. Furthermore, the number of transformations did not agree with the thermodynamic predictions.

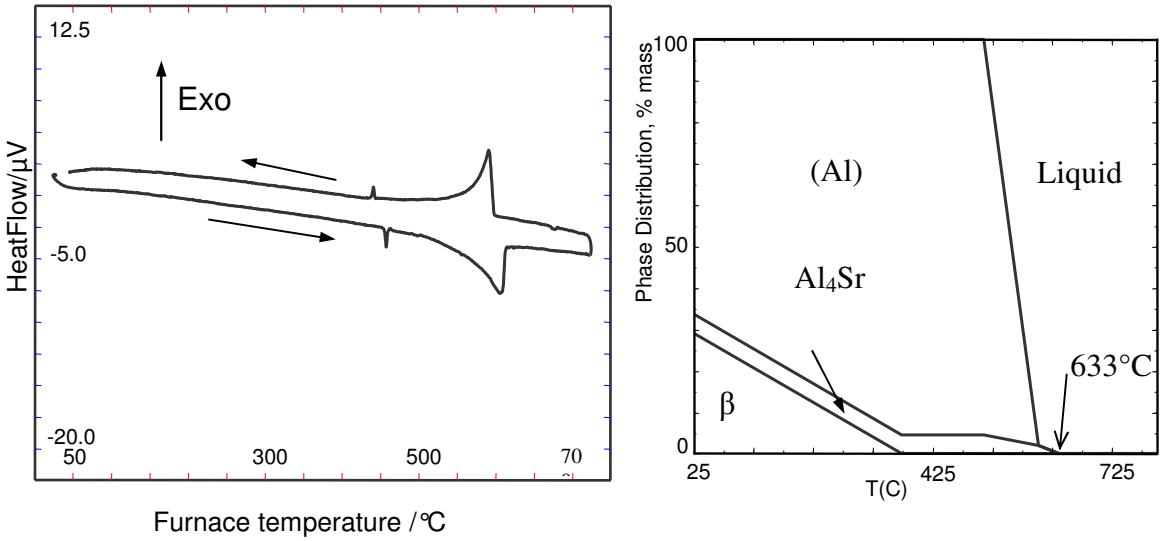

Figure 4-53: (a) DSC spectra and (b) phase assemblage diagram of sample 19.

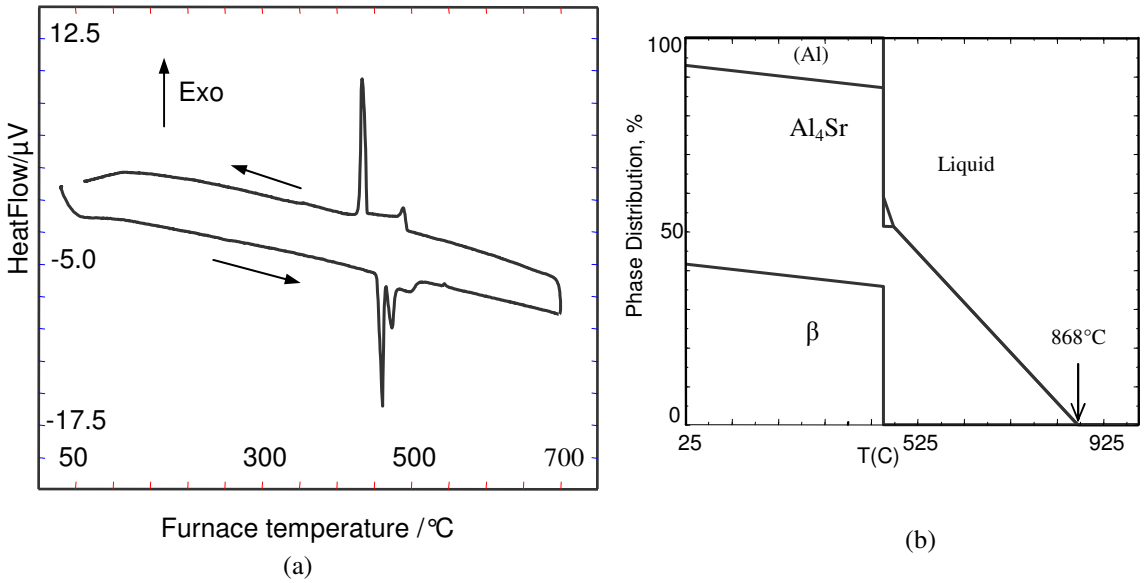

Figure 4-54: (a) DSC spectra and(b) phase assemblage diagram of sample 20.

XRD patterns as shown in Figures 4-55 and 4-56 confirmed that sample 19 and sample 20 have all the three phases predicted by the thermodynamics. Sample 18 was identified positively with Al_4Sr and β, whereas (Al) could not be identified. This may be because this sample is away from (Al) and close to phase boundary of the (Mg)+γ+β phase field.

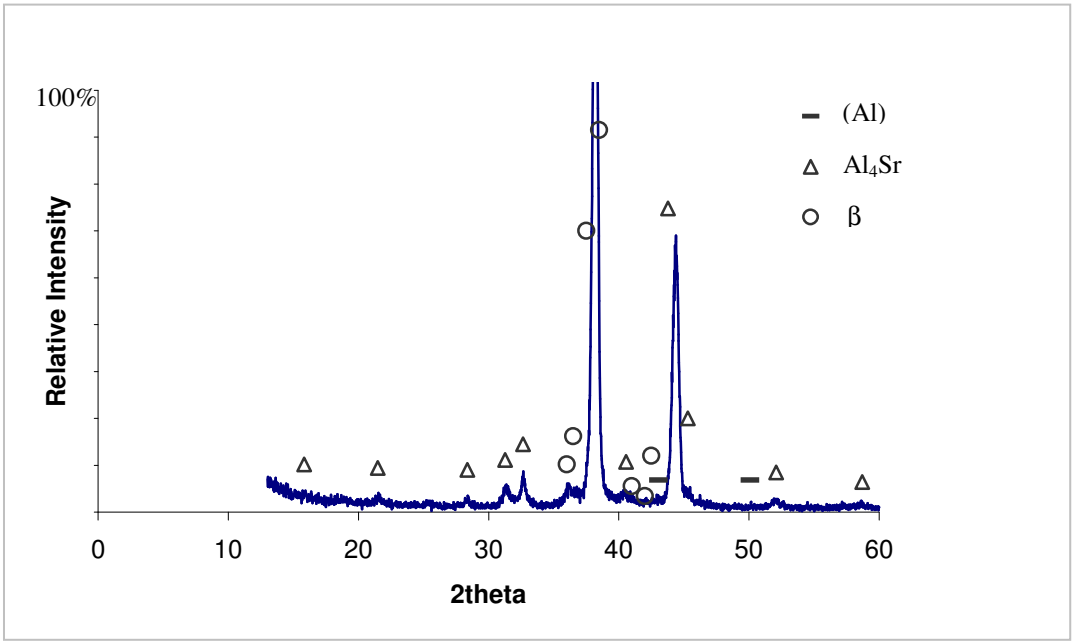

Figure 4-55 : XRD pattern of sample 19 (2.04/10.80/87.16 Sr/Mg/Al wt.%).

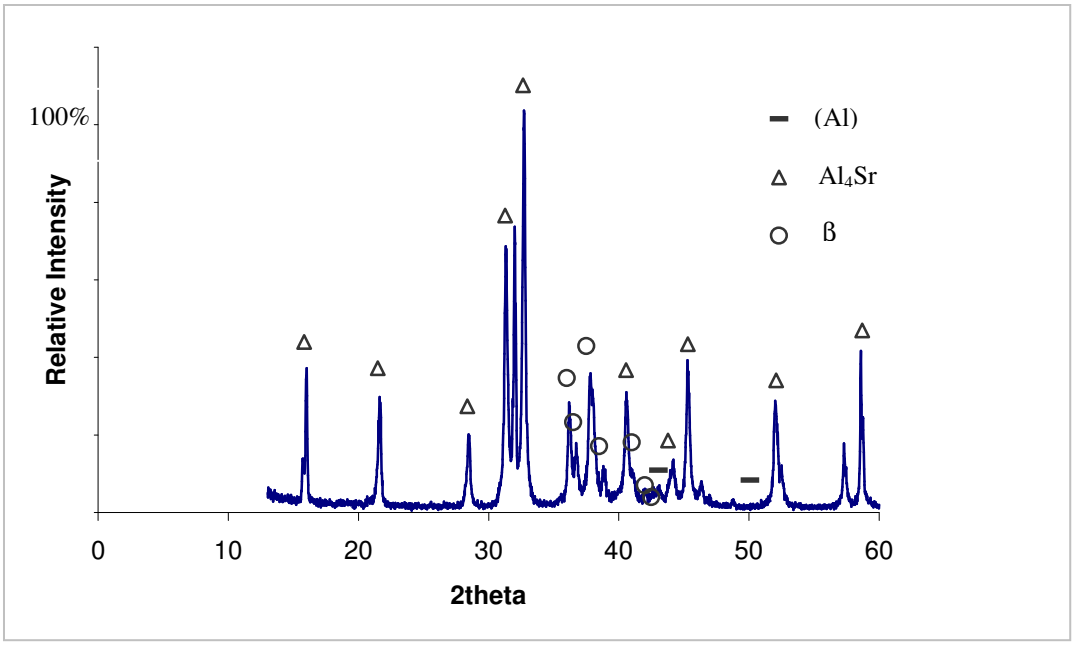

Figure 4-56: XRD pattern of sample 20 (23/15/62 Sr/Mg/Al wt.%).

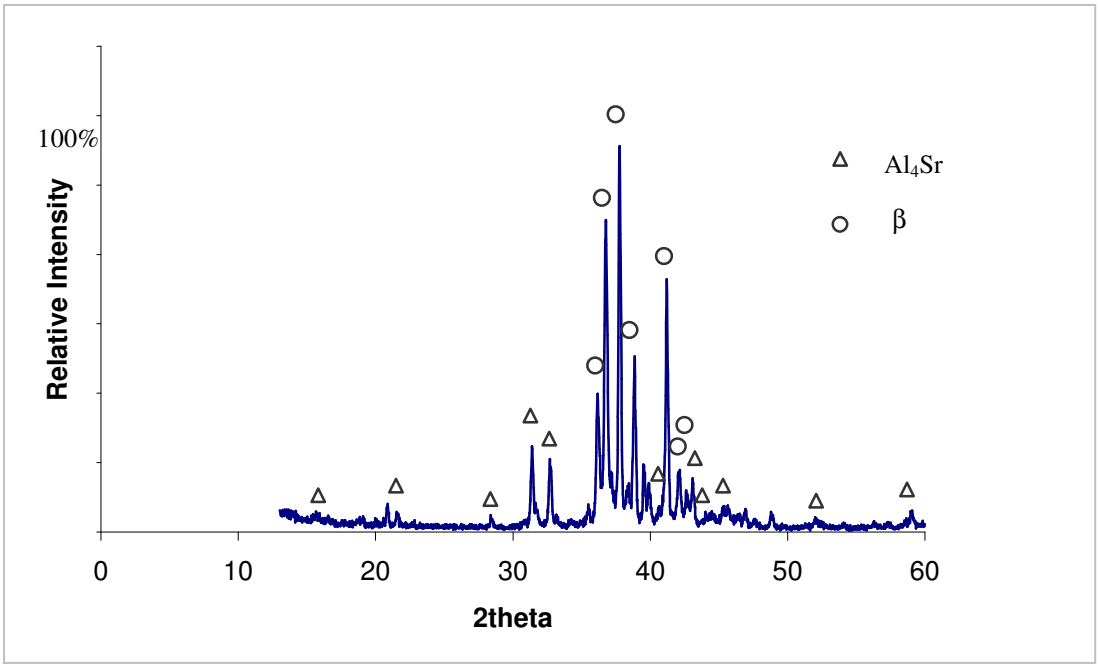

Figure 4-57: *XRD pattern of sample 18 (4.56/31.63/63.81 Sr/Mg/Al wt.%).*

The microstructures of samples 18, 19 and 20 are shown in Figures 4-58 to 4-60. Different microstructure was observed when the composition has been changed. It is very much apparent that the plate-like matrix is Al_4Sr since it was the common phase in most of the investigated samples. It is necessary to use SEM-EDX or microprobe in order to identify the other phases.

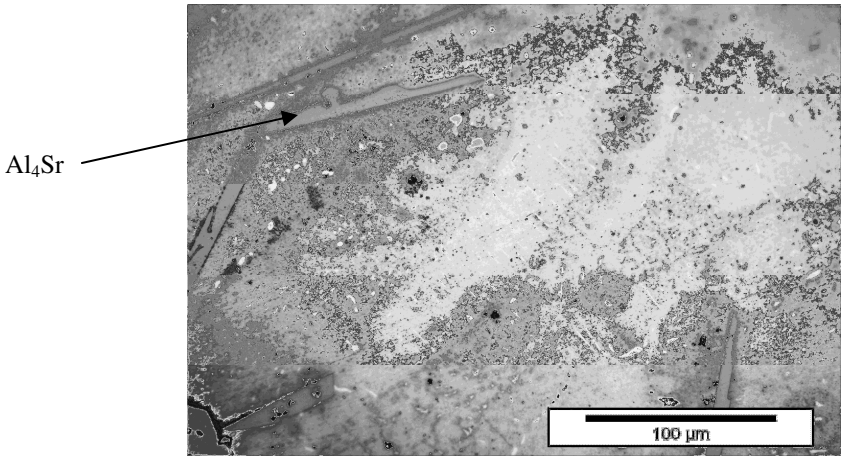

Figure 4-58: Optical micrograph of sample 18.

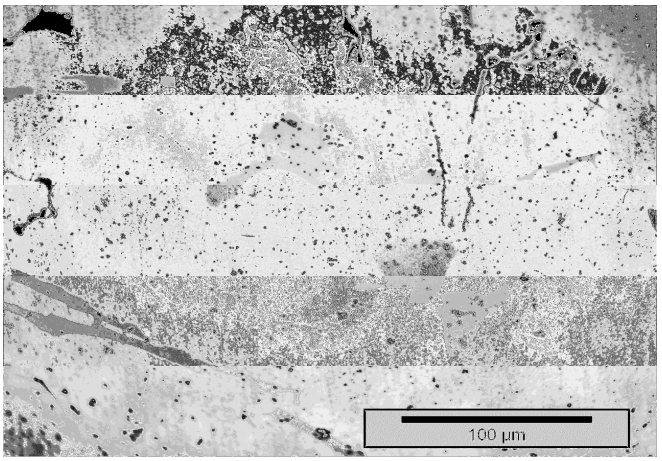

Figure 4-59: Optical micrograph of sample 19.

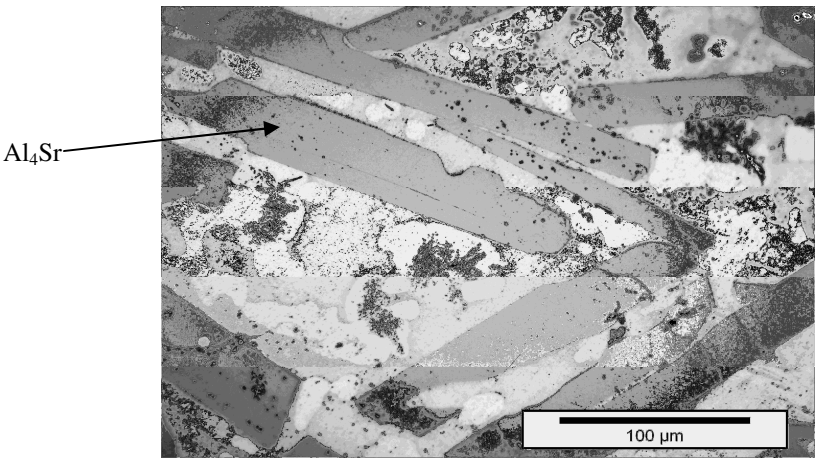

Figure 4-60: Optical micrograph of sample 20.

4.5 Samples in (Mg)+Al_2Sr+ $Mg_{17}Sr_2$ phase field

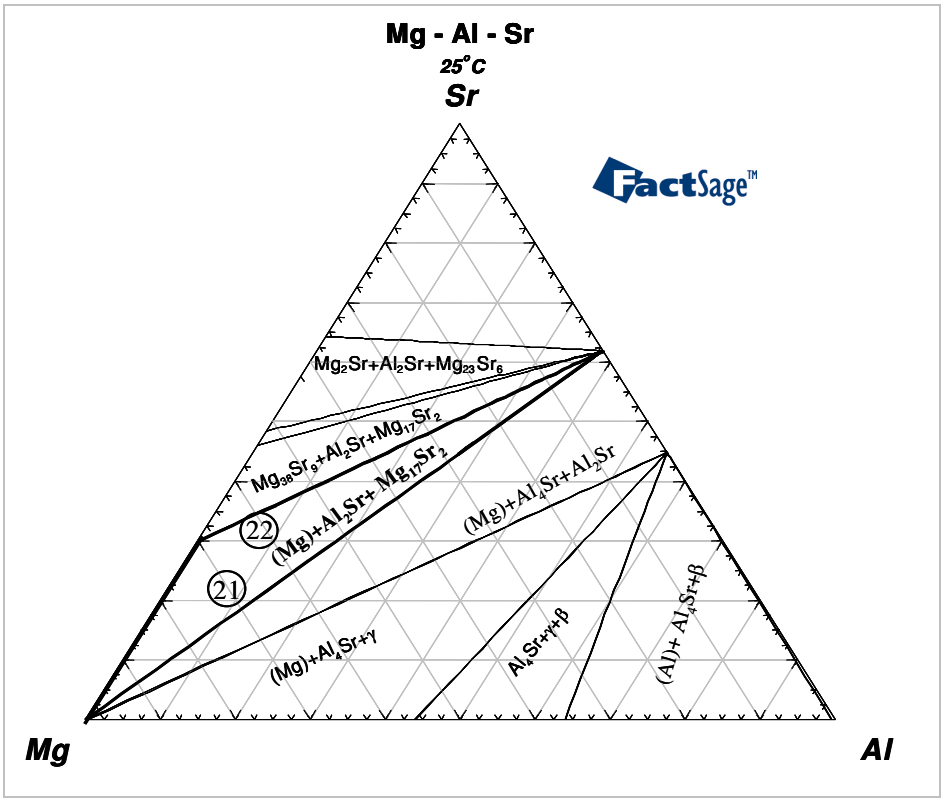

Figure 4-61: Isothermal section at 25°C showing samples in (Mg)+Al_2Sr+$Mg_{17}Sr_2$ phase field.

Only two samples as shown in Figure 4-61 have been prepared in this phase field. DSC spectra and phase assemblage diagram of sample 21 are shown in Figure 4-62. The liquidus temperature of this sample was registered at 607°C by DSC signals whereas the calculated liquidus temperature is 553°C.

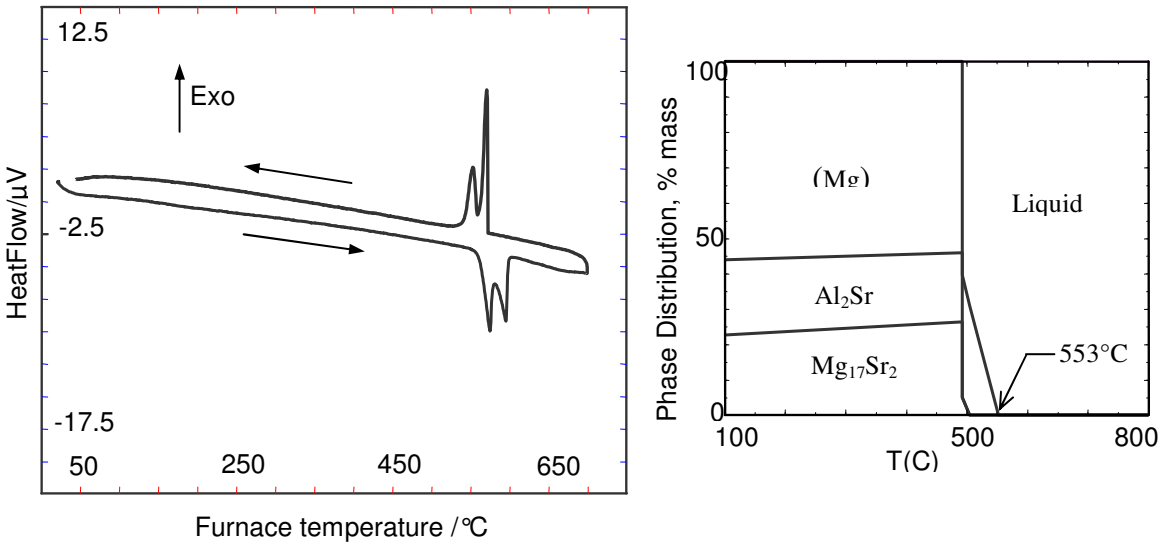

Figure 4-62: (a) DSC spectra and (b) phase assemblage diagram of Sample 21.

DSC spectra and phase assemblage diagram of sample 22 are shown in Figure 4-63 and 4-64 respectively. The DSC signal shows only one peak, hence this composition is at or very close to the eutectic point. From the phase assemblage diagram, although all the three phases did not precipitate at the same temperature, this diagram shows that sample 22 is indeed close to a eutectic composition and thus matches with the DSC result. The enthalpy of melting for this sample was registered as 300J/g.

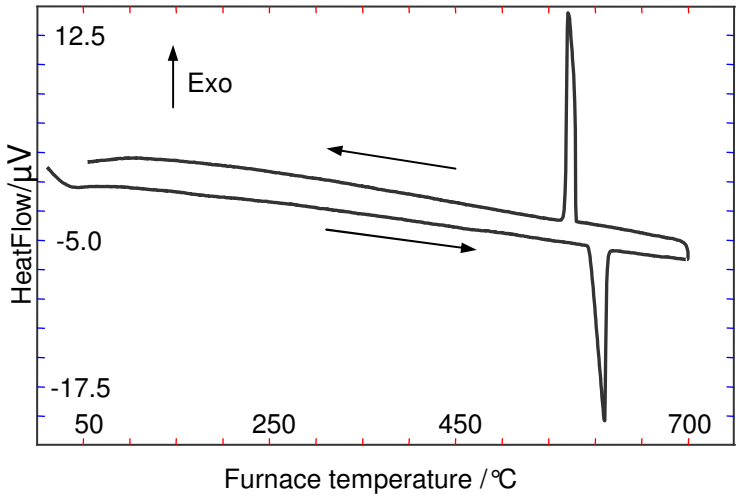

Figure 4-63: DSC spectra of sample 22 (32.74/60.55/6.71 Sr/Mg/Al wt.%) during heating and cooling.

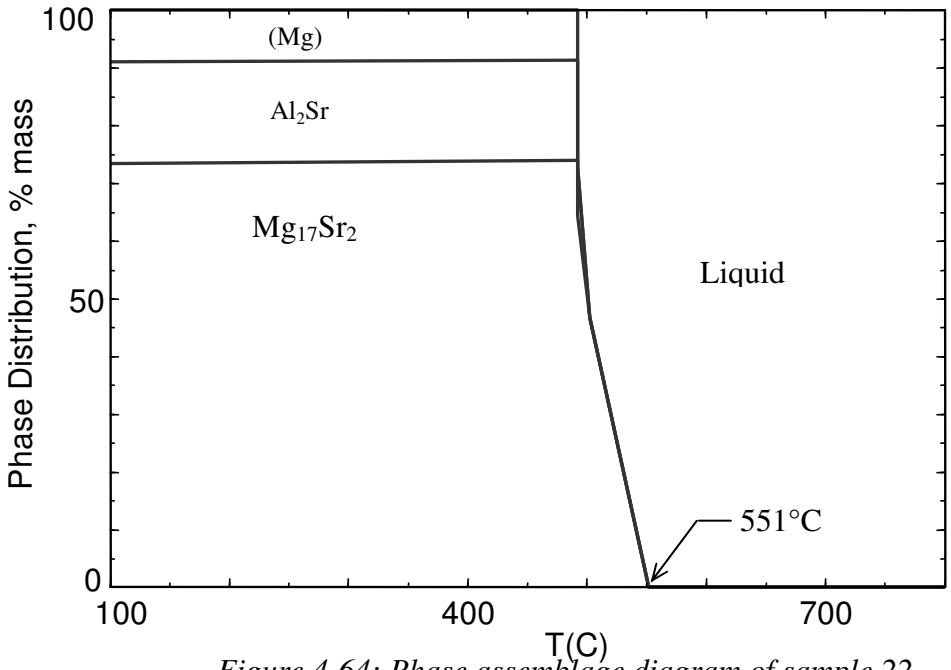

Figure 4-64: Phase assemblage diagram of sample 22.

Sample 21 as shown in Figure 4-65 has been identified with all the three phases predicted by the thermodynamics. However sample 22 has been identified positively with only two phases: (Mg) and $Mg_{17}Sr_2$ and the sample did not contain Al_2Sr. Instead, there are some unknown peaks that do not match with any known binary phase in the Mg-Al-Sr system, therefore these new peaks are identified tentatively as new phase as shown in Figure 4-66. $Mg_{17}Sr_2$ was identified using a hexagonal unit cell (space group $P6_3/mmc$, a = 10.535Å, c=10.356 Å). In this study, it was observed that it is very difficult to identify Al_2Sr compound. This may be due to the reason that near Al_2Sr compound there may be some new binary compound or may be Al_2Sr forms solid solution with the neighboring compounds in the Mg-Al-Sr system.

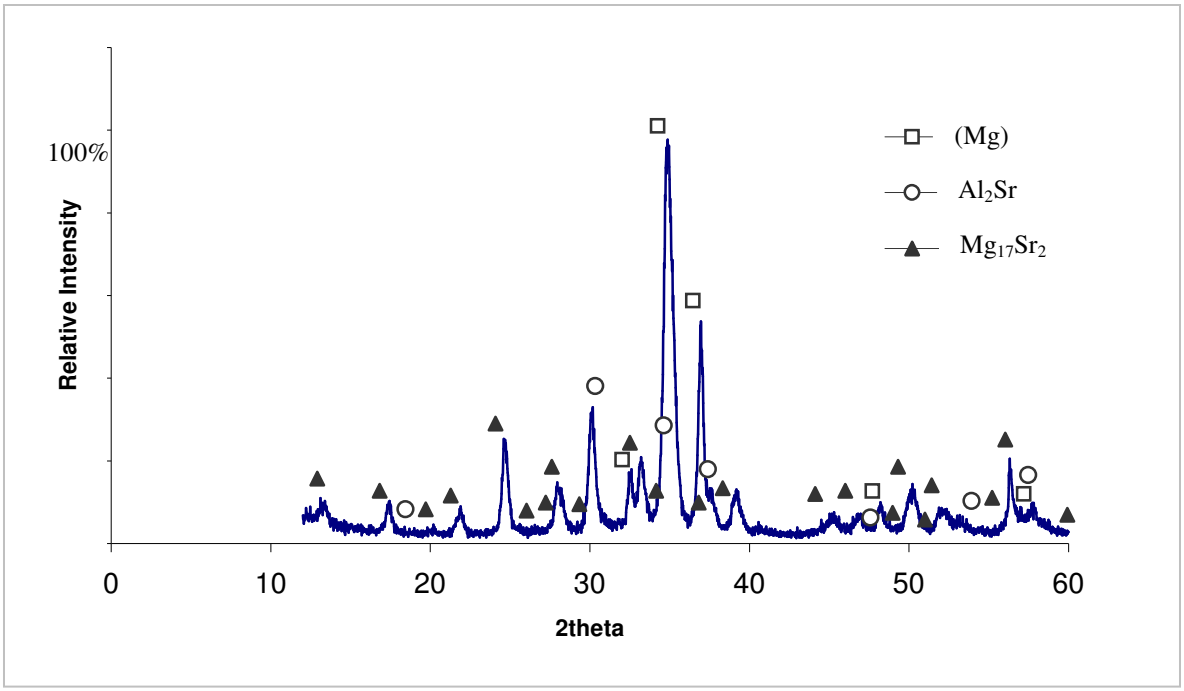

Figure 4-65: X-ray diffraction pattern of sample 21(19.90/72/8.1 Sr/Mg/Al wt.%).

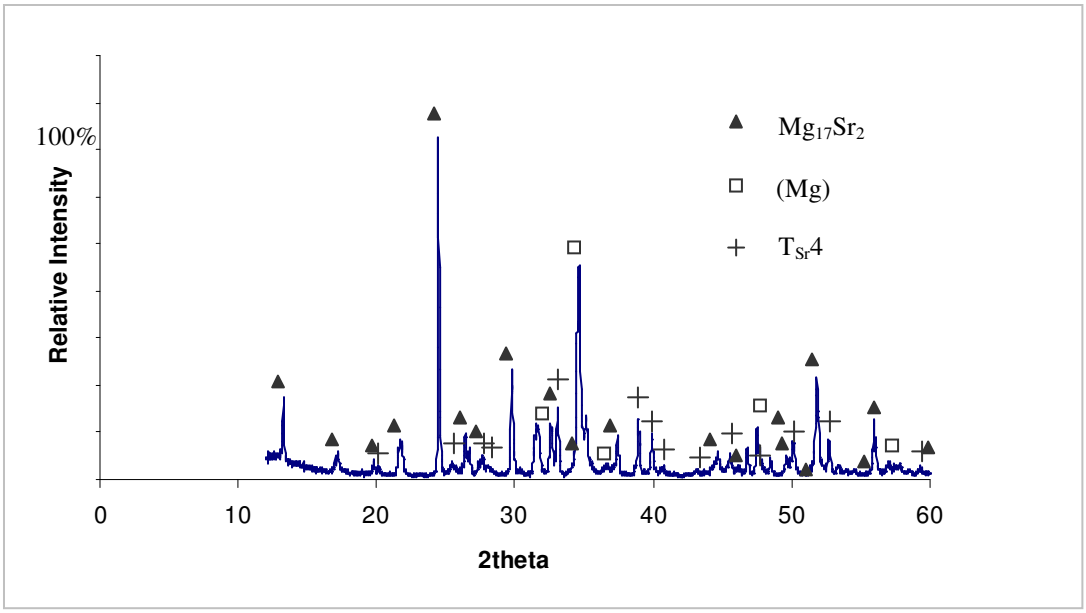

Figure 4-66: X-ray diffraction pattern of sample 22 (32.74/60.55/ 6.71Sr/Mg/Al wt.%)).

Figures 4-67 and 4-68 show the micrograph of samples 21 and 22 respectively. Even though these two samples belong to the same phase field, different microstructures were observed. It can be seen from Figure 4-68 that sample 22 has eutectic morphology. The microstructure of sample 21 is very different compared to the other microstructures and can be clarified using SEM-EDX.

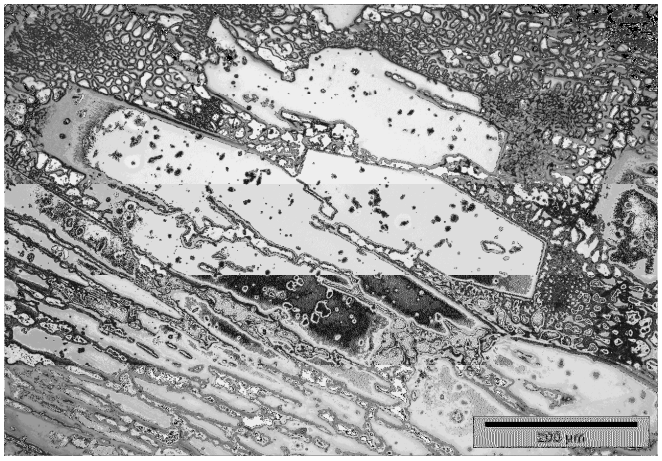

Figure 4-67: Optical micrograph of sample 21.

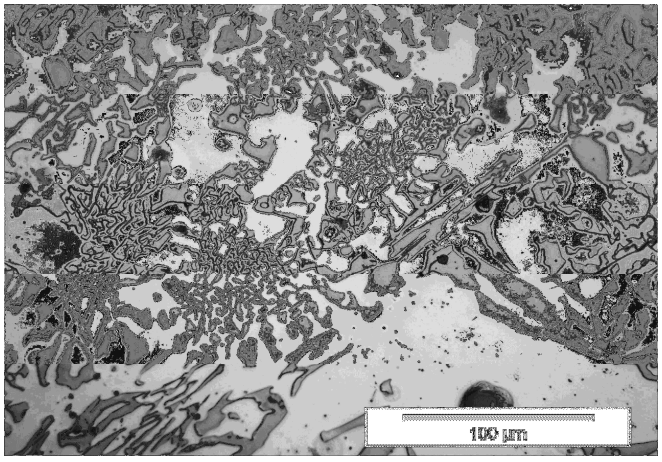

Figure 4-68: Optical micrograph of sample 22.

4.6 Microstructural Evolution

The microstrutural evolution was observed comparing the microstructure of the as-cast with the post-DSC samples. In the as-cast condition, sample 1 has primary (Mg) phase and network of grain boundary phase as shown in Figure 4-69 (a). It can be seen from Figure 4-69 (b) that the morphology and the network nature of the grain boundary phase experienced changes during the heat treatment. The network becomes less complete. The network of the grain boundary phase in the as-cast state collapsed after the heat treatment. The microstructure of sample 4, as shown in Figure 4-70 is characterized as a dendritic microstructure, which has Al_4Sr as the primary phase. Post-DSC sample shows that the intermetallic has grown and the eutectic morphology is more evident. But the most interesting point to be noted is that after the DSC experiment in which the samples were heated from 25°C to 700°C and cooled to room temperature for three times, the microstructure looks similar. It thus indicates that the phases identified in these samples are stable.

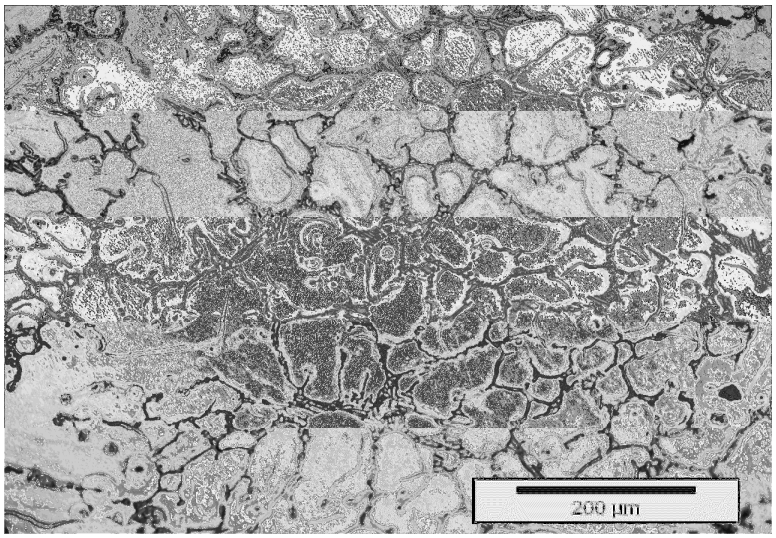

a)

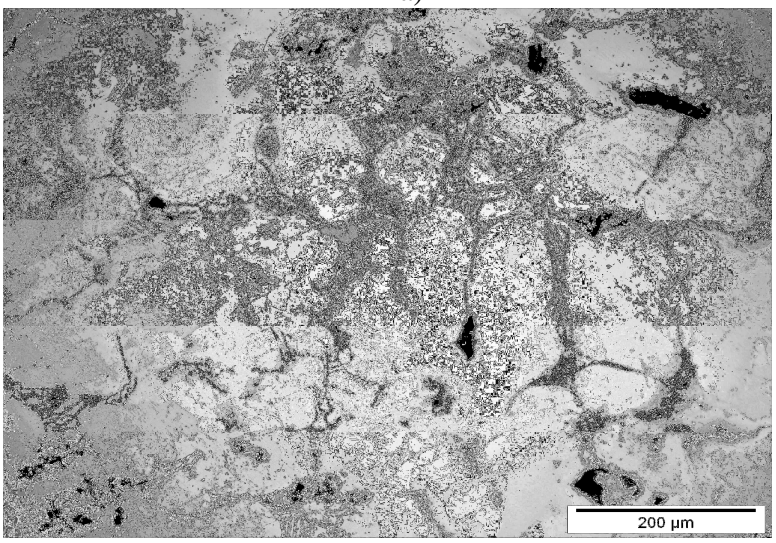

b)

Figure 4-69: Optical micrograph of sample 1 a) as-cast condition, b) post-DSC condition.

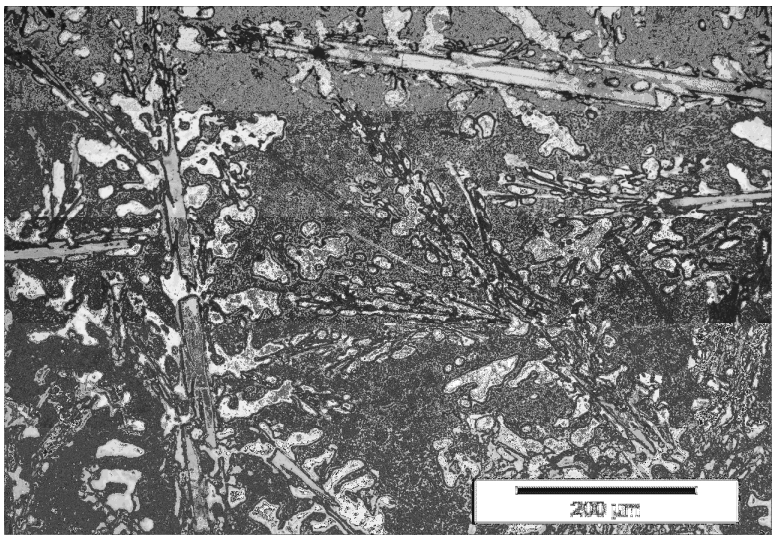

a)

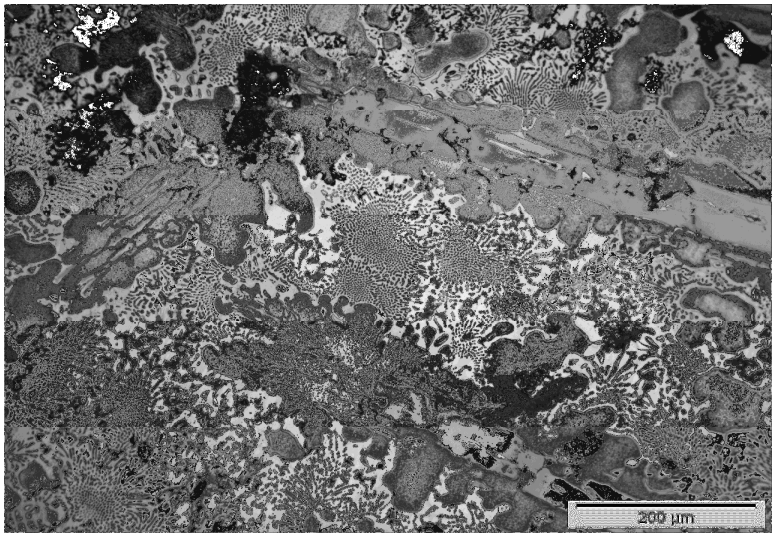

b)

Figure 4-70: Optical micrograph of sample 4 a) as-cast condition, b) post-DSC condition.

4.7 New Ternary Phase Fields

Figure 4-71 shows the ternary phase diagram of the Mg-Al-Sr system, where four new phase fields have been identified using XRD, metallography and DSC. Table 4-4 shows a comparison of some peak positions of $T_{Sr}1$ that matched well with the ternary compound $Al_3Mg_{13}Sr$ designated tentatively by Baril *et al.* [21]. Large solubility of the phase may cause shifting of the peaks. First of all in $T_{sr}2$ and $T_{sr}3$ phase fields, new binary compounds have been predicted by 1st principal method and no experimental information is available till date on them. This new phase may alter the phase field in the calculated Mg-Al-Sr system or may form new ternary phases that have been supported by this investigation. In addition, this is a ternary system and has enormous possibilities to form ternary solid solutions. $T_{sr}4$ phase field is very complex as shown in Figure 2-5, since three stoichiometric compounds remain in very close proximity with each other. The ternary compounds reported by Makhmudov *et al.* [19] were not encountered in this investigation.

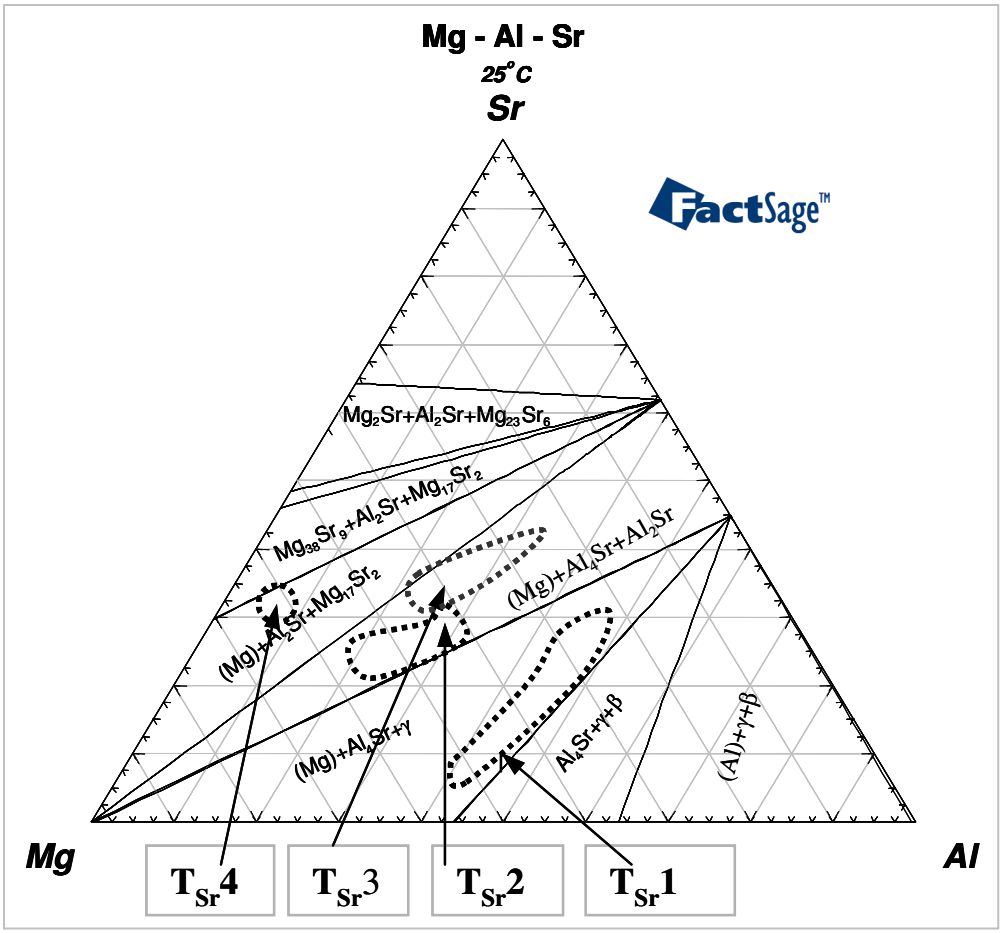

Figure 4-71: New tentative phase fields.

Table 4-4: Comparison of peak position

Ternary phase	Peak position (2theta)
$T_{Sr}1$	**24.16**, 28.02, **30.74**, **35.44**, 37.4, **38.52**, 46.52,**49.06**,53.92
$Al_3Mg_{13}Sr$	24.8, 30.56, 35.28, 39.56, 42.82, 50.8

CHAPTER 5

Conclusions, Contributions and Suggestions for Future Work

5.1 Conclusions

A comprehensive study using DSC, XRD and metallography on the ternary equilibria in the Mg-Al-Sr system was conducted. Based on the experimental results, the following conclusions can be drawn:

1. DSC has permitted real time measurements of the phase change involved in the Mg-Al-Sr system. Onset temperature, enthalpy of melting, liquidus temperaure have been reported.
2. Invariant and univariant reactions in the studied samples were distinguished.
3. Four new phase fields have been identified using XRD and tentatively designated as $T_{Sr}1$, $T_{Sr}2$, $T_{Sr}3$ and $T_{Sr}4$. They may be new ternary soilid solutions or ternary compounds.
4. Al_4Sr and (Mg) were found to be the dominating phases in the investigated alloys. The plate-like crystal structure has been identified as Al_4Sr in most of the samples.
5. Samples 1 and 2 have been identified with (Mg), Al_4Sr and very small amount of γ. Sample 1 is very close to the alloy developed by Baril *et al.* [21] at Noranda. This information may help to setup a window to identify the creep resistant alloy in Mg-Al-Sr syetem.

6. Morphology and the network nature of the grain boundaries have been observed. The microstrutural evolution in two post-DSC samples has been investigated. The identified phases in the as-cast condition were found consistent and thermodynamically stable with the post-DSC sample in the investigated alloys.
7. Thermodynamic calculations e.g. vertical sections and phase assemblage diagrams were obtained using Factsage. The experimental results were compared with the pertinent thermodynamic findings. A considerable discrepancy in transformation temperature was observed. However, the liquidus temperature for few samples agrees well with the experimental results. Furthermore, phase transformations occurring below 400°C were not possible to detect by DSC signals.
8. The literature data were compared with the current experimental results. Two samples were prepared and compared with similar composition of those reported by Makhmudov *et al.* [19]. One of these samples agreed with the current results. Some peak positions of $T_{Sr}1$ matched well with the ternary compound $Al_3Mg_{13}Sr$ designated tentatively by Baril *et al.* [21].
9. Two samples having compositions near or at ternary eutectic points have been identified.
10. Investigation of samples in different phase fields revealed that the extent of the phases is not predicted correctly by the thermodynamic calculations.
11. Predicted phases do not agree with the present XRD results for nine samples that suggests that this system should be remodeled.

5.2 Contributions to Knowledge

- The present work has provided thorough experimental study combined with thermodynamic calculation for a very high potential system. This provided better understanding of the equilibria in this system.
- Four new phase fields have been identified. This will help researchers to narrow down their experimental work and to make key experiments in these phase fields to identify the ternary compounds or solid solutions, which may have direct impact on the creep resistance of the Mg-Al-Sr-based alloys.

5.3 Suggestions for Future Work

- The microstructures can be investigated by EDS or microprobe to positively identify all the phases in the Mg-Al-Sr system.
- Further experimental study is needed to identify the crystal structure and the nature of the ternary phases in the Mg-AL-Sr system. Key experiments can be conducted by selecting samples nearby the new phase fields to identify the crystal structure and the chemical composition.
- A thermodynamic modeling of Mg-Al-Sr system can be carried out to incorporate all the new findings.
- The microstructures of the other post-DSC samples can be investigated to check whether the phases are thermodynamically stable or not.

REFERENCES

1. Gradinger, R. and Stolfig, P., Magnesium Wrought Alloys for Automotive Applications, *Proceedings of the Minerals, Metals & Materials Society* (TMS), pp.231-236, 2003.
2. Pekguleryuz, M., Baril, E., Labelle, P. and Argo, D., Creep Resistant Mg-Al-Sr Alloys, *Journal of Advanced Materials – SAMPE,* 35(3), pp.32-38, 2003.
3. Aghion, E., Bronfin, B., Friedrich, H. and Schumann, S., Dead Sea Magnesium Alloys Newly Developed for High Temperature Applications, *Proceedings of the Minerals, Metals & Materials Society* (TMS), pp.177-182, 2003.
4. Mordike, B.L.**,** Creep Resistant Magnesium Alloys, *Materials Science Engineering A*, 324(1-2), pp.103-112, 2002.
5. Das, S., Magnesium for Automotive Applications: Primary Production Cost Assessment, *Journal of Materials*, 55(11), pp.22-26, 2003.
6. Zhang, Z., Couture, A., An Investigation of the Properties of Mg-Zn-Al Alloys, *Scripta Materialia*, 39(1), pp.45-53, 1998.
7. Blum, W., Watzinger, B., Grossman, B., Haldenwanger, H.G., Comparative Study of Creep of the Die-cast Mg-alloys AZ91, AS21, AS41, AM60 and AE42, *Materials Science and Engineering A*, 319, pp.735-740, 2001.
8. Pekguleryuz, M., Development of Creep Resistant Magnesium Alloys- An Overview, Noranda Technology Center, Quebec, Canada.
9. Pekguleryuz, M. and Renaud, J., Creep Resistance in Mg-Al-Ca Casting Alloys, *Proceedings of the Minerals, Metals & Materials Society* (TMS), pp.279-284, 2000.

10. Gröbner, J., Schmid-Fetzer, R. and Kevorkov, D., Experimental Investigation and Thermodynamic Calculation of Ternary Al-Ca-Mg Phase Equlibria, Ternary Al-Ca-Mg Phase Equlibria, *Z. Metallkde***,** 94, pp.976-982, 2003.
11. Zakulski, W., Thermodynamics of the Al-Mg-Sr Liquid Solutions, *Proceedings of the CALPHAD XXXIII*, Paper: 7.4, June 2004.
12. Gröbner, J., Schmid-Fetzer, R. and Kevorkov, D., Focused Development of Magnesium Alloys Using CALPHAD Approach, *Advanced Engineering Materials*, 3, pp.947-961, 2001.
13. Gröbner, J., Schmid-Fetzer, R. and Kevorkov, D., The CALPHAD Approach in the Focused Design of Magnesium Alloys. *Proceedings of the Minerals, Metals & Materials Society* (TMS), pp. 241-253, 2001.
14. FactSage 5.3, http://www.factsage.com, 2004.
15. Prince, A. and Nikitina, N., Aluminum-Magnesium-Strontium, *Ternary Alloys: A Comprehensive Compendium of Evaluated Constitutional Date and Phase Diagram*, 16, pp.413-425, New York 1998.
16. Makhmudov, M.M., A.V. Vakhovob, A.V., T.D. Dzhuraev and Ganiev, I.N., The Combined Solubility of the Components in the Mg-rich and Al-rich Regions of the Mg-Al-Sr System, *Dokl. Akad. Nauk Tadzh,* SSR 23, pp.25-28, 1980.
17. Makhmudov, M.M., A.V. Vakhovob, A.V., T.D. Dzhuraev, Liquidus Surface of Aluminum and Magnesium Phases of the Magnesium-Aluminum-Strontium Diagram, *Doklady Akademi Nauk Tadzhikskoi SSR*, 24 (7), pp. 435-438. 1981.

18. Makhmudov, M.M., A.V. Vakhovob, A.V., T.D. Dzhuraev, Phase Equilibrium in the Magnesium-Aluminum-Strontium System, *Russian Metallurgy,* 6, pp. 209-212, 1981.

19. Makhmudov, M.M., A.V. Vakhovob, A.V., T.D. Dzhuraev, Examination of the Quasibinary Sections of the Mg-Al-Sr System, *Russian Metallurgy,* 1, pp. 122-124,1982.

20. M Makhmudov, M.M., A.V. Vakhovob, A.V., T.D. Dzhuraev, Determination of the Liquidus Surface in the Sr-Mg_2Sr-Al_4Sr System by the Simplex Method, Zavod. Lab. 48(10),61-62, 1982.

21. Baril, E., Labelle, P. and Pekguleryuz, M., Elevated Temperature Mg-Al-Sr: Creep Resistance, Mechanical Properties, and Microstructure, *Journal of Materials,* 55(11), 34-39, 2003.

22. Landriault E., Characterization of the Magnesium Alloy, Masters Thesis, Ecole Polytechnique, 2004.

23. Chartrand, P. and Pelton, A.D., Critical Evaluation and Optimization of the Thermodynamic Properties and Phase Diagrams of the Al-Mg, Al-Sr, Mg-Sr and Al-Mg-Sr Systems, *Journal of Phase Equilibria*, 5(6), pp.591-605, 1994.

24. Koray, O., Investigation in Mg-Al-Ca-Sr Stsrem by Computational Thermodynamics Approach Coulped with First-Principles Energetics and Experiments, PhD Thesis, The Pensylvania State University, 2004.

25. Murray. J.L., The Al-Mg (Aluminum-Magnesium) System, *Bulletin of Alloy Phase Diagrams*, 3(1), pp.60-74, 1982.

26. Saunders, N., A review and thermodynamic assessment of the Al-Mg and Mg-Li systems. *CALPHAD,* 14(1), pp. 61-70, 1990.

27. Ludecke, D. and Hack, K, A., Thermodynamic Evaluation of the Al-Mg System, *Zeitschrift fuer Metallkunde*, 77, pp.145-161,1986.

28. Zho, Y. and Chang, Y.A., Thermodynamic Calculation of the Al-Mg Phase Diagram, *CALPHAD*, 17(2), pp.161-174,1993.

29. Goel, N.C., Cahoon J.R and Mikkelsen, An Experimental Technique for the Rapid Determination of Binary Phase Diagrams: The Al-Mg-System, *Metallurgical Transactions A*, 20A, pp.197-203, 1998.

30. Moser, Z., Zakulski, W., Gasior, W., Panek, Z., Matsuda, I., Fukuda, Y., Iida, T. and Botor, J., New Thermodynamic Data for Liquid Aluminum-Magnesium Alloys from EMF, Vapor Pressures and Calorimetric Studies, *Journal of Phase Equilibria,* 19 (1), pp.38-47, 1998.

31. Su, H. L., Harmelin, M., Donnadieu, P., Baetzner, C., Seifert, H. J., Lukas, H. L. and Effenberg, G., Experimental Investigation of the Mg-Al Phase Diagram from 47-63 at.% Al, *Journal of Alloy Compounds*, 247(1-2), pp.57-65, 1997.

32. Tomassz, C., Zakuiski, W., Bielanska, E., Study of the Thermal Stability of the Phases in the Mg-Al System, *Journal of Phase Equilibria*, 24(3), pp. 249-254, 2003.

33. Liang, P. and Su, H.L., Experimental investigation and thermodynamic calculation of the central part of the Mg-Al phase diagram, *Zeitschrift fuer Metallkunde*, 89(8), pp. 536-540, 1998.

34. Zhong, Y., Koray, O., Liu, Z.K. and Luo, A., Computational Thermodynamics and Experimental Investigation of the Mg-Al-Ca-Sr Alloys. *Proceedings of the Minerals, Metals & Materials Society* (TMS), pp. 69-73, 2002.

35. Alcock, C.B. and Atkin, V.P., The Al-Sr (Aluminum-Strontium) System, *Bulletin of Alloy Phase Diagrams,* 10(6), pp.624-630, 1989.

36. Closset, B. and Dugas, H., The Aluminum-Strontium Phase diagram, *Metallurgical Transaction A,* 17, pp.1250-1253, 1986.

37. Burylev, B.P., Vakhobov, A.V., and Dzhuraev, T.D., Thermodynamic Activities of the Components in Aluminum with Barium and Strontium, *Zh. Fiz. Khim.,* 48(6), pp.809-811, 1974.

38. Vakhobov A.V. and Dzhuraev, T.D., Vigdotovich, V.N., Study of the Vapor Pressures over Alloys of the Aluminium-Strontium System, *Zhur. Fiz. Khim,* 48(9), pp.2204-2207, 1974.

39. Srikanth, S. and Jacob, K.T., Thermodynamics of Aluminum-Strontium Alloys. *Z. Metallkd.* 82(9), pp.675-683, 1991.

40. Wang, C., Jin, W. and Du, Y.,Thermodynamic Modeling of the Al-Sr system. *Journal of Alloys and Compounds,* 358(1-2), pp.288-293, 2003.

41. Zhang, Z., Bian, X. and Wang, Y., Formation of microstructure of an Al-10wt% Sr Alloy Prepared by Electrolysis and Mixing, *Materials Letters,* 57(7), pp. 1261-1265, 2003.

42. Zhang, J., Calculation Model Of Mass Action Concentration For Mg-Al, Sr-Al And Ba-Al Melts And Determination Of Their Thermodynamic Parameters. *Journal of Iron and Steel Research International,* 10(2), pp.5-9, 2003.

43. Wolverton, C. and Yan, X.Y., Incorporating First-principle Energetics in Computational Thermodynamics Approaches, *Acta Materialia*, 50(9), pp. 2187-2197, 2002.

44. Liu, Z.K., Zhong, Y., Wolverton, C. and Chang, A.Y., A Combine CALPHAD/First-Principles Remodeling of the Thermodynamics of Al-Sr: Unsuspected Ground State Energies by Rounding Up the (Un)Usual Suspects, Acta Materialia, 52(9), pp. 2739-2754, 2004.

45. Nayeb-Hashemi, A.A. and Clark, J.B., The Mg-Sr (Magnesium-Strontium) System. *Bulletin of Alloy Phase Diagram.* 7(2), pp. 149-156,1986.

46. Vosskhuler, H, The Structure of the Magnesium-rich alloys of Magnesium and Strontium, *Metallwirtschaft*. 18, pp.377-378, 1939.

47. Brown J.W., The Strontium-Magnesium Phase System, PhD Thesis, Syracuse University, 1973.

48. Klemm, W. and Dinekelocker, F., On Alloys of Magnesium with Calcium Strontium and Barium. *Z. Anorg*. *Chem*., 255, pp.2-12, 1947.

49. Sommer, F., Determination of Thermodynamic Activities of Liquid Alloys in the Systems Mg-Sr and Ba-Mg, *Z. Metallkd.,* 71(2), pp. 120.123, 1980.

50. Parvez, M.A., Essadiqi, E. and Medraj, Experimental Investigation of Ternary Mg-Al-Sr Phase Diagram, *Proceedings of the CSME Forum*, pp.829-838, 2004.

51. Wang, X., Parvez, M.A., Essadiqi, E. and Medraj, A Differential Scanning Calorimeter Study of Mg-Al-Ca Ternary System, *Proceedings of the* CSME *Forum*, pp.819-828, 2004.

52. Lindermann, A, Schmidt, J, Todte, M, Thermal Analytical investigations of the Magnesium Alloys AM60 and AZ91 including the Melting Range, *Thermochimica Acta*, 382(1-2), pp.269-275, 2002.

53. Gröbner, J., Schmid-Fetzer, R. and Kevorkov, D., The Al-Li-Si System: Experiemntal Study and Thermodynamic Calculation of the Polythermal, *Journal of Solid State Chemistry,* 156, pp. 506-511, 2001.

54. Tkachenko, V.G., Khoruzhaya, V.G., Meleshevich, K.A., Karpets, M.V., and Frizel, V.V., Phase Equilibria in Mg-Al-Ca System, *Powder Metallurgy and Metal Ceramics*, 42 (5-6), pp.268-273, 2003.

55. D.A. Graham, J.Y. Yao, and Couper: A DSC and TEM Study of Precipitation in T1 and T4 Treated Al-Mg-Si Alloys, *Materials Science Forum*, 331-337, pp.1083-1088, 2000.

56. Ogawa, N., Miki, T., Nagasaka, T. and Hino, M., Activity Measurement of the Constituent in Molten Sn-Mg-Zn Ternary Lead Free Solder Alloys by Mass Spectrometry. *Materials Transactions*, 43(12), pp.3227-3233, 2002.

57. Shujian, T., Shixiang, L. and Chaogui, Z., Investigation on the Phase Diagram of the Ternary System $LaCl_3$-NaCl-LiCl. *Journal of Alloys and Compounds,* 279(2), pp.127-131, 1998.

58. Vassilev, V., Feutelais, M., Sghaier, B. and Legendre, B., Thermodynamic Investigation in In-Sb, Sb-Sn and In-Sb-Sn Liquid Systems, *Journal of Alloys and Compounds,* 314(1-2), pp.198-205, 2001.

59. Ohinuma, I., Fujita, Y., Mitusui, H., Ishikawa, K., Kainuma, R. and Ishida, K., Phase Equlibria in the Ti-Al Binary System. *Acta Materalia.* 48(12), pp. 3113-3123, 2000.

60. Dichi, E., Wojakowska, A. and Legendre, B., Study of the Ternary Germanium-Antimony-Tin: Experimental Phase Diagram. *Journal of Alloys and Compound.* 320(2), pp.218-223, 2001.

61. Wiesner, U., Beiger, W. and Krabbes, G., Determination of Phase Diagrams by Heat Evaluation from DTA. *Thermochimica Acta.* 290(1), pp.115-121, 1996.

62. Wojakowska, A., Krzyzak, E. and Wojakowska, A., Phase Diagram for the CuBr-CsBr System. *Thermochimica Acta*. 344(1-2), pp.55-59, 2000.

63. Nakasone, K. Shiokawa, K., Urabe, Y. and Nemoto, N., Symmetrical Ketone/n-Alkane System. 1. Phase Diagrams from DSC, *The* J*ournal of Physical Chemistry*. *B,* 104(31), pp.7483-7489, 2000.

64. Unlu, N., Genc, A. and. Ovecoglu, M.L., Microstructural Evolution During Annealing of the Melt-Spun Ternary Hypoeutectic l-7.6Si-3.3Fe (in Wt%) Alloy. *Journal of Alloys and Compounds.* 343(1-2), pp. 223-233, 2002.

65. Yao, J.Y., Graham, D.A. and Couper, A DSC and TEM Study of Precipitation in T1 and T4 Treated Al-Mg-Si Alloys, *Materials Science Forum*. 331-337, pp.1083-1088, 2000.

66. http://user.chollian.net/~jpkim3/tascience/applist/dsccruv1.htm

67. Freidina, E.B. and Fray, D.J., Study of the Ternary System $CaCl_2$-NaCl-CaO by DSC. *Thermochimica Acta,* 354(1-2), pp. 59-62, 2000.

68. Mahendran, K.H., Sujatha, K., Sridharan, R. and Gnannasekaran, T., Studies on the Phase Diagram of LiBr-$SrBr_2$ System. *Journal of Alloys and Compounds*, 358(1-2), pp.42-47, 2003.

69. Mahendran, K.H., Sujatha, K., Sridharan, R. and Gnannasekaran, T., Differential Scanning Calorimetric Studies on the Phase Diagram of the Binary LiCl-$Cacl_2$ System, *Journal of Alloys and Compounds,* 325(1-2), pp.78-83, , 2001.

70. Galina, G.C., A Differential Scanning Calorimetry Study of a Binary System. *Journal of Colloid and Interface Science,* 141(2), pp.400-408, 1991.

71. Szecsebyi, K.M., Tomor, K. and Pokol, G., The Phase Diagram of the $AgNO_3$-KNO_3 System Determined by Differential Scanning Calorimetry, *Journal of Thermal Analysis.* 41, pp.125-134, 1994.

72. Koray, O. and Luo, A., Phase Identification and Microanalysis in the Mg-AL-Ca Alloy System. *Proceedings of the Minerals, Metals & Materials Society* (TMS), pp.195-200, 2003.

73. Kraus, W., Nolze, G. "PowderCell for Windows, Federal Institute for Materials Research and Testing Berlin, Version 2.3, 1999.

74. **Parvez**, M.A., Wang, X., Essadiqi, E. and Medraj, M., Experimental Investigation of the Equilibria in Mg-Al-(Ca,Sr) Systems, *Proceedings of the Minerals, Metals & Materials Society* (TMS), pp.179-184, 2005.

75. **Parvez**, M.A., Essadiqi, E. and Medraj, M, Experimental Investigation of the equilibria in th eternary Mg-Al-Sr System, submitted to COM 2005, Calgary.

76. Villars, P., Pearson's Handbook, Crystallographic data for Intermetallic Phases, 1997.

77. Akhtar, D., Gopalan, R., Rajasekharan, T.P., On a New Metastable Phase in the Al-Mg System, Z. F. Metalkunde, 78, pp. 201-203, 1987.

APPENDIX

A-1 XRD pattern calculation of Al_2Sr

Table A-1: Crystal Structure data of Al_2Sr [76].

Structure	Rhombic		
Spacegroup	*Fd3m*		
Spacegroup number	227		
Lattice parameter (Å)	a	b	c
	8.325(5)	8.325(5)	8.325(5)
Angles	α	β	γ
	90.00	90.00	120.00
Atoms in unit cell	24		

Table A-2: Atoms positions in the unit cell of Al_2Sr [76].

Atom	Wyckoff position	x	y	z
Sr	8a	0	0	0
Al	16d	0.625	0.625	0.625

Error!

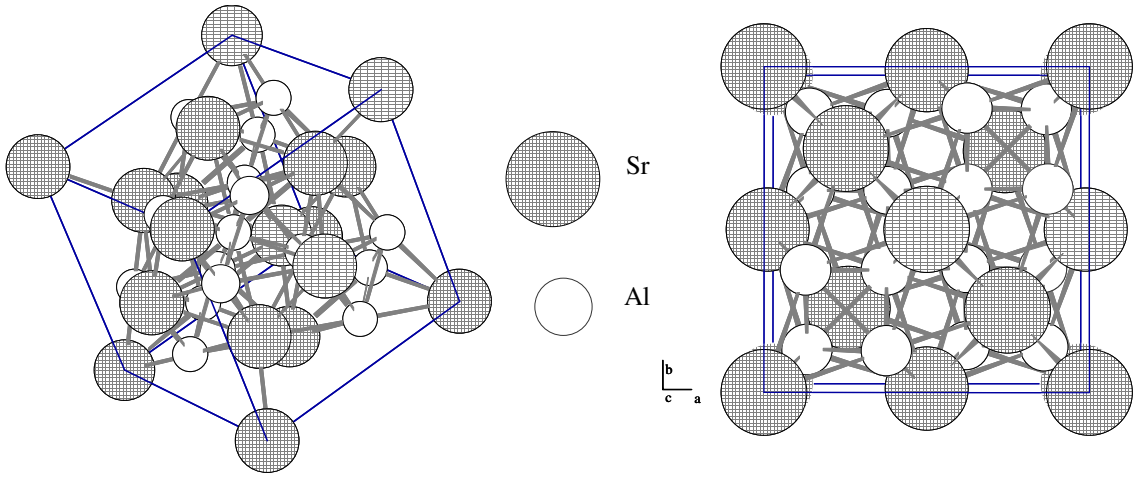

Figure A-1: (a) Al_2Sr unit cell, (b) (001) projection.

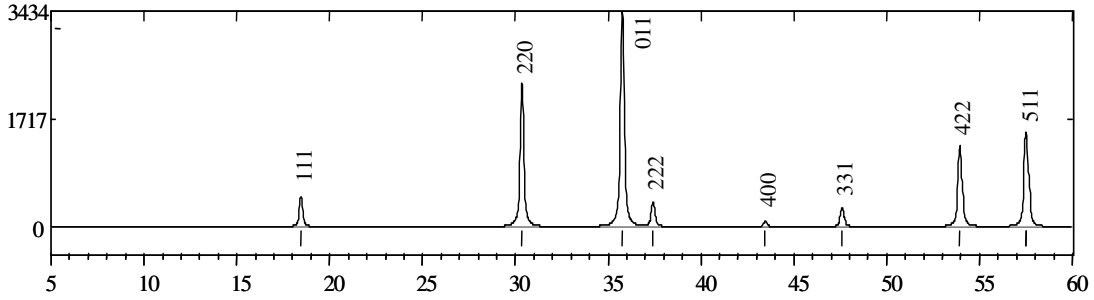

Figure A-2: Calculated XRD diffraction pattern for Al_2Sr.

A-2 XRD pattern calculation of γ

Table A-3: Crystal Structure data of γ [76].

Structure	*Cubic*		
Spacegroup	I43m		
Spacegroup number	217		
Lattice parameter (Å)	a	b	c
	10.55(3)	10.55(3)	10.55(3)
Angles	α	β	γ
	90.00	90.00	120.00
Atoms in unit cell	58		

Table A-4: Atoms positions in the unit cell of γ [76].

Atom	Wyckoff position	x	y	z
Mg1	2a	0	0	0
Mg2	8c	0.3240	0.3240	0.3240
Mg3	24g	0.3582	0.3582	0.0393
Al	24g	0.0954	0.0954	0.2725

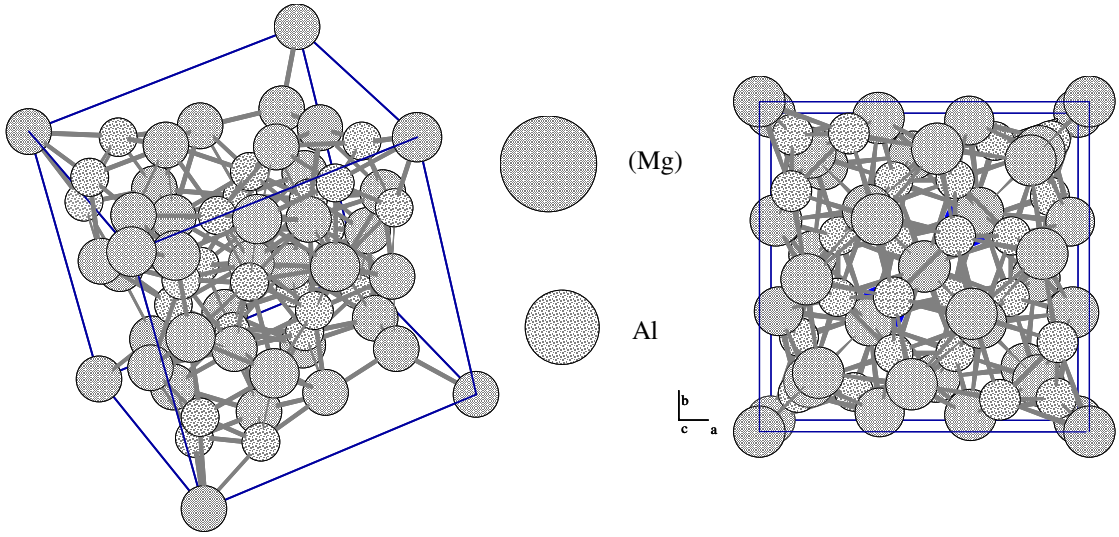

Figure A-3: (a) γ unit cell, (b) (001) projection.

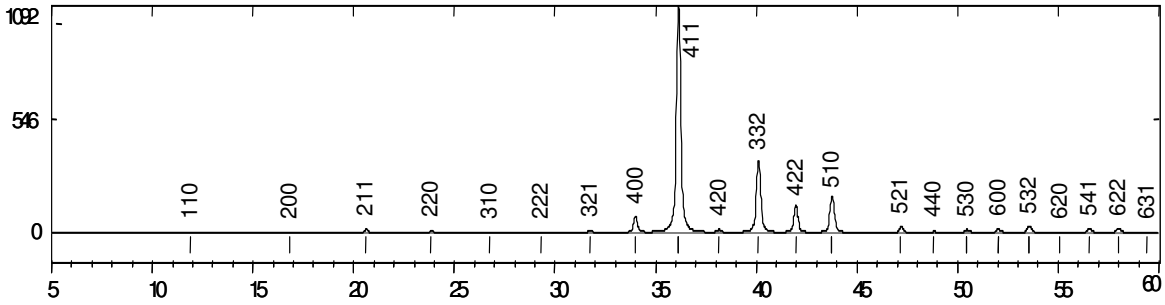

Figure A-4: Calculated XRD diffraction pattern for γ.

A-3 XRD pattern calculation of $Mg_{17}Sr_2$

Table A-5: Crystal Structure data of $Mg_{17}Sr_2$ [76].

Structure	*Hexagonal*		
Spacegroup	$P6_3/mmc$		
Spacegroup number	194		
Lattice parameter (Å)	a	b	c
	10.535(5)	10.535(5)	10.356(5)
Angles	α	β	γ
	90.00	90.00	120.00
Atoms in unit cell	38		

Table A-6: Atoms positions in the unit cell of $Mg_{17}Sr_2$ [76].

Atom	Wyckoff position	x	y	z
Sr1	2b	0	0	0.25
Sr2	2d	0.3333	0.6666	0.75
Mg1	4f	0.3333	0.6666	0.1041
Mg2	6g	0.5	0	0
Mg3	12j	0.3283	0.9627	0.25
Mg4	12k	0.1652	0.3305	0.9805

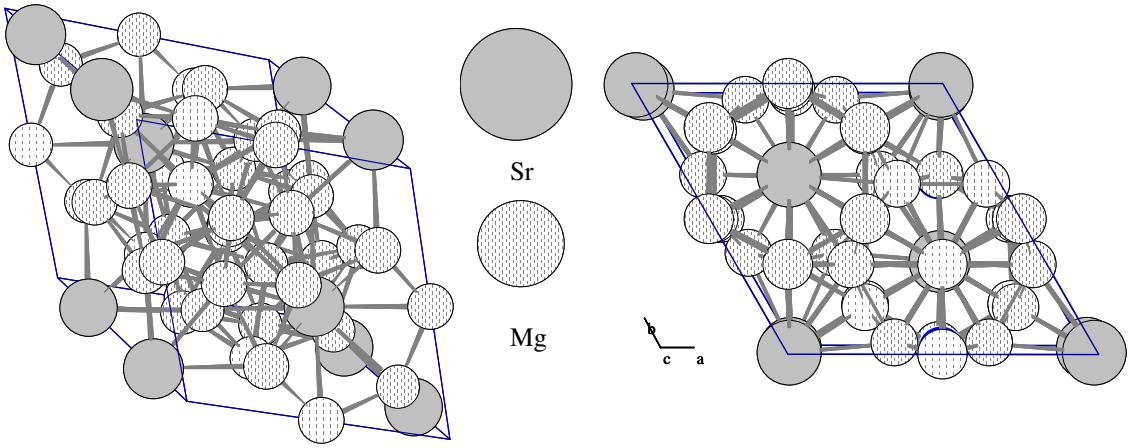

Figure A-5: (a) $Mg_{17}Sr_2$ unit cell, (b) (001) projection.

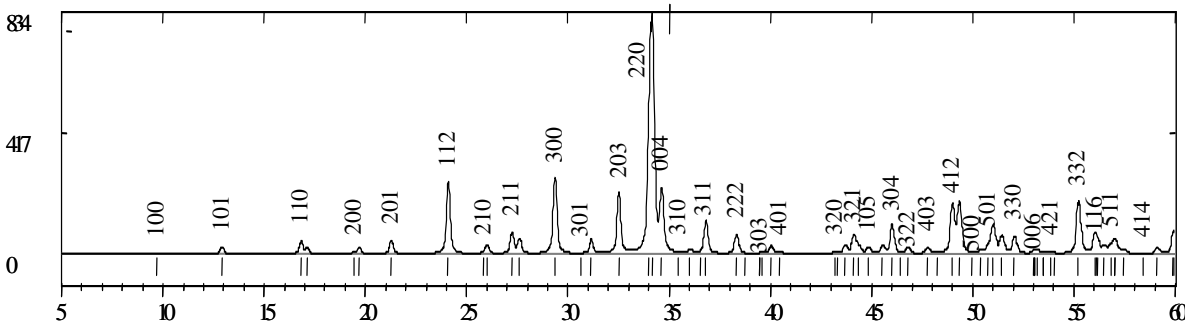

Figure A-6: Calculated XRD diffraction pattern for $Mg_{17}Sr_2$.